



# **Three-Dimensional Effects Induced by Charged Particle Beams and Radiation Pulses in Plasmas**

SUBMITTED AS PARTIAL FULFILLMENT OF THE  
REQUIREMENTS FOR THE DEGREE OF  
DOCTOR OF PHILOSOPHY  
IN  
FUNDAMENTAL AND APPLIED PHYSICS

**Supervisor:**

Professor Renato Fedele

**Co-supervisors:**

Professor Dusan Jovanović

Dr. Sergio De Nicola

**Candidate:**

Fatema Tanjia

XXV cycle

GRADUATE SCHOOL OF PHYSICAL SCIENCES  
DIPARTIMENTO DI FISICA  
UNIVERSITÀ DEGLI STUDI DI NAPOLI "FEDERICO II"

NAPOLI, ITALY

APRIL 2, 2013

UNIVERSITÀ DEGLI STUDI DI NAPOLI “FEDERICO II”  
DIPARTIMENTO DI FISICA

The undersigned hereby certify that they have read and recommend to the Fundamental and Applied Physics for acceptance a thesis entitled “**Three-Dimensional Effects Induced by Charged Particle Beams and Radiation Pulses in Plasmas**” by **Fatema Tanjia** as partial fulfillment of the requirements for the degree of **Doctor of Philosophy**.

Dated: **April 2, 2013**

Research Supervisor: \_\_\_\_\_  
Professor Renato Fedele

Co-Supervisors: \_\_\_\_\_  
Professor Dusan Jovanović

\_\_\_\_\_  
Dr. Sergio De Nicola

Examiners: \_\_\_\_\_  
\_\_\_\_\_  
\_\_\_\_\_  
\_\_\_\_\_

UNIVERSITÀ DEGLI STUDI DI NAPOLI “FEDERICO II”

Date: **April 2, 2013**

Author: **Fatema Tanjia**

Title: **Three-Dimensional Effects Induced by Charged  
Particle Beams and Radiation Pulses in Plasmas**

Department: **Dipartimento di Fisica**

Degree: **PhD**

---

Signature of Author

*Long long years back, a person incepted a beautiful dream  
inside the heart of his little daughter. I am nothing but a  
proud daughter today, who accomplished his father's  
long-cherished dream.*

*To the simplest and honest man of this universe,  
**MY FATHER***

# Contents

<b>List of Figures</b>	<b>viii</b>
<b>List of Symbols</b>	<b>xii</b>
<b>List of Acronyms</b>	<b>xix</b>
<b>Abstract</b>	<b>xx</b>
<b>Acknowledgements</b>	<b>xxii</b>
<b>Introduction</b>	<b>1</b>
<b>1 Basic Physics</b>	<b>6</b>
1.1 Characteristic parameters of plasma . . . . .	6
1.1.1 Charge neutrality and the Debye length . . . . .	7
1.1.2 Plasma oscillations . . . . .	8
1.1.3 Dawson limit . . . . .	9
1.2 Ponderomotive force . . . . .	10
1.3 Wake field generated by a charged particle . . . . .	12
1.4 Plasma Fluid Model . . . . .	14
1.4.1 Lorentz-Maxwell system . . . . .	15
1.5 Plasma wave excitation mechanisms . . . . .	16
1.5.1 Plasma Beat Wave excitation . . . . .	18
1.5.2 Laser Wake Field excitation . . . . .	20
1.5.3 Plasma Wake Field excitation . . . . .	22

<b>2</b>	<b>Wave Optics of Paraxial Beams</b>	<b>24</b>
2.1	Correspondence between optics and mechanics . . . . .	24
2.1.1	Geometrical optics and classical mechanics . . . . .	26
2.1.2	Paraxial approximation . . . . .	27
2.2	Quantization procedure . . . . .	27
2.2.1	Electromagnetic beam: Paraxial diffraction . . . . .	28
2.2.2	Charged particle beam . . . . .	29
<b>3</b>	<b>Self-consistent PWF Excitation</b>	<b>35</b>
3.1	Plasma fluid model . . . . .	36
3.1.1	Introducing perturbations and Gauge transformations . . . . .	37
3.1.2	Introducing the self-similar variable . . . . .	38
3.1.3	Long beam limit . . . . .	39
3.2	Transverse beam dynamics . . . . .	39
3.2.1	Hartree's approximation . . . . .	40
3.2.2	Quantum-like description: thermal regime . . . . .	40
3.2.3	Quantum description: quantum regime . . . . .	41
3.3	The self-consistent system . . . . .	44
3.4	Envelope description of the beam . . . . .	44
3.5	Linear regime . . . . .	45
3.6	Nonlinear regime . . . . .	50
3.6.1	Strictly local regime . . . . .	50
3.6.2	Moderately nonlocal regime . . . . .	54
3.6.3	Strongly nonlocal regime . . . . .	57
<b>4</b>	<b>Self-consistent LWF excitation</b>	<b>58</b>
4.1	Basic assumptions . . . . .	58
4.2	Governing equations . . . . .	61
4.2.1	Dimensionless equations in the moving frame . . . . .	63
4.3	Modulational representation and scalings . . . . .	66
4.4	Weak and moderate laser intensities . . . . .	68
4.4.1	1D longitudinal evolution of the pulse . . . . .	70

4.4.2	Evolution of the pulse in two dimensions: self focusing . . . .	73
4.5	Regime of very large intensities . . . . .	75
<b>5</b>	<b>Quantum Plasma Lenses</b>	<b>77</b>
5.1	Basic concept of plasma lens . . . . .	77
5.2	Thin plasma lens approximation . . . . .	78
5.3	Governing equations . . . . .	79
5.3.1	Aberration-less approximation . . . . .	80
5.3.2	Inside the slab . . . . .	81
5.3.3	In vacuo . . . . .	83
5.4	Numerical evaluation . . . . .	84
5.4.1	Inside the lens . . . . .	85
5.4.2	In vacuo . . . . .	85
	<b>Conclusion</b>	<b>87</b>
	<b>List of Publications related to the thesis</b>	<b>93</b>
<b>A</b>	<b>Kinetic model: The Vlasov-Maxwell system</b>	<b>95</b>
<b>B</b>	<b>Fluid model: Lorentz-Maxwell system</b>	<b>99</b>
B.1	EM and ES modes in unmagnetized plasma . . . . .	102
B.1.1	High-frequency modes . . . . .	103
<b>C</b>	<b>Slowly-varying amplitude approximation</b>	<b>107</b>
<b>D</b>	<b>Virial equation</b>	<b>109</b>
	<b>Bibliography</b>	<b>113</b>

# List of Figures

1.1	Schematic diagram of the fields in a plasma waves (a) Isopotential contours (b) Longitudinal $\mathbf{E}$ field, with accelerating region (for $e^+$ ) shown enhanced (c) Transverse $\mathbf{E}$ - field with focusing region (for $e^+$ ) shown enhanced (d) Wave potential, with regions of both acceleration and focusing shown enhanced (Figure courtesy Ref. [1]) . . . . .	19
1.2	Amplitudes of $E_{1z}$ and $\mathbf{E}_{1\perp}$ (in arbitrary units) from the secular term of Eqs. (1.5.5) and (1.5.6), respectively, for $k_p\sigma_{\perp} = 3$ . . . . .	20
3.1	$ \psi_{p,m} ^2$ as a function of $x/\sigma$ and $y/\sigma$ for several combinations of $p$ and $m$ ( $p, m = 0, 1, 2, 3$ ). Note that, for a given $m$ , the number of the “lateral” maxima increases as $p$ increases. For a given $p$ , the peaks corresponding to $m \neq 0$ are shifted with respect to those with $m = 0$ ; the shift increases as $m$ increases. . . . .	46
3.2	Density plot for $ \psi_{p,m} ^2$ in the transverse $x - y$ plane normalized by $\sigma$ . The combinations of $p$ and $m$ are the same as Figure 3.1. Note that, for given $m$ , the number of rings increases as $p$ (number of “lateral” maxima in Figure 3.1 increases. In particular, when $m = 0$ , the structure of the density plots is always constituted by a central core plus $p$ rings. When $m \neq 0$ , due to the shift of the peaks (see Figure 1), the density plots appear without core (hollow beam corresponding to Figure 1). For the given value of $p$ , the ring radii increase as $m$ increases. . . . .	48

3.3	$\sigma$ , as the function of $\xi$ , for three different values of $K_b$ . Left plot: $K_b = 0.5(\sigma_0 < \mathcal{E}_{0,0}/K)$ ; middle plot: $K_b = 1.0(\sigma_0 = \mathcal{E}_{0,0}/K)$ ; right plot: $K_b = 2.0(\sigma_0 > \mathcal{E}_{0,0}/K)$ . The plots account for the periodic transverse breathing of the beam that is not visible in Figures 3.1 and 3.2, due to the use of the normalized variables $x/\sigma$ and $y/\sigma$ . . . . .	49
3.4	3D plots of $ \psi_m ^2$ as the function of $x/\sigma$ and $y/\sigma$ for different values of the dimensionless time $\xi$ for $m = 0$ : $K_b = 0.25; \delta = 0.5; \tilde{\mathcal{A}}_m = 0.5$ (first row); $K_b = 0.5; \delta = 1.0; \tilde{\mathcal{A}}_m = 0.5$ (second row); $K_b = 1.0; \delta = 1.3; \tilde{\mathcal{A}}_m = 0.675$ (third row). . . . .	52
3.5	3D plots of $ \psi_m ^2$ as the function of $x/\sigma$ and $y/\sigma$ for different values of the dimensionless time $\xi$ for $m = 1$ : $K_b = 0.25; \delta = 0.25; \tilde{\mathcal{A}}_m = 1.21875$ (first row); $K_b = 0.9375; \delta = 0.5; \tilde{\mathcal{A}}_m = 1.875$ (second row); $K_b = 1.7; \delta = 1.5; \tilde{\mathcal{A}}_m = 2.5125$ (third row). . . . .	53
3.6	3D plots of $ \psi_m ^2$ as the function of $x/\sigma$ and $y/\sigma$ for different values of the dimensionless time $\xi$ for $m = 2$ : $K_b = 0.25; \delta = 0.25; \tilde{\mathcal{A}}_m = 3.70313$ (first row); $K_b = 0.953125; \delta = 0.75; \tilde{\mathcal{A}}_m = 5.71875$ (second row); $K_b = 2.5; \delta = 2.7; \tilde{\mathcal{A}}_m = 9.99375$ (third row). . . . .	54
3.7	Ring soliton of a moderate beam. The evolution of the wave function (left) and of the wake potential (right). The initial wave function was adopted as a slab soliton [Eq. (3.6.11)] with the amplitude $a = 1.5$ and with the velocity equal to zero, $b = 0$ . The azimuthal wavenumber is adopted as $m = 2$ , and the coefficient of the restoring force is $K = 0.1$ . All normalizations are given in Eq. (3.6.7). . . . .	55
3.8	The evolution of the wave function (left) and of the wake potential (right). All parameters are the same as in Figure 3.7, except a finite initial velocity of the structure, $b = 0.7$ . . . . .	56
4.1	The electrostatic potential $-\phi$ (black line), found as the solution of Eq. (4.4.4) driven by a laser pulse with the Gaussian shape. The square amplitude of the vector potential (red line) is taken as $ A_{\perp 0}(z) ^2 = (1/2L) \exp(-z^2/2L^2)$ , with different dimensionless pulse widths ranging from 1 to 5. . . . .	70

4.2	The evolution of a moderately focused laser pulse. The laser amplitude $a =  A_{\perp 0} $ (black), the phase $\theta = \arg A_{\perp 0}$ (blue) and the electrostatic potential $\phi$ (red) are obtained as the numerical solutions of Eqs. (4.4.3) and (4.4.4) in the 1D regime $\nabla_{\perp} \rightarrow 0$ . The initial condition is soliton-like, i.e. $A_{\perp 0}(z, 0) = 2\sqrt{C_1} \exp(i\delta kz) \operatorname{sech}(\sqrt{C_1}z)$ , with $\delta k = -0.5$ and with a larger amplitude, $C_1 = 5.75$ . . . . .	71
4.3	The evolution of the envelope of a weak intensity regime FLAME laser pulse, found as the numerical solution of Eqs. (4.4.3) and (4.4.4) in the 2D regime $\nabla_{\perp}^2 \ll \partial^2/\partial x^2$ . The initial condition was adopted in the form of an unchirped NLS soliton, that is modulated in the perpendicular direction by a Gaussian, $A_{\perp 0}(z, 0) = 2\sqrt{C_1} \exp(i\delta kz) \operatorname{sech}(\sqrt{C_1}z)$ , with $L_x = 25$ , $C_1 = 0.07$ , and $\delta k = -0.5$ . The initial electrostatic potential was adopted to be zero, $\phi(x, z, 0) = 0$ . . . . .	72
4.4	The evolution of the electrostatic potential produced by a weak intensity regime displayed in Figure 4.3. . . . .	73
4.5	The evolution of the envelope of a laser pulse with the amplitude typical for the accelerator scheme under investigation here (referred to in the text as a moderate intensity regime). All parameters are the same as in Figure 4.3 except the amplitude, which is adopted as $C_1 = 5.5$ . . . . .	74
4.6	The evolution of the electrostatic potential produced by a moderate intensity regime displayed in Figure 4.5. . . . .	75
5.1	Periodic Breathing of $\sigma^2$ [in $\mu\text{m}^2$ ] as a function of $z$ [in cm] inside the plasma with the initial condition of $\sigma(0) = \sigma_0$ and $\sigma'(0) = 0$ . . . . .	81
5.2	Density plot of $ \psi^2 $ in transverse $x - y$ plane corresponding to FIG. 1. The focusing and defocusing of the profile indicates the periodicity of $\sigma$ inside the plasma . . . . .	81
5.3	Variation of $\sigma$ [in $\mu\text{m}$ ] as a function of $z$ [in cm] inside the lens with the initial condition of $\sigma(0) = \sigma_0$ and $\sigma'(0) = 0$ . For a lens of thickness $l = 1$ mm, it has been found that $\sigma(l) = 9.91 \mu\text{m}$ and $f = 5.55$ cm. . . . .	82

5.4	Variation of $\sigma$ as a function of $z$ in the vacuum with initial condition $\sigma(0) = \sigma(l)$ and $\sigma'(0) = \sigma(l)/\rho(l)$ . $\sigma$ experiences strong focusing due to the dominance of the magnetic field term $K$ . When $\sigma$ becomes very small near the final focus, the space charge effects becomes dominant compared magnetic field and it blows up. The beam spot size in the interaction point is $\sigma^* = 56$ nm. . . . .	82
5.5	A closer look on the variation of $\sigma$ around the interaction point. It shows the hyperbolic structure of $\sigma$ . . . . .	83
5.6	The cross section of $\sigma$ with continuous $z$ around the interaction point corresponding to Figure 5.5, showing the hyperbolic shape . . . . .	83
5.7	The focusing of $\sigma$ with continuous $z$ till the interaction point shows the trumpet structure . . . . .	84
5.8	Density plot of $ \psi ^2$ in the transverse $x - y$ plane at the final focus corresponding to Figures 5.5 and 5.6 . . . . .	84

# List of Symbols

- A** – Vector potential
- A<sub>1</sub>** – Vector potential perturbation
- A<sub>1z</sub>** – Longitudinal component of vector potential perturbation
- A<sub>1⊥</sub>** – Transverse component of vector potential perturbation
- A<sub>⊥0</sub>** – Amplitude of the EM wave **A<sub>⊥</sub>**
- A<sub>max</sub>** – Maximum amplitude of **A<sub>⊥0</sub>**
- A<sub>m</sub>** – Constant of motion in nonlinear regime corresponding to  $\sigma_m$  with positive integer  $m$
- B** – Magnetic field
- B<sub>0</sub>** – External constant magnetic field
- B<sub>1</sub>** – Magnetic field perturbation
- c** – Speed of light
- d<sub>e</sub>** – Collisionless skin depth
- E** – Electric field
- E<sub>1</sub>** – Electric field perturbation
- E<sub>z</sub>** – Longitudinal component of **E**
- E<sub>⊥</sub>** – Transverse component of **E**
- E<sub>max</sub>** – Cold wave-breaking field
- ℰ** – Kinetic energy of the electron quiver motion in the laser field
- ℰ<sub>m</sub>** – Total energy of the charged-particle beam
- ℰ<sub>m,p</sub>** – Averaged energy corresponding to the Laguerre-Gauss ( $m, p$ ) mode
- ℰ<sub>0,0</sub>** – Averaged energy corresponding to the Laguerre-Gauss (0, 0) mode
- e** – Absolute value of electron charge
- F** – Lorentz force

$F$	– Collisionless Boltzmann distribution function
$f$	– Focal length of the plasma lens, Boltzmann distribution function
$\mathbf{f}_{\text{NL}}$	– Ponderomotive force acting on single particle
$H$	– Hamiltonian
$H_0$	– Unperturbed relativistic Hamiltonian
$\mathcal{H}$	– Effective dimensionless Hamiltonian
$\hbar$	– Planck's constant
$I_{\text{max}}$	– Maximum laser intensity
$\mathbf{J}$	– Current density
$K$	– Constant related to external magnetic field
$k$	– Wave number of the electromagnetic wave
$k_B$	– Boltzmann constant
$k_p$	– Electron plasma wave number
$L$	– Lagrangian for light rays
$\mathcal{L}$	– Lagrangian of a mechanical system
$L_{\perp}$	– Transverse laser spot size
$L_z$	– Longitudinal laser pulse length
$l$	– Thickness of the plasma lens
$m$	– Integer/vortex charge
$m_0$	– Electron's rest mass
$m_e$	– Electron mass
$m_i$	– Ion mass
$m_s$	– Mass of species $s$
$N$	– Number of beam particles
$n$	– Refractive index, plasma electron number density
$n_0$	– Unperturbed refractive index, unperturbed plasma density
$n_1$	– Plasma density perturbation
$n_b$	– Unperturbed beam number density
$n_e$	– Plasma electron number density
$n_{e0}$	– Unperturbed plasma electron density
$n_{e1}$	– Plasma electron density perturbation

- $n_i$  – Plasma ion number density
- $n_{i0}$  – Unperturbed plasma ion density
- $n_{i1}$  – Plasma ion density perturbation
- $n_p$  – Plasma number density
- $n_s$  – Fluid density associated with species  $s$
- $n_\alpha$  – Hydrodynamic density of generic particle species  $\alpha$
- $\mathbf{P}$  – Canonical momentum
- $\mathcal{P}$  – Dimensionless canonical momentum
- $\mathcal{P}_\perp$  – Dimensionless transverse canonical momentum
- $\mathbf{p}$  – Mechanical momentum
- $p$  – Integer
- $p_0$  – Unperturbed mechanical momentum
- $p_s$  – Scalar pressure of species  $s$
- $q$  – Electric charge
- $\mathbf{r}$  – position vector
- $\mathbf{r}_0$  – Initial position vector
- $\mathbf{r}_\perp$  – Transverse position vector
- $r_\perp$  – Transverse space position in cylindrical coordinate
- $s$  – Electron/positron spin
- $T$  – Temperature, time period
- $T_p$  – Plasma period
- $T_s$  – Temperature of species  $s$
- $T_{th}$  – Beam temperature threshold
- $t$  – Time coordinate
- $U$  – Potential energy
- $\mathcal{U}$  – Dimensionless potential energy
- $U_i$  – Ionization potential
- $U_w$  – Dimensionless wake potential
- $\mathbf{u}$  – Plasma electron fluid velocity
- $u$  – Velocity of the moving reference frame along  $z$  – direction
- $\mathbf{u}_1$  – Plasma electron fluid velocity perturbation

- $\mathbf{u}_b$  – Beam fluid velocity
- $\mathbf{V}_s$  – Macroscopic velocity associated with the generic species  $s$
- $\mathbf{V}_{s1}$  – First order perturbation of  $\mathbf{V}_s$
- $\mathbf{v}$  – Plasma electron fluid velocity, velocity of a single particle  
in configuration space
- $v$  – Speed
- $\mathbf{v}_0$  – Initial velocity of a single electron
- $\mathbf{v}_1$  – Early time velocity of a single electron
- $\mathbf{v}_2$  – Additional correction of velocity of a single electron in longer time scale
- $\mathbf{v}_e$  – Plasma electron fluid velocity
- $\mathbf{v}_i$  – Plasma ion fluid velocity
- $\mathbf{v}_\alpha$  – Hydrodynamic velocity of generic particle species  $\alpha$
- $\mathbf{v}_z$  – Longitudinal component of  $\mathbf{v}$
- $\mathbf{v}_\perp$  – Transverse component of  $\mathbf{v}$
- $\mathbf{W}$  – Wake field
- $W_{max}$  – Maximum laser power
- $\alpha$  – Constant related to the square of the quiver velocity, particle species
- $\beta$  –  $v/c$
- $\Gamma$  – Keldysh parameter
- $\gamma$  – Relativistic factor
- $\gamma_0$  – Unperturbed relativistic factor
- $\gamma_s$  – Ratio of specific heats at constant pressure and constant volume of species  $s$
- $\delta$  – Inter-particle distance, constant related to the nonlinearity,  
small change of generic physical quantities
- $\epsilon$  – Emittance ( $\epsilon = \epsilon_t, \epsilon_c$  generic dispersion parameter),  
emittance of the lowest quantum state
- $\epsilon_c$  – Relativistic Compton wavelength ( $\lambda_c/\gamma_0$ )
- $\epsilon_t$  – Transverse thermal emittance
- $\epsilon_x$  –  $x$  component of  $\epsilon_t$
- $\epsilon_y$  –  $y$  component of  $\epsilon_t$
- $\lambda$  – Wavelength of the electromagnetic wave, Characteristic length of the  
spatial variation of generic physical quantities involved in fluid description

- $\lambda_c$  – Compton wavelength
- $\lambda_p$  – Plasma wavelength
- $\lambda_D$  – Debye length
- $\lambda_{pe}$  – Electron plasma wavelength
- $\lambda_T$  – Thermal de Broglie wavelength
- $\lambda$  – Inverse of wave number ( $1/k = \lambda/2\pi$ )
- $\mu$  – Phase space
- $\nu$  – Quiver velocity
- $\nu_{max}$  – Maximum quiver velocity
- $\nu_{rep}$  – Repetition rate
- $\xi$  – Self-similar time-like displacement variable  $\xi = z - \beta ct$
- $\vec{\xi}$  – Displacement vector in lagrangian coordinates
- $\rho$  – Charge density, curvature radius
- $\rho_0$  – Initial curvature radius
- $\rho_b$  – Charged particle beam number density
- $\sigma$  – Charged-particle beam spot size (transverse)
- $\sigma_0$  – Intial beam spot size
- $\sigma_j$  – Second order moments of  $j(j = x, y)$
- $\sigma_m$  – Effective beam spot size with integer  $m$
- $\sigma_{m,p}$  – Effective beam spot size with positive integers  $m, p$
- $\sigma_p$  – Total averaged transverse momentum associated to EM beam
- $\sigma_{p_x}$  –  $x$  component of  $\sigma_p$
- $\sigma_{p_y}$  –  $y$  component of  $\sigma_p$
- $\sigma_r$  – Effective EM beam radius in cylindrical coordinat
- $\sigma_x$  –  $x$  component of  $\sigma_{\perp}$
- $\sigma_y$  –  $y$  component of  $\sigma_{\perp}$
- $\sigma_z$  – Laser pulse/charged particle beam length
- $\sigma_{\perp}$  – Laser/charged-particle beam spot size (transverse)
- $\sigma'$  – Differentiation of  $\sigma$  with respect to  $\xi$
- $\sigma^*$  – Beam spot size at the final focus

- $\sigma_x^*$  –  $x$  component of  $\sigma^*$
- $\sigma_y^*$  –  $y$  component of  $\sigma^*$
- $\tau$  – Laser pulse duration
- $\Phi_{NL}$  – Ponderomotive potential acting on the single particle
- $\phi$  – Scalar potential
- $\phi_1$  – Scalar potential perturbation
- $\phi_{m,p}$  – Phase associated to Laguerre-Gauss mode  $(m, p)$
- $\varphi$  – Azimuthal coordinate
- $\varphi_{NL}$  – Ponderomotive potential per unity volume
- $\chi$  – Constant
- $\chi_w$  – Constant associate to the plasma lens effect
- $\chi_{sp}$  – Constant associate to the space charge effect
- $\Psi$  – Beam wave function
- $\vec{\Psi}$  – Single particle spinor
- $\Psi_s$  – Component of spinor
- $\psi_m$  – Beam wave function in cylindrical symmetry of  $(m, 0)$  mode
- $\psi_{m,p}$  – Beam wave function in cylindrical symmetry of  $(m, p)$  mode
- $\Omega$  – Wake potential
- $\omega$  – Frequency of electromagnetic wave
- $\omega_{ce}$  – Electron cyclotron frequency
- $\omega_p$  – Plasma frequency
- $\omega_{pe}$  – Electron plasma frequency
- $\omega_{uh}$  – Plasma upper hybrid frequency

## Operators

$\nabla$	– Gradient operator
$\nabla_{\perp}$	– Transverse gradient operator
$\nabla^{(6)}$	– Gradient operator in 6 – dimensional $\mu$ – space
$\nabla_{\mathbf{r}}$	– Gradient operator in the configuration space
$\nabla_{\mathbf{v}}$	– Gradient operator in the velocity space
$\hat{f}$	– Quantum operator associated to the generic observable $f$
$\langle f \rangle$	– General notation for average of the the generic quantity $f$ (time average, space average, quantum average, statistical average, etc.)
$\hat{\mathbf{I}}$	– Identity tensor
$\mathbf{k}\mathbf{k}$	– Dyadic product of $\mathbf{k}$
$\hat{L}_s$	– Differential operator in hexa dimensional $\mu$ space
$\hat{\mathbf{P}}_s$	– Flux momentum density tensor of the species $s$
$\hat{\mathbf{p}}_s$	– Tensor pressure of the species $s$
$\mathbf{v}\mathbf{v}$	– Dyadic product of $\mathbf{v}$

# List of Acronyms

BSI	Barrier Suppression Ionization
BWF	Beam Wave Function
COMB	Coherent plasma Oscillations excitation by Multiple electron Bunches
EM	Electromagnetic
ES	Electrostatic
FAI	Fondo Affari Internazionale
FLAME	Frascati Laser for Acceleration and Multidisciplinary Experiments
INFN	Istituto Nazionale di Fisica Nucleare
LOA	Laboratoire d'Optique Appliquée
LWF	Laser Wake Field
MIR	Moderate Intensity Regime
NLS	Nonlinear Schrödinger
PBW	Plasma Beat Wave
PLASMONX	PLASma acceleration and MONochromatic X-ray production
PWF	Plasma Wake Field
LM	Lorentz-Maxwell
SIR	Strong Intensity Regime
SITE	Self Injection Test Experiment
SL	SPARC LAB
SLAC	Stanford Linear Accelerator Center
TWM	Thermal Wave Model
UCLA	University of California, Los Angeles
WIR	Weak Intensity Regime

# Abstract

This PhD thesis concerns the 3D effects that are generated by the self-consistent interaction of very intense relativistic charged-particle beams or ultra-short and ultra-intense laser pulses with a plasma. These effects are usually encountered in the new plasma-based accelerator techniques, in the inertial fusion and in a number of astrophysical problems. This thesis work is a theoretical investigation within the context of the general beam physics, but oriented to the applications for the new plasma-based acceleration schemes. When very intense relativistic charged-particle beams or ultra-short and ultra-intense electromagnetic radiation beams are traveling in a plasma, due to both their longitudinal and transverse profiles, a modification of the local properties of the plasma are introduced. The general mechanism is called *wake field interaction*. In the case of charged particles, the violation of the local plasma neutrality caused by the traveling beam excites large amplitude plasma fields, leading to the so-called Plasma Wake Field (PWF) excitation. These fields have a 3D character in terms of components and profiles. They are driven by the particle beam, but on longer time scales the plasma wake fields act on the beam itself. Sufficiently long beams experience the transverse PWF effects, such as self-focusing, filamentation and collapse. However, in a controlled way, they can be used to manipulate the beam in a plasma lens, usable to enhance the luminosity in the final stage of very compact linear colliders for nano-sized beams.

In the case of ultra-short and ultra intense laser pulses, the ultra-strong ponderomotive effects introduced by both the ultrashort longitudinal and transverse profiles modifies the local plasma density associated with large amplitude electric fields, leading to the so-called Laser Wake Field (LWF) excitation. Similarly to the case of particle beams, the laser pulse drives this mechanism, but on the longer time scales it experiences the reaction of the plasma that affects the beam propagation.

Starting from a fluid model of the system “plasma + beam”, the self consistent PWF and LWF excitations have been described obtaining in both cases a Zakharov-like system of equations, coupling a sort of nonlinear Schrödinger equation (describing the

spatio-temporal evolution of a complex function whose squared modulus is proportional to the beam density/intensity profile). Within both quantum-like (Thermal Wave Model) and quantum context, novel linear and nonlinear collective vortex states of a charged-particle beam (as a collective manifestation of the orbital angular momentum) have been obtained, nonlocal effects investigated, and conditions for the self-focusing and collapse discussed. In addition a scheme of plasma lens for nanobeams has been put forward.

Taking into account the weak and moderate nonlocal regimes, the dynamics of the ultra-short and ultra-intense laser pulses have been investigated in the case of self-injection plasma acceleration; additionally, solitary solutions have been found and the evolution of the beam collapse has been observed.

All the above investigations have been carried out both analytically and/or numerically. They have been carried out within the INFN national collaboration NTA SL COMB and NTA SL SITE (former PLASMON-X project) devoted to the PWF- and LWF-based acceleration, respectively, also in collaboration with the following distinguished scholars: the late Professor Padma Kant Shukla (Ruhr-Universität Bochum, Bochum, Germany; Professor Dusan Jovanović (Institute of Physics, University of Belgrade, Belgrade, Serbia); Dr. Sergio De Nicola (INO-C.N.R., Pozzuoli, Italy).

# Acknowledgements

It is a matter of great pleasure for me to record my deepest sense of gratitude, honour, and thankful acknowledgement to my supervisor Professor Renato Fedele, one of the best teachers I have encountered in my entire student life. It is his indispensable guidance, un-tiring efforts, and invaluable suggestions that helped to grow my knowledge throughout the total duration of my research work. I must thank my co-supervisors Professor Dusan Jovanović and Dr. Sergio De Nicola for their continuous support and help, specially for the purpose of numerical computations. Without their guidance, my PhD training would have been incomplete. I found myself lucky and honoured to have the opportunity to learn directly from all these respected and distinguished physicists.

During my PhD, as a part of collaboration, I had the opportunity to visit regularly and to work directly with the late Professor Padma Kant Shukla, a distinguished plasma physicist and was International Chair of Physics and Astronomy at the Ruhr-Universität Bochum, Germany. I wish I could thank personally while presenting him a copy of my thesis! May GOD rest his soul in peace.

I am very much thankful to GOD for letting me born in such a beautiful family. If my father was the first person to teach me how to dream a beautiful dream, my mother was always the source of strength and continuous support to peruse it. I found them and all my siblings always besides me in every thick and thin, even when I was incorrect with them. A special mention and love for two of the youngest family members, my dearest nephew and niece, Adyan and Mayameen. I consider my PhD times very lucky, because they arrive in this universe during this period. Another special thanks for my dearest sister 'Aapi' and dear brother-in-law 'Aslam Bhai'. After long tiring work-loaded academic semesters, all those vacations with you two and Adyan were simply priceless.

I thank all my long-time friends from Bangladesh, who always kept in touch with me despite my lack of regular contact with them. My heartiest apology for not communicating regularly.

Every international student of the Physics Department of “Federico II” meets an Angel as PhD secretary named Guido Celentano. I really don’t know how would we survive through the Italian bureaucratic process of getting a legal permit of stay without his help. Moreover, it is impossible to thank or acknowledge this extremely kind, down-to-earth, and humble human being. Dear Guido, please, at least today accept my heartiest thanks! It was really an honour to meet and know a person like you.

I should acknowledge not only ‘my supervisor Professor Fedele’, but also the ‘kind human Renato’ inside him. Three years ago, an Easter weekend like this one, he realised the heart of a sad, homesick girl and invited her to spend Easter Sunday with his beautiful family. That Sunday lunch of spending my first weekend abroad within warm welcoming by Atena, Alessandro, and Francesca is one of my most beautiful memories in Napoli. Thanks for being available for any help, whenever needed.

When I first came to Napoli, I was alone, being far away from family and dear ones for the first time. But gradually I started to realise that people around me are taking care of my well-beings. Too many precious memories are coming in my mind! In the beginning, Srdjan’s spontaneous help of very first day, Ebrahim-Rahil’s everyday ‘How are you today?’, LiuJi’s silent peace-spreading smile, or Priya’s continuous giggle at home in the evening. Later with time, I just discovered more and more a bunch of beautiful people around me in the name of friends and colleagues.

I am really afraid to mention specific person’s name from my integrated family-like friends in Napoli, with the fear that I might miss to take some names. But I can not help myself from mentioning some very special dear ones. Abolfazl Baharampour- and his continuous loud laughter, sharing small little happiness/tears with him. Sara Karam- my little dear ‘more than a sister’ and spending all those beautiful times with her in chatting/shopping. Thanks a lot for allowing me to be part of your life.

Many other friends, colleagues, and well-wishers from Napoli whom I am not mentioning specifically. Whether it is each laughter everyday in PhD room, during lunch-time, or beautiful times during weekends with all of you, I treasure them as precious moments of my life.

Finally, last but not the least, to my dearest ‘Vampire’- life could have been even more difficult without you and your Skype!

*Fatema Tanjia*

March 30, 2013

Napoli, Italy

# Introduction

The strong development of high-energy physics registered in the last two decades has required that particle accelerators have to work at the extreme conditions of luminosity  $10^{34} \text{ cm}^{-2} \text{ s}^{-1}$  or brightness (high-intensity beams) and beam energy of the order of several tens of TeV. To satisfy these requirements, but at same time keeping very compact both the experimental set-up and the accelerating machines, very intense electromagnetic (EM) fields of about  $100 \text{ GV m}^{-1}$  are needed to manipulate (acceleration/deceleration, focusing/defocusing) the beams/bunches in suitable ways. Unfortunately, limitations in terms of costs and technology encountered in the use of the present generation of conventional accelerators fix the maximum acceleration gradient at a few tens of MeV/m. To overcome the limitations, the use of plasmas to conceive new acceleration schemes and, in perspective, new non-conventional accelerating machines, seems to be very promising.

Plasma is an attractive medium for particle acceleration [1–3] because of the high electric field it can sustain with studies of acceleration processes remaining one of the most important areas of research in both laboratory, space and astrophysical plasma. The accelerating gradients and focusing strength that have been demonstrated in plasma accelerators are as high as of the magnitude of the order of  $\text{GVm}^{-1}$ . In a plasma-based accelerator [4], particles gain energy from a longitudinal plasma wave. To accelerate particles to relativistic energies, the plasma waves have to be sufficiently intense, with a phase speed close to the speed of light in vacuum.

Recently, the study of the EM pulses propagations in plasmas has rapidly grown in connection with a wealth of nonlinear effects investigated as well as a number of techniques and devices realized at the frontiers of nonlinear optics. Techniques and devices have been improved to extreme conditions in terms of ultra-high radiation intensities and ultra-short pulse durations. This is testified, in the diverse applications, by a number of very spectacular nonlinear effects observed as well as physical mechanisms used. During the pioneering activity of the plasma based acceleration schemes, a resonant excitation of a plasma wave by means of beat waves of two co-linear lasers

was predicted [5] and soon recognized as an important mechanism to be used for particle acceleration, usually referred to as Plasma Beat Wave (PBW) excitation [4]. These predictions have been observed in a number of numerical simulations [6–11] as well as experiments [12, 13].

When the technology concerning very intense and very short (picosecond duration) laser pulses became matter of fact, the experience matured with PBW excitation was fruitfully used to conceive a new generation of plasma acceleration schemes with non-resonant mechanism of plasma wave excitation, the so-called Laser Wake Field (LWF) excitation [14–16]. After a few years, a decisive improvement of that laser technology lead to the use of ultra-intense and ultra short (femtoseconf duration). Then, the LWF became the primary goal for future accelerator technology in most of the advanced countries [17, 18]. In experiments of ultra-intense laser pulse propagation, the wake field have been excited to provide ultra-intense plasma electric fields [19–24]. On the other hand, the study of relativistic charged-particle beam dynamics in plasmas has increased gradually in connection with the richness of nonlinear and collective effects induced by the propagation of very intense or very short charged-particle bunches. Intense charged-particle beams/bunches propagating in a plasma excites ultra-intense plasma fields. These fields provided, in turn, intense acceleration of particles. The related acceleration is usually referred to as Plasma Wake Field (PWF) acceleration [25–27]. In all the above referred mechanisms behind the driver (laser wave packet or charged particle bunch) a wake appears much like the wake of a fast motor boat.

Since the early 1990s significant progress has been made in both laser and particle beam driven plasma accelerators. The accelerating gradient although important is not the only parameter necessary to build a successful accelerator, luminosity and emittance are two others that have to match or be better than that in conventional accelerators. Plasma accelerators are ideal for providing compact, short pulses and they may also be useful in increasing the energy of conventional accelerators using the afterburner concept.

## **Chapter wise brief summary**

### **Chapter 1: Basic Physics**

In this chapter the basic theory of the plasma based acceleration is described. First some fundamental phenomena of the plasma physics, such as plasma oscillations, Dawson limit, ponderomotive force, etc. are described briefly. Then the simple plasma model is presented in terms of fluid equations of plasma together with the Maxwell's equations. This Lorentz-Maxwell fluid plasma model is described both for EM pulses and charged particles beam. During the interaction with the plasma the beam becomes

the driver of large amplitude plasma waves via wake field excitations. The generation of wake field inside the plasma is then explained and different relativistic plasma wave excitation mechanisms are described briefly. In particular, the basic idea of Plasma Wake Field (PWF) and Laser Wake Field (LWF) excitations (PWF for charged particle beams and LWF for laser pulses) have been put forward which are the major ingredients of this dissertation. In chapter 3 and 4, the theoretical model based on these two excitation mechanisms will be described elaborately.

## **Chapter 2: Optics and dynamics of beams**

In PWF and LWF excitations, the interaction of plasma with charged particle beams and radiation pulses, respectively, are of great scientific interest. Before going to the particular theoretical model in the next chapters, in this chapter, the optics and dynamics of these beams are described starting from an analogy between optics and mechanics. Then the transverse beam dynamics is described both for EM and charged particle beams, thus ignoring the longitudinal dynamics. We describe the beam motion under the paraxial approximation, which, in the classical electron optics language means that the beam rays slightly deviate from the propagation direction. Since the longitudinal motion is relativistic, this implies that the transverse motion should be non relativistic, in order to be consistent with the paraxial approximation. In the case of charged particle beams, the paraxial behavior is described in two different regimes. This has been done by giving a ‘quantum-like’ and ‘quantum’ description to the beam, which in turn result two different regimes, *thermal* and *quantum*, respectively (*thermal paraxial dispersion* and *quantum paraxial diffraction*).

## **Chapter 3: Self-consistent PWF excitation**

In this chapter, within the framework of the INFN project SPARC LAB (SL) COMB, a theoretical investigation of the quantum transverse beam motion for a cold relativistic charged particle beam travelling in a cold, collisionless, strongly magnetized plasma is carried out [28,29]. This is done by taking into account both the individual quantum nature of the beam particles (single-particle uncertainty relations and spin) and the self consistent interaction generated by the plasma wake field excitation. By adopting a fluid model of a strongly magnetized plasma, the analysis is carried out in the overdense regime (dilute beams) and in the long beam limit. It is shown that the quantum description of the collective transverse beam dynamics is provided by a pair of coupled nonlinear governing equations. It comprises a Poisson-like equation for the plasma wake potential (driven by the beam density) and a 2D spinorial Schrödinger equation for the wave function, whose squared modulus is proportional to the beam

density, that is obtained in the Hartree's mean field approximation, but disregarding the exchange interactions. The analysis of this pair of equations, that in general exhibits a strong nonlocal character, is carried out analytically as well as numerically in both the linear and the nonlinear regimes, showing the existence of the quantum beam vortices in the form of Laguerre-Gauss modes and ring envelope solitons, respectively. In particular, when the relation between the plasma wake field response and the beam probability density is strictly local, the pair of the governing equations is reduced to the 2D Gross-Pitaevskii equation that allows us to establish the conditions for the self focusing and collapse. These conditions include the quantum nature of the beam particles. Finally, when the relation between the plasma wake field response and the beam probability density is moderately nonlocal, the above pair of equations permits to follow the spatio-temporal evolution of a quantum ring envelope soliton. Such a structure exhibits small or violent breathing but it remains very stable for long time.

#### **Chapter 4: Self-consistent LWF excitation**

In this chapter, within the framework of the INFN project SPARC LAB (SL) SITE (former NTA PLASMON-X), a theoretical (both analytical and numerical) investigation of the interaction of an ultra-strong and ultra-short laser pulse with unmagnetized plasma is carried out and applied to the specifications of the Ti:Sa Frascati Laser for Acceleration and Multidisciplinary Experiments (FLAME) [30]. The three-dimensional character of the effects that are produced by the wake field excitation of ultra-short and ultra-intense EM radiation pulses and the concomitant nonlinear and nonlocal character of the plasma response are investigated. The analysis is based on the Lorentz-Maxwell fluid model for the plasma in the fully relativistic regime taking the pancake approximation. The latter is self-consistently coupled with the set of equations governing the modification of the medium (plasma) on the time scale that is long compared to that of the carrier EM pulse. We demonstrate that the nonlinear and nonlocal effects come mostly from the interaction between the electromagnetic pump wave with a Langmuir wave, whose frequency is considerably lower than that of the electromagnetic (laser) pump. To this end and within a relatively simple model, we develop an analytical approach (used also for numerical evaluations) that may provide satisfactory physical interpretations for the purely numerical results obtained from the usual simulation codes. We use the standard assumption [4, 5, 14–16] that the evolution of the pulse is relatively slow in the reference frame that travels with the pulse, which greatly simplifies the hydrodynamic equations for the electrons. In particular, we show that, beyond the slowly-varying amplitude approximation, the above coupled equations are reduced to a non-trivial pair of Zakharov-like equations. These equations are

governing the self-consistent 3D spatio-temporal nonlinear and nonlocal evolution of the four-potential and suitably take into account both the ultra-short longitudinal and transverse spatio-temporal variations of the laser pump amplitude while propagating through the plasma. The system of equations, describing the spatio-temporal nonlinear and nonlocal evolution of a pancake-shaped laser pulse, is obtained beyond the slowly-varying amplitude approximation and for arbitrary intensities. The system is then further analyzed for different cases of laser intensity regimes, namely weak and moderate intensity. It is shown that the pancake structure is unstable in two dimensions (2D) but the collapse occurs over a distance much longer than the typical active plasma length. Our analytical and numerical investigations are finalized to give new insights on the feasibility or limitations in the realization of an efficient plasma acceleration that has been already tested in preliminary experiments devoted to the diverse aspects of very high energy gain, very intense focusing and production of radiation of very small wavelengths.

### **Chapter 5: Applications towards focusing: plasma lenses**

On the basis of the theory that has been described in Chapter 3, here we describe possible applications towards focusing of the beam. We carry out a preliminary study of the transverse effects experienced by a cold relativistic beam through a thin plasma slab (plasma lens). In the strongly nonlocal regime, in which the beam experiences very strong focusing effect, the scheme of quantum plasma lens is reviewed in terms of the wave description provided by the above quantum theory.

### **Conclusion**

Finally, a summary of the thesis work is given.

# Chapter 1

## Basic Physics

In this chapter, we present the basic physics related to plasma theory and the basic concept of plasma wave excitation mechanisms. The theory that have been described here was gathered starting from my previous background on plasma physics that continued to grow during last 3 years of PhD training.

### 1.1 Characteristic parameters of plasma

About almost 85 years ago Tonks and Langmuir [31] first introduced the term ‘plasma’ to describe the inner region (remote from the boundaries) of a glowing ionized gas produced by means of an electric discharge in a tube. The term plasma comes from Greek *πλάσμα* which means “anything formed”. It represents a macroscopically neutral gas containing many interacting charged particles (electrons and ions) and neutrals.

There are some physical quantities by which it is sufficient to establish the condition of a gas to be plasma and to predict the behavior of external electromagnetic (EM) radiation that interacts with it. For this reason the measurement of these quantities, even though not so easy, is essential. To overcome the problems related to the experimental measurement of these parameters refined techniques have been developed over time which constitute the discipline known as plasma diagnostics. These quantities are called characteristic parameters of plasma. Parameters to which literatures [32–34] often refer are: charge neutrality, the Debye length, plasma frequency of oscillations, number density  $n_s$  and mass  $m_s$  associated to the species  $s$  of the observed particles, Dawson limit, etc. In the next sections we will describe how they characterize the plasma state.

### 1.1.1 Charge neutrality and the Debye length

Let us consider a plasma initially with a uniform density of  $n_0$  for both protons and electrons. There is no net charge density, so that we can assume that there is initially no electric field. Now, let us suppose that the proton density is changed from  $n_0$  to  $(1 - \delta)n_0$  in the region  $-L < x < L$ . If  $L$  is sufficiently small, the electric field due to this change will be so small that the electrons will suffer negligible disturbance. On the other hand, if  $L$  is sufficiently large, the change will have a drastic effect on the electron distribution. We are going to estimate the range of  $L$  at which transition takes place.

If there were no change in electron density, the Poisson's equation would lead to the following equation for the electric potential

$$\frac{d^2\phi}{dx^2} = 4\pi\delta n_0 e. \quad (1.1.1)$$

Assuming that the plasma as a whole (outside the disturbance) is maintained at potential  $\phi = 0$ , the appropriate solution of Eq. (1.1.1) is

$$\begin{aligned} \phi &= 2\pi\delta n_0 e(x^2 - L), & \text{for } |x| < L, \\ \phi &= 0 & \text{for } |x| > L. \end{aligned} \quad (1.1.2)$$

Hence in particular,

$$\phi(0) = -2\pi\delta n_0 e L^2. \quad (1.1.3)$$

Now suppose that the plasma has a temperature  $T$ , so that each particle has mean kinetic energy  $k_B T/2$  in each degree of freedom ( $k_B$  is the Boltzmann constant). If  $\phi(0)$  is so small that an electron of average thermal energy can easily reach  $x = 0$ , there will be only a small change in the state of plasma. On the other hand, if  $\phi(0)$  is so large that a very few electrons can reach  $x = 0$ , there will be a drastic change in the state of the plasma. Hence the requirement that the plasma remain 'quasi-neutral' is that

$$\frac{1}{2}k_B T > 2\pi\delta n_0 e^2 L^2. \quad (1.1.4)$$

This can be rewritten in the form

$$\delta < \left(\frac{\lambda_D}{L}\right)^2, \quad (1.1.5)$$

where we have introduced the quantity called the 'Debye length':

$$\lambda_D = \frac{k_B T}{4\pi n e^2}.$$

Numerically this can be expressed as

$$\lambda_D = 10^{0.84} n^{-1/2} T^{-1/2}. \quad (1.1.6)$$

Suppose, for instance, that  $\delta = -1$ , so that protons are completely removed from the range  $-L < x < L$ . Then we see that plasma remains quasi-neutral if  $L \ll \lambda_D$ . If  $L \gg \lambda_D$ , the region indicated behaves as vacuum.

### 1.1.2 Plasma oscillations

If a number of electrons is moved from one region to another inside a plasma, an electric field, that pushes the charges of opposite sign (electrons and ions) towards each other, is generated. If the displacement occurs quickly enough, because of the large mass difference, the electrons find themselves in their initial position with a non-zero speed before the ions motion becomes significant, i.e., ions can be considered immobile forming an uniform background. The plasma electron motion induces charge separation, which results in high electric fields and a strong restoring Coulomb force that drives the oscillation of the plasma electrons.

It is possible to provide a simple mathematical description of this phenomenon by assuming a cold, collisionless plasma with distribution of plasmas ions of fixed uniform background. Limiting ourselves to the one-dimensional case, we consider a rigid layer of electrons that are displaced along the  $x$  direction lead by the vector displacement  $\vec{\xi}$  (with respect to ions). The Poisson equation in one dimension determines the field in the new electrostatic (ES) configuration of charges. In analogy to the case of the plate capacitor, the electric field produced by the capacitor is  $\mathbf{E} = 4\pi e n_e \vec{\xi}$ , where  $n_e$  is the plasma electron number density and  $e$  being the absolute value of electron charge, respectively). Then the electric restoring force on an electron is  $\mathbf{F} = -e\mathbf{E} = -4\pi e^2 n_e \vec{\xi}$ . Therefore, the electron motion equation gives

$$\ddot{\xi}^2 + \omega_p^2 \xi = 0, \quad (1.1.7)$$

$$\ddot{\mathbf{E}}^2 + \omega_p^2 \mathbf{E} = 0, \quad (1.1.8)$$

where  $\omega_p = (4\pi e^2 n_e / m_0)^{1/2}$  and  $m_0$  is the rest mass of electron. Equations (1.1.7) and (1.1.8) are the equations for simple harmonic motion describing the oscillations frequency of the fluctuating plasma electrons around the equilibrium position and of the electric field, respectively. Note that  $2\pi\omega_p^{-1}$  estimates the characteristic time of the charge separation.  $\omega_p$  is called *electron plasma frequency*.

### 1.1.3 Dawson limit

As we have seen, the violation of the local neutrality of a cold and quiescent plasma, it induces an ES oscillation of frequency  $\omega_p$  of the electric field in the plasma that is described by Eq. (1.1.8). This is similar to a dielectric field plane capacitor to accelerate charged particles, where acceleration increases as the potential between two plates increases. However if the electric field overcomes the intrinsic limit of dielectric rigidity, breakdown and ‘perforation’ of dielectric occurs. On the contrary, breakdown can not occur in a fully ionized plasma: it can support ultra-high electric fields. For a plasma, a limit to this field also exists [2, 3]. It’s expression follows from Poisson’s equation  $\nabla \cdot \mathbf{E} = -4\pi en_1$ , where  $n_1$  is the number density perturbation. It is obvious that the intensity of  $\mathbf{E}$  is related to  $n_1$  and grows with it. It must be expected so that the maximum electric field is sustainable by plasma that has been perturbed as much disturbance as possible. Physically, this means a total depletion of electrons of the perturbed region. An estimate of the maximum field can be obtained from Poisson’s equation where  $n_1 \sim n_0$ :

If the unperturbed plasma density is  $n_0$  then an estimate of the maximum value of the intensity of  $\mathbf{E}$  is given by

$$\nabla \cdot \mathbf{E}_{max} \approx -4\pi en_0. \quad (1.1.9)$$

It is reasonable to assume that in a cold plasma the wave that comes from the maximum perturbation has phase velocity close to  $c$ . The Fourier transform of Eq. (1.1.9) gives us  $i\mathbf{k} \cdot \mathbf{E}_{max} \approx -4\pi en_0$ , so if  $k \approx \omega_p/c \approx k_p$ , where  $k_p$  is the electron plasma wave number we find the range of Dawson limit

$$E_{max} \sim \frac{4\pi en_0 e}{\omega_p/c} = \frac{m\omega_p c}{e}, \quad (1.1.10)$$

which can be cast as

$$E_{max} [\text{V/cm}] \approx 0.96 \sqrt{n_0 [\text{cm}^{-3}]}. \quad (1.1.11)$$

This is the famous *Dawson limit* first introduced by John Dawson in 1959 [2, 3]. This limit is sometimes also referred to as the *cold wave-breaking field* because it is the amplitude at which a cold plasma wave steepens and becomes double valued so that the crest begins to fall into trough. For  $n_0 \approx 10^{18} \text{cm}^{-3}$ , the Dawson limit is  $E_{max} \sim 1 \text{GV/cm}$ , which is about  $10^4$  times larger than the ones employed in conventional accelerators to manipulate the charged particles to pursue three different goals: accelerate particle bunches to high-energy, focus particle beams to produce high luminosity in colliders and produce coherent radiation of small wavelengths by wiggling particles of a beam with a periodic fields.

It should be emphasized that due to the modest value of these fields in the conventional accelerators, these goals can not be easily fulfilled to meet the demand of the frontiers of high-energy physics in terms of energy and luminosity to be reached or of the frontiers of the nano and sub nano meters free electron laser (FEL) physics. On the contrary, the so large field that can be generated in a plasma surely meet (provided some technological aspects are suitably solved) those demands for the most extreme conditions in terms of ultra-high accelerator energy, ultra-high collider luminosity, and ultra-short FEL wavelengths.

## 1.2 Ponderomotive force

One of the discoveries of the 20th century, derived from studies of electromagnetism, is that light exerts pressure on the medium in which it propagates. This phenomenon takes the name of radiation pressure and for particularly intense beams plays a fundamental role in the dynamics of plasma. To describe the phenomena involving the radiation pressure effects on the charged particles of a plasma (macroscopic Compton effect), the notion of *ponderomotive force* appears to be helpful. This is a nonlinear force experienced by charged particles in an homogenous oscillating electromagnetic field. For example, when high-powered microwaves or laser beams of high intensity (electromagnetic pumps) are used to heat or confine a plasma, the radiation pressure (which can reach also many hundred thousands of atmospheres), is essentially proportional to the square of the EM field intensity. Typically, the intensity associated with such EM pumps has a spatial profile, then the gradient of it introduces a force that acts on the particles, called ponderomotive force. This force pushes out the particles from high intensity regions to the lower ones. It is clear that the ponderomotive force has a 3D character, because in general, the EM intensity profile depends on longitudinal as well as transverse space coordinates. This means that the ponderomotive force has both longitudinal and transverse components.

Let us give now a quantitative description of the ponderomotive force.

We first start considering the motion of a single electron that is traveling in the presence of oscillating electric and magnetic ( $\mathbf{E}$  and  $\mathbf{B}$ ) fields of a wave. The motion equation of the electron and the Maxwell's equation for  $\nabla \times \mathbf{E}$  are

$$m_0 \frac{d}{dt} \mathbf{v}(t) = -e[\mathbf{E}(\mathbf{r}(t), t) + \mathbf{v}(t) \times \mathbf{B}(\mathbf{r}(t), t)], \quad (1.2.1)$$

$$\frac{\partial}{\partial t} \mathbf{B}(\mathbf{r}(t), t) = -c \nabla \times \mathbf{E}(\mathbf{r}(t), t), \quad (1.2.2)$$

where  $\mathbf{v}$ ,  $m_0$ , and  $e$  are the velocity, mass, and magnitude of the electron charge, respectively. We then assume that the wave has a non-uniform amplitude modulating a carrier part with a frequency  $\omega$ , viz.,  $\mathbf{E}(\mathbf{r}, t) = \mathbf{E}_s(\mathbf{r}, t) \cos \omega t$ , where  $\mathbf{E}_s$  is slowly varying, i.e.,

$$\frac{1}{|\mathbf{E}_s|} \left| \frac{\partial \mathbf{E}_s}{\partial t} \right| \ll \omega.$$

Let us use a standard iterative method of solving the motion equation. We then assume that at  $t = 0$ ,  $\mathbf{v} = \mathbf{v}_0 = 0$  and  $\mathbf{r} = \mathbf{r}_0$ . In the early times, the particle experiences the action of the electric field at the position  $\mathbf{r}_0$  while the effects of the magnetic field through the Lorentz force are still negligible because of the smallness of  $\mathbf{v}$  during these times. But, nevertheless, in the early times, the electric field  $\mathbf{E}(\mathbf{r}_0, t)$  through Eq. (1.2.2) excites the early times magnetic field. Then, from Eqs. (1.2.1) and (1.2.2), we get the equations for the early times velocity and magnetic field  $\mathbf{v}_1$  and  $\mathbf{B}_1$ , respectively, viz.,

$$\frac{d\mathbf{v}_1}{dt} = -\frac{e}{m_0} \mathbf{E}(\mathbf{r}_0, t) = -\frac{e}{m_0} \mathbf{E}_s(\mathbf{r}_0, t) \cos \omega t, \quad (1.2.3)$$

$$\frac{\partial \mathbf{B}_1}{\partial t} = -c \nabla \times \mathbf{E}_s(\mathbf{r}, t)|_{\mathbf{r}=\mathbf{r}_0} \cos \omega t. \quad (1.2.4)$$

After integrating Eqs. (1.2.3) and (1.2.4) with respect to  $t$ , we get

$$\mathbf{v}_1 = -\frac{e}{m_0 \omega} \mathbf{E}_s(\mathbf{r}_0, t) \sin \omega t, \quad (1.2.5)$$

$$\mathbf{B}_1 = -\frac{c}{\omega} \nabla \times \mathbf{E}_s(\mathbf{r}, t)|_{\mathbf{r}=\mathbf{r}_0} \sin \omega t. \quad (1.2.6)$$

During the early times the particle performs a displacement  $\delta \mathbf{r}_1$  such that it moves to a new position  $\mathbf{r} = \mathbf{r}_0 + \delta \mathbf{r}_1$ , where  $\delta \mathbf{r}_1$  is obtained by integrating  $\mathbf{v}_1$  over the early times. Consequently, in this new position the particle experiences another value of the electric field given by  $\mathbf{E}(\mathbf{r}_0 + \delta \mathbf{r}_1)$  that can be expanded as

$$\mathbf{E}(\mathbf{r}_0 + \delta \mathbf{r}_1) \approx \mathbf{E}(\mathbf{r}_0, t) + (\delta \mathbf{r}_1 \cdot \nabla) \mathbf{E}(\mathbf{r}, t)|_{\mathbf{r}=\mathbf{r}_0} = \mathbf{E}_s(\mathbf{r}_0, t) \cos \omega t + (\delta \mathbf{r}_1 \cdot \nabla) \mathbf{E}_s(\mathbf{r}, t)|_{\mathbf{r}=\mathbf{r}_0} \cos \omega t, \quad (1.2.7)$$

where, according to Eq. (1.2.5), we have

$$\delta \mathbf{r}_1 = \frac{e}{m_0 \omega^2} \mathbf{E}_s \cos \omega t. \quad (1.2.8)$$

On a longer timescale, the velocity acquires an additional correction, say  $\mathbf{v}_2$ , due to the incremented total Lorentz force  $\mathbf{E}(\mathbf{r}_0 + \delta \mathbf{r}_1) + \mathbf{v}_1 \times \mathbf{B}_1/c$ , viz.,

$$\frac{d}{dt} (\mathbf{v}_1 + \mathbf{v}_2) = -\frac{e}{m_0} \left[ \mathbf{E}(\mathbf{r}_0 + \delta \mathbf{r}_1) + \frac{\mathbf{v}_1}{c} \times \mathbf{B}_1 \right]. \quad (1.2.9)$$

Then, by using Eqs. (1.2.5) - (1.2.8), we can write

$$m_0 \frac{d\mathbf{v}_1}{dt} + m_0 \frac{d\mathbf{v}_2}{dt} = -e\mathbf{E}_s(\mathbf{r}_0, t) \cos \omega t - \frac{e^2}{m_0\omega^2} \left[ (\mathbf{E}_s \cdot \nabla)_{\mathbf{r}=\mathbf{r}_0} \cos^2 \omega t + [\mathbf{E}_s \times (\nabla \times \mathbf{E}_s)]_{\mathbf{r}=\mathbf{r}_0} \sin^2 \omega t \right]. \quad (1.2.10)$$

This is the total force on the particle up to the second-order correction. Since it is an oscillating function in time, to evaluate its effectiveness on the particle we need to take its average on the period of the carrier component of the fields, i.e.,  $T = 2\pi/\omega$ . We observe that the average of the first-order force is zero, whilst the one of the second-order gives an effective nonlinear force, called *ponderomotive force*, whose expression is

$$\mathbf{f}_{NL} = \left\langle m_0 \frac{d\mathbf{v}_2}{dt} \right\rangle = -\frac{e^2}{4m_0\omega^2} \nabla \mathbf{E}_s^2 \equiv -\frac{e^2}{2m_0\omega^2} \nabla \langle \mathbf{E}^2 \rangle. \quad (1.2.11)$$

This quantity represents the effective nonlinear force on a single electron. The presence of the gradient in Eq. (1.2.11) also suggests the idea of expressing the ponderomotive force as a gradient of a scalar potential, called *ponderomotive potential*  $\Phi_{NL}$  as  $\mathbf{f}_{NL} = \nabla \Phi_{NL}$  with

$$\Phi_{NL} = -\frac{e^2}{2m_0\omega^2} \langle \mathbf{E}^2 \rangle \quad (1.2.12)$$

Ponderomotive force is independent of the sign of the charges on which it acts, is generated by a nonuniform electric field amplitude and is independent of its orientation and is also directed towards the regions where it is less intense. Such magnitude is a non-linear effect arises because the effect is of the second order. The link with the radiation pressure is evident, since being proportional to  $\mathbf{E}^2$ . Note that the concept of ponderomotive force is conveniently introduced for cases when  $\mathbf{E}_s$  is slowly varying, so that the wave field is a low frequency envelope modulating a high frequency oscillation  $\omega$ . This is usually referred to as “low frequency response”.

### 1.3 Wake field generated by a charged particle

In order to describe the beam-plasma interaction, let us consider for the time being the motion of a relativistic test charged particle moving in the presence of an EM field represented by the fields  $\mathbf{E}$  and  $\mathbf{B}$ . Then we are going to show that, under suitable conditions, the particle motion can be described as a particle in an effective scalar potential. This result will be suitably applied to the effects experienced by the charged particles of a beam that is traveling through a plasma in the presence of the external magnetic field of the plasma itself (see Chapter 3). To this end, let us consider the

Lagrangian of such a relativistic test charged particle in an e. m. field [35] as

$$\mathcal{L}(\mathbf{r}, \mathbf{v}, t) = -m_0c^2 \sqrt{1 - \frac{v^2}{c^2}} - q \left[ \phi(\mathbf{r}, t) - \frac{\mathbf{v}}{c} \cdot \mathbf{A}(\mathbf{r}, t) \right], \quad (1.3.1)$$

where  $\mathbf{v}$  is the velocity of the test charged particle and  $(\mathbf{A}, \phi)$  is the four potential related to  $\mathbf{E}$  and  $\mathbf{B}$  [ $\mathbf{E} = -\nabla\phi - (1/c)\partial\mathbf{A}/\partial t$  and  $\mathbf{B} = \nabla \times \mathbf{A}$ ]. Thus, the Euler-Lagrange equation viz.,

$$\frac{d}{dt} \frac{\partial \mathcal{L}}{\partial \mathbf{v}} - \frac{\partial \mathcal{L}}{\partial \mathbf{r}} = 0 \quad (1.3.2)$$

leads to

$$\frac{d\mathbf{P}}{dt} = q \left[ \nabla \left( \mathbf{A} \cdot \frac{\mathbf{v}}{c} - \phi \right) \right], \quad (1.3.3)$$

where  $\mathbf{P} = \mathbf{p} + q\mathbf{A}/c$  is the canonical momentum of the test charged particle,  $\mathbf{p} = m\gamma\mathbf{v}$  is the mechanical momentum, and  $\gamma$  is the relativistic factor. Note that, here the time derivative of  $\mathbf{P}$  is the gradient of the scalar potential  $\nabla(\mathbf{A} \cdot \mathbf{v}/c - \phi)$ . On the other hand, the Lorentz force on the test charged particle is

$$\mathbf{F} = \frac{d\mathbf{p}}{dt} = q \left[ \mathbf{E} + \frac{\mathbf{v}}{c} \times \mathbf{B} \right], \quad (1.3.4)$$

that, expressed in terms of the four potential becomes

$$\mathbf{F} = q \left[ \nabla \left( \mathbf{A} \cdot \frac{\mathbf{v}}{c} - \phi \right) + \frac{1}{c} \frac{d\mathbf{A}}{dt} \right], \quad (1.3.5)$$

where  $d/dt = \partial/\partial t + \mathbf{v} \cdot \nabla$ . Now, we assume that the particle motion is relativistic only in  $z$ -direction (hereafter longitudinal direction), viz.,  $\mathbf{v} = \hat{z}v_z + \mathbf{v}_\perp$ , where  $|\mathbf{v}_\perp| \ll v_z = \beta c$  and the generic physical quantity  $f$  (scalar or vector, i.e.,  $\mathbf{E}$ ,  $\mathbf{B}$ ,  $\mathbf{A}$ ,  $\phi$  etc.) depends on  $\mathbf{r}$  and  $t$  as  $f(\mathbf{r}, t) = f(\mathbf{r}_\perp, \xi)$ , where  $\xi \equiv z - \beta'ct$  and  $\mathbf{r}_\perp$  is the transverse component of  $\mathbf{r}$  ( $\mathbf{r} = \hat{z}z + \mathbf{r}_\perp$ ). Thus, it is easy to see that Eq. (1.3.5) becomes

$$\mathbf{F} = q \left[ \nabla (\beta A_z - \phi) + (\beta' - \beta) \frac{\partial \mathbf{A}}{\partial \xi} \right], \quad (1.3.6)$$

where  $A_z$  is the longitudinal component of  $\mathbf{A}$  ( $\mathbf{A} = \hat{z}A_z + \mathbf{A}_\perp$ ) and  $\nabla = \hat{z}\partial/\partial \xi + \nabla_\perp$ . It can be easily seen that if  $\beta' = \beta$ , i.e., the particle is moving with the same speed as the fields, the force per unitary charge  $\mathbf{W}$  exhibits a sort of ES character and can be derived by the scalar function  $\Omega = \beta A_z - \phi$ , viz.,

$$\mathbf{W} = \nabla \Omega. \quad (1.3.7)$$

Note that, under the same assumptions given above, the right hand side of Eq. (1.3.3) coincides with Eq. (1.3.4).  $\Omega$  has the following physical interpretation. According

to Eq. (1.3.4), the longitudinal component of  $\mathbf{W}$ , e.g.,  $\mathbf{W}_{\parallel}$ , is the longitudinal electric field at the point  $(\mathbf{r}_{\perp}, \xi)$  while the transverse one, e.g.,  $\mathbf{W}_{\perp}$  is the transverse Lorentz force per unitary charge

$$\mathbf{W}_{\parallel} = \hat{z}E_z = \hat{z}\frac{\partial}{\partial\xi}\Omega, \quad (1.3.8)$$

$$\mathbf{W}_{\perp} = \frac{\mathbf{F}_{\perp}}{q} \simeq \mathbf{E}_{\perp} + \hat{z}v_z \times \mathbf{B}_{\perp} = \nabla_{\perp}\Omega, \quad (1.3.9)$$

where to get the second equation we have neglected  $\mathbf{v}_{\perp}$  since  $|\mathbf{v}_{\perp}| \ll v_z$ . Note that an equivalent result of Eq. (1.3.9) can be obtained assuming that the magnetic field has no longitudinal component  $B_z$  but retaining  $\mathbf{v}_{\perp}$ .  $\mathbf{W}$  and  $\Omega$  are here defined as the *wake field* and the *wake potential*, respectively. The ES character of Eq. (1.3.7) or the pair of equations (1.3.8) and (1.3.9) in the  $(\mathbf{r}_{\perp}, \xi)$  coordinate, where particle and fields are traveling at same speed, corresponds to the well known condition known as Panofsky-Wenzel theorem [36], viz.,

$$\nabla_{\perp}\mathbf{W}_{\parallel} = \hat{z}\frac{\partial}{\partial\xi}\mathbf{W}_{\perp}, \quad (1.3.10)$$

where

$$\mathbf{W}_{\parallel} = \hat{z}\frac{\partial}{\partial\xi}\Omega \quad \text{and} \quad \mathbf{W}_{\perp} = \nabla_{\perp}\Omega.$$

## 1.4 Plasma Fluid Model

The plasma electrodynamics within the context of the kinetic description is typically provided by the Vlasov equation coupled with the Maxwell's equation for the self-consistent electromagnetic fields, (Vlasov-Maxwell system). It accounts the Lorentz force, but disregards the short-range collisions. From this model, one can obtain an approximate plasma description in terms of a set of fluid equations. These equations are obtained from the moments of the Vlasov equation by integrating over velocities and assuming the local field equals the average field, provided that the resulting chain of moment equations are truncated to the second order by fixing a closure relation among the second order moment of the distribution function (pressure term) with the zero and first order moments (number density and current density, respectively. For more details, see Appendix A and Ref. [32]).

According to the above truncation, one reduces the Vlasov-Maxwell system to a set of equations (the so called ‘‘Lorentz-Maxwell (LM) system’’), consisting of the continuity equation and the fluid motion equation for each plasma component (ions and electrons) coupled with the Maxwell's equations (for details, see Appendix B). In

order to describe, in the next sections, the mechanism of plasma wave excitation in simple way, it is enough to assume that the plasma particles have a non relativistic motion. Actually, in principle, the plasma particle motion regime under the action of an oscillating field with maximum amplitude  $E_M$  at frequency  $\omega$  is described in terms of the so called *quiver velocity*  $v = qE_M/m\omega c$ . It turns out that if  $v \ll 1$ , the plasma particle motion is non relativistic. Then, increasing gradually the amplitude, the plasma particle velocity will gradually become a significant fraction of  $c$ . It happens when  $v \approx 1$  corresponding to radiation intensity of the order of  $10^{13} - 10^{16}$  W/cm<sup>2</sup>. Larger intensities ( $\gtrsim 10^{17}$  W/cm<sup>2</sup>) lead the plasma particles to be fully relativistic.

### 1.4.1 Lorentz-Maxwell system

Let us consider a simple cold, unmagnetized plasma of classical electrons with mass  $m_e$  and velocity  $\mathbf{v}_e$ . Ions are assumed to be immobile ( $\mathbf{v}_i = 0$ ), creating a homogeneous background with  $n_0$ . Another important assumption is that thermal motion of electron is neglected. For these assumptions, the plasma fluid equations (in CGS) can be written as

$$\left( \frac{\partial}{\partial t} + \mathbf{v}_e \cdot \nabla \right) \mathbf{v}_e = -\frac{e}{m_e} \left[ \mathbf{E} + \frac{1}{c} \mathbf{v}_e \times \mathbf{B} \right], \quad (1.4.1)$$

$$\frac{\partial n_e}{\partial t} + \nabla \cdot (n_e \mathbf{v}_e) = 0, \quad (1.4.2)$$

$$\nabla \cdot \mathbf{E} = -4\pi\rho, \quad (1.4.3)$$

$$\nabla \cdot \mathbf{B} = 0, \quad (1.4.4)$$

$$\nabla \times \mathbf{E} = -\frac{1}{c} \frac{\partial \mathbf{B}}{\partial t}, \quad (1.4.5)$$

$$\nabla \times \mathbf{B} = \frac{1}{c} \frac{\partial \mathbf{E}}{\partial t} + \frac{4\pi}{c} \mathbf{J}, \quad (1.4.6)$$

where  $n_e$  and  $\mathbf{v}_e$  are the electron number density and velocity, respectively,  $\rho = -e(n_0 - n_e)$  charge density, and  $\mathbf{J} = -en_e \mathbf{v}_e$  is the current density. Expressing  $\mathbf{E}$  and  $\mathbf{B}$  fields in terms of four potential ( $\mathbf{A}, \phi$ ) (similarly done in Section 1.3), the LM fluid model becomes

$$\left(\frac{\partial}{\partial t} + \mathbf{v}_e \cdot \nabla\right) \mathbf{v}_e = -\frac{e}{m_e} \left[ -\nabla\phi - \frac{1}{c} \frac{\partial \mathbf{A}}{\partial t} + \frac{1}{c} \mathbf{v}_e \times \nabla \times \mathbf{A} \right], \quad (1.4.7)$$

$$\frac{\partial n_e}{\partial t} + \nabla \cdot (n_e \mathbf{v}_e) = 0, \quad (1.4.8)$$

$$\nabla^2 \phi - \frac{1}{c^2} \frac{\partial^2 \phi}{\partial t^2} = 4\pi e(n_0 - n_e), \quad (1.4.9)$$

$$\nabla^2 \mathbf{A} - \frac{1}{c^2} \frac{\partial^2 \mathbf{A}}{\partial t^2} = \frac{4\pi}{c} e n_e \mathbf{v}_e, \quad (1.4.10)$$

where we have taken the Lorentz gauge  $c\nabla \cdot \mathbf{A} + \partial\phi/\partial t = 0$ .

## 1.5 Plasma wave excitation mechanisms

Plasma as a medium for particle acceleration has a number of advantages. As we can see from section 1.1.3, it has no electrical breakdown limit like conventional accelerating structures, whose acceleration gradients are not exceeding strengths of 50 MV/m. A plasma supports longitudinal plasma waves, in which the plasma electrons oscillate back and forth at the plasma frequency  $\omega_p$ .

A plasma wave can be excited by injecting EM radiation beams or charged-particle beams in a plasma. If a radiation beam modulated with a wave packet traveling in the plasma along  $z$  direction with 3D profile of the form

$$\mathbf{E}(\mathbf{r}, t) = \frac{1}{2} \mathbf{E}_s(\mathbf{r}, t) \exp[i(kz - \omega t)] + c.c., \quad (1.5.1)$$

where  $\mathbf{E}_s(\mathbf{r}, t)$  is a complex amplitude slowly varying compared to the carrier term  $\exp(ikz - i\omega t)$ , then a ponderomotive force per unity volume is produced. According to Section 1.2, it is obtained by the gradient of the following ponderomotive potential per unity volume:

$$\varphi_{NL} = n_0 \Phi_{NL} = -\frac{\omega_p^2}{\omega^2} \frac{\langle \mathbf{E}^2 \rangle}{8\pi} = -\frac{\omega_p^2}{\omega^2} \frac{|\mathbf{E}_s|^2}{16\pi}. \quad (1.5.2)$$

Ponderomotive effect acts on the plasma on the time scales longer than the carrier wave of the beam envelope so that, it changes the properties of the medium. It is a key element for developing and sustaining oscillation modes of different frequencies which can meet with each other through spontaneous beats (wave-wave interaction). These effects are only possible when the system plasma-radiation gradually moves away from the conditions of the linear regime where an ES or EM wave of large amplitude (called external pump) starts to propagate in the plasma. Therefore effects of modulation of amplitude and phase in the plasma arise spontaneously which depend on intensity of

the waves propagating through it. Once generated, these modulations introduce the ponderomotive effect. The ponderomotive force is set up as a forcing term introduced by the external pump. If we make the conditions for which this forcing is resonant with the modulations, the coupling between the modes is increased and this will inevitably lead to an intensification of the same ponderomotive effect and consequently that of the excited modes. This process obviously corresponds to an instability of the system which is associated to the continuous growth of the amplitudes of the modes excited at the expense of the external pump.

Working with an external pump, we may assume that the amplitude  $\mathbf{E}_s$  is moving with the group velocity which is almost equal to the speed of light, i.e.,  $v_g = \beta c \simeq c$ . Then we put  $\mathbf{E}_s = \mathbf{E}_s(\mathbf{r}_\perp, \xi)$ , where  $\xi = z - \beta ct \simeq z - ct$ .

If now the external pump is a relativistic charged-particle beam, then its motion in the plasma produces a violation of the local charge neutrality. Therefore, a plasma density perturbation is generated and oscillations start and this way the charged-particle beam is the driver of the oscillations. Here also we can assume that the beam density is represented by a traveling function of the form:  $\rho_b = \rho_b(\mathbf{r}_\perp, \xi)$ .

We found out that the excitation of plasma waves is produced by radiation or charged particle beams. Then a unified description can be used governing the spatio-temporal evolution of the plasma density perturbation  $n_1$ , viz.,

$$\frac{\partial^2 n_1}{\partial \xi^2} + k_p^2 n_1 = g(\mathbf{r}_\perp, \xi), \quad (1.5.3)$$

where

$$g(\mathbf{r}_\perp, \xi) = \begin{cases} -1/m_0 c^2 \nabla^2 \varphi_{NL}(\mathbf{r}_\perp, \xi), & \text{in case of radiation beams} \\ (q/e) k_p^2 \rho_b(\mathbf{r}_\perp, \xi), & \text{in case of charged-particle beams} \end{cases}$$

and  $k_p = \omega_p/c$  is the plasma wave number.

The typical form assumed for ponderomotive potential are basically two. One, that was also used in pioneering age of plasma accelerators, is given by the envelope of a beating of two laser field of nearby frequencies such as in Plasma Beat Wave (PBW) excitation.

The other is the one induced by a short, intense radiation beam that propagates in the plasma, produces wake field and drives collective oscillations of plasma electrons in a background of plasma ions, such as in the case of Laser Wake Field (LWF) excitation.

In case of charged particle beams, large amplitude relativistic plasma waves excitation is produced via the generation of wake field, e.g., in Plasma Wake Field (PWF) excitation. In the next sections, we will describe PBW, LWF, and PWF excitations elaborately.

### 1.5.1 Plasma Beat Wave excitation

The first mature plasma acceleration scheme is the PBW acceleration. Resonant excitation of a plasma wave using two laser pulses had been first analyzed by Rosenbluth and Liu in 1972 [5] for plasma heating applications. Later on, the scheme of beating two laser resonantly towards acceleration was proposed by Tajima and Dawson [4] since compact, ultrashort pulse, ultrahigh power laser technology was not available at that time to produce wake field. A large amplitude relativistic plasma wave is generated by the ponderomotive force of two lasers separated in frequency by the plasma frequency, such that the energy and momentum conservation relations are satisfied.

In PBW excitation, two co-propagating laser beams at nearby frequencies are injected into a plasma and beat together so that the difference in frequencies and wave numbers of these lasers imposes that of the plasma wave, viz.,  $\Delta\omega = |\omega_1 - \omega_2| \sim \omega_p$  and  $\Delta k = |k_1 - k_2| \sim k_p$ , where  $\omega_{1,2}$  and  $k_{1,2}$  are the frequencies and wave numbers of the two lasers and  $\omega_{1,2} \gg \omega_p$ . In the case of resonant excitation, the frequency difference of the lasers matches exactly the plasma frequency, i.e.,  $|\omega_1 - \omega_2| = \omega_p$ . The plasma electrons feel the periodic ponderomotive force of these laser pulses. Since this frequency difference matches the natural oscillation frequency of the electron plasma wave,  $\omega_p$ , the plasma responds resonantly to the ponderomotive force and large amplitude plasma waves are built up. Since,  $\omega_{1,2} \gg \omega_p$ , the group velocity  $v_g$  of either laser pulse is equal to the phase velocity of the plasma wave  $v_p = \omega_p/k_p$ . Since  $v_g$  is nearly the speed of light  $c$ , the plasma oscillation can be used for acceleration.

A two dimensional effects occur when a plasma wave has a finite width, as shown schematically in Figure 1.1 (Figure courtesy Ref. [1]). Such a wave has both longitudinal and transverse component of fields which is  $90^\circ$  out of phase.

According to Ref. [8], assuming for the two pumps of the form

$$\mathbf{E}_j(\mathbf{r}, t) = \mathbf{E}_0 \exp(-r_\perp^2/\sigma_\perp^2) \cos(k_j z - \omega_j t),$$

where  $\sigma_\perp$  is the laser spot size and  $j = 1, 2$ . Then the resulting field (beat wave) is

$$\mathbf{E}(\mathbf{r}, t) = 2\mathbf{E}_0 \exp(-r_\perp^2/\sigma_\perp^2) \cos(\Delta k \xi) \cos(k_0 z - \omega_0 t), \quad (1.5.4)$$

which, once compared to Eq. (1.5.1), the quantity  $2\mathbf{E}_0 \exp(-r_\perp^2/\sigma_\perp^2) \cos(\Delta k \xi)$  can be identified as the envelope term  $\mathbf{E}_s(\mathbf{r}_\perp, \xi)$ . Here  $\Delta\omega/\Delta k \simeq v_g \simeq \beta c \simeq c$ ,  $\Delta k = (k_1 - k_2)/2$ ,  $\Delta\omega = (\omega_1 - \omega_2)/2$ ,  $k_0 = (k_1 + k_2)/2$ , and  $\omega_0 = (\omega_1 + \omega_2)/2$ . The

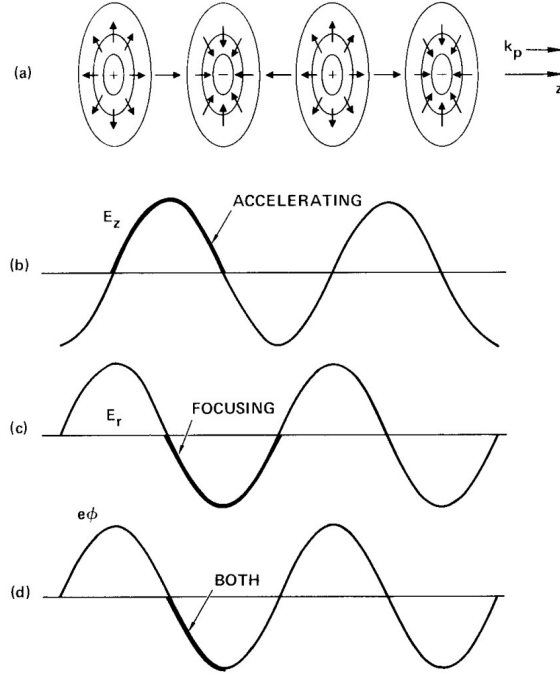


Figure 1.1: Schematic diagram of the fields in a plasma waves (a) Isopotential contours (b) Longitudinal  $\mathbf{E}$  field, with accelerating region (for  $e^+$ ) shown enhanced (c) Transverse  $\mathbf{E}$ - field with focusing region (for  $e^+$ ) shown enhanced (d) Wave potential, with regions of both acceleration and focusing shown enhanced (Figure courtesy Ref. [1])

resonant solutions of the longitudinal and transverse electric field are

$$E_{1z}(\mathbf{r}_\perp, \xi) = -\frac{m_0 c^2 k_p \alpha}{2e} \exp\left(\frac{-2r_\perp^2}{\sigma_\perp^2}\right) \left[2k_p \xi \cos(k_p \xi) + 2 \cos^2(k_p \xi) \sin(k_p \xi) - \cos(k_p \xi) \sin(2k_p \xi)\right], \quad (1.5.5)$$

$$\mathbf{E}_{1\perp}(\mathbf{r}_\perp, \xi) = -\hat{\mathbf{e}}_r \frac{4m_0 c^2 k_p \alpha}{2e} \frac{r_\perp}{k_p \sigma_\perp^2} \exp(-2r_\perp^2/\sigma_\perp^2) \left[2k_p \xi \sin(k_p \xi) + 4 + 2 \cos^3(k_p \xi) + \sin(k_p \xi) \sin(2k_p \xi)\right], \quad (1.5.6)$$

where  $\alpha$  is related to the square of the quiver velocity  $4\alpha = e^2 E_0^2 / m_0^2 \omega_0^2 c^2$ . The terms containing  $2k_p \xi \cos(k_p \xi)$  and  $2k_p \xi \sin(k_p \xi)$  are responsible for the growth of the large amplitude longitudinal and transverse fields, respectively, by the ponderomotive effect in the plasma that is oscillating. Particles must be injected in the quarter cycle in which  $E_{1z}$  is accelerating and  $\mathbf{E}_{1\perp}$  is focusing [8]. The amplitudes of the secular terms for longitudinal and transverse fields of Eqs. (1.5.5) and (1.5.6) for  $k_p \sigma_\perp = 3$  are shown in Figure 1.2 [8].

Prior to 1985, the technology for generating ultra-intense picosecond laser pulses did not exist. Thus only existing feasible concept was PBW excitation, which relied

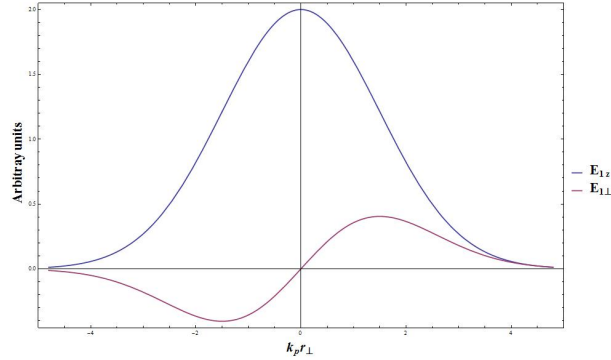


Figure 1.2: Amplitudes of  $E_{1z}$  and  $E_{1\perp}$  (in arbitrary units) from the secular term of Eqs. (1.5.5) and (1.5.6), respectively, for  $k_p \sigma_{\perp} = 3$ .

on long pulses of modest intensity. The PBW acceleration was subsequently studied (analytically as well as numerical simulations) by various works [6, 7, 9–11, 37]. The observation of plasma wave generation in the PBW accelerator via Thomson scattering was first demonstrated by Clayton *et al.* in 1985 [38]. Later, in experiments performed at the University of California at Los Angeles (UCLA), a 28 MeV energy gain was observed using a 2 MeV injected electron bunch, corresponding to a gradient of 2.8 MV/m and a plasma wave amplitude of  $\delta n/n_0 = 0.28$  (relative density perturbation) by the same group in 1993 [12].

## 1.5.2 Laser Wake Field excitation

In the Laser Wake Field (LWF) excitation [4, 14–16], a short (ps), high intensity ( $\geq 10^{17}$  W/cm<sup>2</sup>) laser pulse envelope provides both a transverse and longitudinal ponderomotive force on the plasma electrons. For LWF excitation, the laser pulse must be extremely intense for a substantial wake to be generated. The intensity can become sufficiently great so that electron motion in the pulse is relativistic. As an intense laser pulse propagates through an underdense plasma (i.e.,  $\omega_p \ll \omega_L$ , where  $\omega_L$  is the laser frequency), the transverse ponderomotive force expels electrons outward while the leading edge of the laser pulse exerts a forward force on the electrons, thus generating large amplitude plasma waves or wake. If the laser pulse length is large compared to the electron plasma wavelength, then the energy in the plasma wave is re-absorbed by the trailing part of the laser pulse. However, if the pulse length is approximately equal to or shorter than the plasma wavelength, the ponderomotive force excites plasma waves or wake fields with a phase velocity equal to the laser group velocity, and the energy is not re-absorbed. Thus, any pulse with a sharp rise or a sharp fall on a scale of  $c/\omega_p$  will excite a wake.

For a laser pulse profile with normalized intensity  $a_L(\mathbf{r}, t)$ , in the limit  $a_L \ll 1$ , the solution for the wake field (see Ref. [39]) is:

$$\mathbf{E}_1(\mathbf{r}, t) = -E_{max}c \int_0^t dt' \sin[\omega_p(t-t')] \nabla a_L^2(\mathbf{r}, t)/2, \quad (1.5.7)$$

where laser pulse profile  $a_L$ , is proportional to the ponderomotive potential such that  $a_L^2/2 = -(1/m_0c^2n_0)\varphi_{NL}$  and  $E_{max} = m_0c\omega_p/e$  is the cold nonrelativistic wave breaking field. Solution (1.5.7) indicates that the wakefield amplitude is maximum for pulse lengths  $\sigma_z$  is of the order of the plasma wavelength  $\sigma_z \simeq \lambda_p$ . The radial extent of the wake is on the order of the laser spot size  $\sigma_\perp$ . Let us consider a circularly polarized laser pulse, averaging over the fast oscillation, with a normalized intensity  $a_L^2(\mathbf{r}_\perp, \xi) = a_{L_0}^2 \exp(-2r_\perp^2/\sigma_\perp^2) \sin^2(\pi\xi/\sigma_z)$  intensity. The axial and transverse wake fields are

$$E_{1z}(\mathbf{r}_\perp, \xi) = -\frac{\pi}{4} E_0 a_{L_0}^2 \exp(-2r_\perp^2/\sigma_\perp^2) \cos k_p(\xi), \quad (1.5.8)$$

$$\mathbf{E}_{1\perp} = -\hat{\mathbf{e}}_r \frac{\pi r_\perp}{k_p \sigma_\perp^2} E_0 a_{L_0}^2 \exp(-2r_\perp^2/\sigma_\perp^2) \sin k_p(\xi). \quad (1.5.9)$$

Note that, The transverse wakefields are related to the axial wakefield by the Panofsky-Wenzel theorem [36], viz.,  $\nabla_\perp E_{1z} = \partial \mathbf{E}_{1\perp} / \partial \xi$ .

In LWF excitation, since the plasma wave is not resonantly driven, as in the beat wave, the plasma density does not have to be of a high uniformity to produce large amplitude waves. The LWF accelerator was first proposed by Tajima and Dawson in 1979 [4]. The LWF accelerator was later reinvented independently by Gorbunov and Kirsanov in 1987 and Sprangle *et al.* in 1988 [14–16]. Perhaps the first experimental evidence for plasma wave generation by the LWF excitation mechanism was obtained by Hamster *et al.* in 1993 [40], where 4.6 THz radiation at the plasma frequency was observed for a 0.1 ps laser of pulse length  $\simeq \lambda_p$  propagating in a plasma of density  $10^{17} \text{ cm}^{-3}$ . Later several experiments reported the observation of electron acceleration in LFW experiments. Amiranoff *et al.* [17] observed LWF accelerated electrons with an energy gain of 1.6 MeV (3 MeV injected) using a 3.5 TW laser system. One of the most impressive results for LWF acceleration have come from Malka's group at Laboratoire d'Optique Appliquée (LOA) [18], where electron energies up to 200 MeV have been by observed in plasmas as small as a millimetre using a Ti:Sa laser operating at 10 Hz with a pulse length of 30 fs delivered energies up to 1 J on target with a pulse length of 30 fs. The maximum longitudinal electric field was estimated to be 1.5 GV/m. Kitagawa *et al.* [41] observed electron acceleration to 100 MeV using a  $\sim 1\mu\text{m}$ , 0.5 ps duration laser exciting a plasma wave in a glass capillary with plasma density of  $10^{16} \text{ cm}^{-3}$ .

### 1.5.3 Plasma Wake Field excitation

The typical charged particle beam-driven plasma wave excitation is the well known Plasma Wake Field (PWF) excitation in which existing high energy particle beams are used to create wake fields in plasmas [25–27]. In a beam driven PWF excitation, a large amplitude relativistic plasma wave is excited by a short (in comparison to the plasma wavelength), high charge relativistic charged particle beam or bunch (driver). If a particle bunch travels in a neutral plasma of electron density  $n$ , the Coulomb force of the beam's space charge expels plasma electrons, which rush back in after the beam and produce a plasma wave or wake [25]. The plasma wake oscillates at the electron plasma frequency  $\omega_p$  and follows the driver bunch much the same way water wakes follow a fast boat (driven beam). Its phase velocity is therefore equal to the driver beam velocity, and is independent of the plasma density. Both electrons or positrons can be used to excite the plasma wake field; in the case of positrons, electrons from the background plasma are pulled in by the bunch these electrons overshoot and set up the plasma oscillation.

According to Ref. [25], assuming the separation of variables in beam density  $\rho_b(\mathbf{r}_\perp, \xi)$  the plasma density perturbation Eq. (1.5.3) can be found as

$$n_1(\mathbf{r}_\perp, \xi) \equiv \frac{q}{e} \rho_b(\mathbf{r}_\perp, \xi), \quad (1.5.10)$$

which allows us to find the expression for wake potential (for  $\beta = 1$ ) as:

$$\left(\nabla_\perp^2 - k_p^2\right)(A_{1z} - \phi_1) = 4\pi q \rho_b. \quad (1.5.11)$$

This is the master equation for the plasma wake fields excited by either an electron or positron beam. For a beam spot size much greater than the plasma wavelength, i.e.,  $\sigma_z \gg \lambda_p$ , it corresponds to  $\nabla_\perp^2 \Omega \ll k_p^2 \Omega$ . Then from Eq. (1.5.11), we get the wake potential is directly proportional to beam density, viz.,

$$(A_{1z} - \phi_1) = -\frac{4\pi q}{k_p^2} \rho_b(\mathbf{r}_\perp, \xi). \quad (1.5.12)$$

Therefore, the longitudinal and transverse wake fields can be simply expressed as

$$\mathbf{W}_\parallel = -\hat{z} \frac{4\pi q}{k_p^2} \frac{\partial \rho_b(\mathbf{r}_\perp, \xi)}{\partial \xi}, \quad (1.5.13)$$

$$\mathbf{W}_\perp = -\frac{4\pi q}{k_p^2} \nabla_\perp \rho_b(\mathbf{r}_\perp, \xi). \quad (1.5.14)$$

The first experimental observation of PWF accelerator was demonstrated in 1988 [26]. Later, a series of experiments has demonstrated successfully the beam driven PWF

accelerator (see Ref. [42] and references therein). In particular, the recent spectacular progress in PWF acceleration experiments at the Stanford Linear Accelerator Center (SLAC) was made possible by the unique properties of the electron beams available at SLAC: high energy (28.5 and 42 GeV) and charge ( $\approx 3$  nC), low normalized emittance ( $< 5 \times 10^{-5}$  m-rad) and ultra-short bunch length ( $\approx 700$  to  $< 20$   $\mu\text{m}$ ). This is particularly important for application of plasma-based accelerators to high-energy physics. In this context, plasma-based accelerators could one day allow for a significant reduction in the size [43] and cost of a future electron/positron linear collider.

## Chapter 2

# Wave Optics of Paraxial EM Radiation and Charged Particle Beams

In this chapter, we present the basic ingredients of wave optics of electromagnetic radiation and charged-particle beams in paraxial approximation. All the description and the related mathematical properties that have been learnt in attending several courses of PhD schools during last 3 years, are used as main tools for the development of the theory that have been presented in next chapters.

### 2.1 Correspondence between optics and mechanics

Since its early formulation, the analogy between optics and mechanics has proved to be fruitful in producing important physical insights. For example, it is well known that this analogy was very important to arrive, passing through the construction of wave mechanics, at the present formulation of quantum mechanics that has been recognized as the fundamental theory of nature. It is worth mentioning some important steps of the development of this analogy.

The first analogy put geometrical optics in correspondence with classical mechanics, on the basis of the similarity between the formulation of the Fermat principle and the Hamilton principle. The above analogy was quickly recognized to be useful in the study of the charged-particle motion in the presence of electromagnetic fields. The natural development of this branch was the formulation of electron optics, which was employed for several scientific and technological applications, such as electron microscopy and particle accelerators. For many years, electron optics remained to be formulated at the level of geometrical optics. Within this framework, the formulation of electron optics can be given in a way very similar to electromagnetic geometrical optics provided that one replaces the notion of light rays and refractive index with

electronic rays and potential, respectively.

It is possible to describe many optical phenomena using a simplified scalar wave theory in which light is described by a single scalar wave function. This approximate way of treating light is called scalar wave optics, or simply wave optics. It is also well known that in the limit of short wavelengths, wave optics can be reduced to geometrical optics (or ray optics): Maxwell's equations can be reduced to the eikonal equations of geometrical optics. Going from optics to mechanics, the analogy has been extended to the wave level by de Broglie [44] and Schrödinger [45]; as a result, wave mechanics and subsequently quantum mechanics were constructed. The transition from classical to wave mechanics has been induced by just considering the relationship between geometrical and wave optics. The same kind of transition has been performed by Bohr [46] with a formal procedure called quantization based mainly on a set of formal prescriptions called quantization rules, where the Planck's constant  $\hbar$  played a crucial role. These rules allow to go from the classical formulation of mechanics to another formulation in terms of operators; in such a way, to obtain an evolution equation for the physical system under consideration.

Within the framework of the above procedure, when the transition from classical to quantum mechanics has been performed, the Schrödinger equation was recognized as the nonrelativistic limit of a more general wavemechanical formulation induced by the correspondence with wave optics [47]. In fact, the nonrelativistic limit of the Klein-Gordon equation, which was a certain correspondence with the d'Alambert equation, is just the Schrödinger equation.

While quantum mechanics has continued to grow, its success has placed it in a special position in front of the other physical theories. In fact, quantum mechanics is now considered the benchmark of all other theories. Its languages, its formalism, and its results are imported by other disciplines to provide new or alternative key of reading, new description, frameworks and prediction of new effects. In particular, the counterpart of quantum mechanics, namely optics, led to further developments and acquired new interpretations of the EM phenomena, for example, to developments of nonlinear optics [48], parametric processes [49], quantum optics [50, 51]. But the first significant transfer of experiences by "quantum-like" wave optics took place between 1944 and 1946, thanks to the contributions of Fock and Leontovich [52, 53]. Going back to the analogy between the quantum mechanics and wave optics, they considered the above nonrelativistic limit for the d'Alambert equation, i.e., for the Helmholtz equation, while considering the problem of radiation-beam propagation through an arbitrary medium. They showed that the equation, which governs this propagation, is a sort of Schrödinger equation, where  $\hbar$  and time were replaced by the inverse of the wave

number and the propagation coordinate, respectively. The Schrödinger-like equation by Fock and Leontovich was actually obtained from the electromagnetic-wave equation in *paraxial approximation*, where the slopes of the light rays were considered as very small with respect to the propagation coordinate. It is possible to see that this approximation is equivalent to the so-called *slowly-varying amplitude approximation* (for details, see Appendix C), widely used in nonlinear optics [54, 55] and plasma physics [49], as well as to the nonrelativistic limit of the electromagnetic-wave equation. The above correspondence, going back from quantum mechanics to wave optics, has been extended more recently by Gloge and Marcuse [56] by performing the transition from geometrical optics to wave optics in a way quite similar to the one of Bohr. In the formal quantization of Gloge and Marcuse, a set of quantization rules (in which  $\hbar$  and time are replaced by the inverse of the wave number and the propagation coordinate, respectively) are introduced in the Hamiltonian for the electromagnetic rays. The result is the electromagnetic-wave equation whose limit, in the paraxial approximation, gives the Fock-Leontovich equation.

### 2.1.1 Geometrical optics and classical mechanics

It is well known that geometrical optics and classical mechanics can be derived from similar variational principle, Fermat's principle and Hamilton's principle, respectively, usually formulated as

$$\delta \int n(x, y, z) ds = 0, \quad (2.1.1)$$

$$\delta \int \mathcal{L}(\mathbf{q}, \dot{\mathbf{q}}, t) dt = 0, \quad (2.1.2)$$

where  $n(x, y, z)$  is the refractive index of the medium and  $\mathcal{L}$  is the Lagrangian of a mechanical system. Here  $ds = \sqrt{dx^2 + dy^2 + dz^2}$  and  $\mathbf{q} = (q_1, q_2, \dots, q_N)$  are the Lagrangian coordinates. Following the procedure of Gloge-Marcuse [56], Eq. (2.1.1) can be cast as a Hamilton-like principle:

$$\delta \int L(x, y, x', y'; z) dz = 0, \quad (2.1.3)$$

where  $x$  and  $y$  play the role of space coordinates,  $t$  the role of time, and  $L = n(x, y, z)(1 + x'^2 + y'^2)^{1/2}$  plays the role of a Lagrangian of the light rays. Here, the prime denotes the differentiation with respect to  $z$ . According to the Hamiltonian terminology, we introduce the components of the kinetic momenta  $p_x$  and  $p_y$  that are canonically conjugate

of  $x$  and  $y$ , respectively.

$$p_x = \frac{\partial L}{\partial x'} = n \left( \frac{\dot{x}}{\sqrt{1 + x'^2 + y'^2}} \right), \quad (2.1.4)$$

$$p_y = \frac{\partial L}{\partial y'} = n \left( \frac{\dot{y}}{\sqrt{1 + x'^2 + y'^2}} \right). \quad (2.1.5)$$

Then, we define the Hamiltonian of the light rays, as

$$H = p_x x' + p_y y' - L = -\sqrt{n^2 - p_x^2 - p_y^2}. \quad (2.1.6)$$

Note that, here the coordinate  $z$  has taken the place of time variable of the theory of point particles.

### 2.1.2 Paraxial approximation

Paraxial approximation is a frequently used approximation, essentially assuming small angular deviations of the light rays with respect to the propagation direction. Many calculations in optics can be greatly simplified by making the paraxial approximation. In an EM beam, the propagation direction coincides with the beam axis. Then, paraxial rays have direction close to the beam axis, say  $z$ -axis. Consequently the slopes of the rays with respect to  $z$  is small, i.e.,  $x' \equiv dx/dz \ll 1$  and  $y' \equiv dy/dz \ll 1$ . Thus, Eqs. (2.1.4) and (2.1.5) can be approximated as

$$p_x \simeq n(x, y, z)x', \quad (2.1.7)$$

$$p_y \simeq n(x, y, z)y'. \quad (2.1.8)$$

Note that, to be consistent with the paraxial motion, one has to assume that the refractive index is slowly modulated in space with respect to an unperturbed value, say  $n_0$ . Then, according to Eqs. (2.1.7) and (2.1.8),  $p_x$  and  $p_y$  can be assumed to be small to justify the ‘‘classical expansion’’ of the Hamiltonian  $H$ , viz.,

$$H = \frac{1}{2n_0}(p_x^2 + p_y^2) - n(x, y, z). \quad (2.1.9)$$

Eq. (2.1.9) is the analog of a 2D Hamiltonian of a non-relativistic single-particle of mass  $n_0$  and moving in the potential well  $U(x, y, z) = -n(x, y, z)$  on the  $(x, y)$  plane.

## 2.2 Quantization procedure

To give a ‘quantum-like’ description to the propagation of EM radiation beams, a quantization procedure, in which classical canonical momenta  $p_x$ ,  $p_y$ , and Hamiltonian  $H$  are interpreted as operators similar to the Bohr Correspondence rules [46], is

required. This is done in the next section. Subsequently, we extend this procedure to the charged-particle beam to construct the quantum-like as well as the quantum model of the paraxial charged-particle beam propagation. For the time being, in Section 2.2.1, we confine our attention to the wave propagation of paraxial radiation beams. Within this framework, the formulation of electron optics can be given in a way very similar to electromagnetic geometrical optics provided that one replaces the notion of *light beams* with *electronic rays* and consequently refractive index  $n(x, y, z)$  with potential  $U(x, y, z)$ .

### 2.2.1 Electromagnetic beam: Paraxial diffraction

Remarkably, paraxial approximation is appropriate for describing an EM beam propagation. We assume that the relativistic EM beam is traveling along  $z$ - direction, for which the so-called paraxial electron-ray approximation holds.

For EM beam the quantization procedure requires that  $p_x$ ,  $p_y$ , and  $H$  are interpreted as operators of the form  $\hat{p}_x \rightarrow -i\lambda\partial/\partial x$ ,  $\hat{p}_y \rightarrow -i\lambda\partial/\partial y$ , and  $\hat{H} \rightarrow -i\lambda\partial/\partial z$  acting on a complex EM wave amplitude  $\Psi$ . Here  $\lambda = \lambda/2\pi$  is the inverse of the wavenumber ( $\lambda$  being the wavelength) associate with the EM wave. Using this quantization procedure in Eq. (2.1.9), a Schrödinger-like equation can easily be obtained as

$$i\lambda\frac{\partial\Psi}{\partial z} = -\frac{\lambda^2}{2}\nabla_{\perp}^2\Psi + \mathcal{U}\Psi, \quad (2.2.1)$$

where  $\mathcal{U} = -n/n_0$  is the effective potential (refractive index). Here, for simplicity, we normalized  $p_x$ ,  $p_y$ , and  $H$  with  $n_0$  (i.e.,  $\mathcal{P}_x = p_x/n_0$ ,  $\mathcal{P}_y = p_y/n_0$ , and  $\mathcal{H} = H/n_0$ ). Equation (2.2.1) referred as to Fock-Leontovich [53] equation. If  $\Psi$  fulfills the normalized condition

$$\int_{-\infty}^{+\infty} \int_{-\infty}^{+\infty} |\Psi(x, y, z)|^2 dx dy = 1, \quad (2.2.2)$$

the function  $|\Psi(x, y, z)|^2$  gives the normalized EM power density as well as the probability density of finding a EM ray at location in the transverse plane  $(x, y)$ . Since the evolution of an EM beam is governed by a Schrödinger-like equation for the complex field amplitude  $\Psi$ , it is easy to prove the following well-known uncertainty relation

$$\sigma_r \sigma_p \geq \lambda, \quad (2.2.3)$$

where

$$\sigma_r \equiv \left[ \frac{\int_{-\infty}^{+\infty} r^2 |\Psi|^2 d^2r}{\int_{-\infty}^{+\infty} |\Psi|^2 d^2r} \right]^{1/2} \equiv \langle r^2 \rangle^{1/2}, \quad (2.2.4)$$

is the effective beam radius ( $r$  being the radial-cylindrical coordinate) and

$$\sigma_p \equiv \left[ \lambda^2 \frac{\int_{-\infty}^{+\infty} r^2 |\nabla_{\perp} \Psi|^2 d^2 r}{\int_{-\infty}^{+\infty} |\Psi|^2 d^2 r} \right]^{1/2}, \quad (2.2.5)$$

is the total EM averaged transverse momentum associated with the EM beam. It is worth to recall that the limit  $\lambda \rightarrow 0$  recover geometrical optics (light ray equations). This means that the physical meaning of  $\lambda$  is thus given in terms of diffraction parameter. In fact, the condition  $\lambda \neq 0$  in paraxial approximation is connected to a weak displacement of light rays from the beam propagation direction in such a way to produce a mixing between them (*paraxial diffraction*).

### 2.2.2 Charged particle beam

Electron optics [57] and the concept of electron rays have been developed by using the similarity between the charged particle beam motion and the behavior of light beams in geometrical optics. On the basis of the optical language, refraction and reflection laws for electron rays can be introduced and their formulation is fully similar to the one that is used for light beams. If we have several particles moving together in an arbitrary potential, each particle trajectory can be thought of as an electron ray. When the potential is a function of the coordinates, it corresponds to an inhomogeneous refractive index. Thus, an electron trajectory through this inhomogeneous-potential region corresponds to the light-beam propagation through an inhomogeneous medium. Furthermore, the basic electron-optics concepts have been developed in connection with the first experimental investigations of charged-particle motion (ions and electrons) in oscilloscopes and mass spectrometers. The general statement, from which we recover the above optical description, is again the similarity between Hamilton principle and Fermat principle of geometrical optics.

Let us consider a relativistic charged-particle beam is traveling along the  $z$ -axis with velocity  $\beta c$  ( $\beta \simeq 1$ ) under the action of an external potential. The motion of each single particle is associated with an unperturbed total energy  $m_0 \gamma_0 c^2$  ( $m_0$  and  $\gamma_0$  being the particle rest mass and the unperturbed relativistic factor, respectively). Let us additionally suppose that the beam has an interaction with the surroundings in the transverse plane only in such a way that, in the co-moving frame, the transverse motion of each single-particle is associated with an effective Hamiltonian  $\mathcal{H} = \mathcal{H}(\mathbf{r}_{\perp}, \mathcal{P}_{\perp}, \xi)$ :

$$\mathcal{H}(\mathbf{r}_{\perp}, \mathcal{P}_{\perp}, \xi) = \frac{1}{2} \mathcal{P}_{\perp}^2 + \mathcal{U}, \quad (2.2.6)$$

where,  $\mathbf{r}_{\perp}$  and  $\mathcal{P}_{\perp}$  are the conjugate variables of transverse position and momentum, respectively,  $\xi = z - \beta ct \simeq z - ct$  is the time-like variable, and  $\mathcal{U}$  is the external

potential. The quantities  $\mathcal{H}$  and  $\mathcal{U}$ , and  $\mathcal{P}_\perp$  are dimensionless quantities with respect to  $m_0\gamma_0c^2$  and  $m_0\gamma_0c$ , respectively.

### A. Thermal regime

In order to take into account the thermal spreading among electronic rays, a charged particle beam can be considered as a special case of a particle system, for which the so-called paraxial electron-ray approximation holds [58]. We can describe statistically the behavior of the paraxial electron rays by determining their second-order moments, which are elements of the diffusion matrix, and whose determinant essentially defines the squared diffusion coefficient. If  $F(x, y, p_x, p_y, \xi)$  is a collisionless Boltzmann distribution function (the beam is assumed sufficiently diluted as to render negligible the effects of collisions at short range between the particles), then we can calculate the second-order moments of  $F$  as follows:

$$\sigma_j(\xi) = \left\langle \left( x_j - \langle x_j \rangle \right)^2 \right\rangle^{1/2}, \quad (2.2.7)$$

$$\sigma_{p_j}(\xi) = \left\langle \left( p_{x_j} - \langle p_{x_j} \rangle \right)^2 \right\rangle^{1/2}, \quad (2.2.8)$$

$$\sigma_{jp_j}(\xi) = \left\langle \left( x_j - \langle x_j \rangle \right) \left( p_{x_j} - \langle p_{x_j} \rangle \right) \right\rangle^{1/2}, \quad (2.2.9)$$

where  $j = x, y$ . With these moments we construct the quantities:

$$\epsilon_x(\xi) = 2 \left[ \sigma_x^2(\xi) \sigma_{p_x}^2(\xi) - \sigma_{xp_x}^2(\xi) \right]^{1/2}, \quad (2.2.10)$$

$$\epsilon_y(\xi) = 2 \left[ \sigma_y^2(\xi) \sigma_{p_y}^2(\xi) - \sigma_{yp_y}^2(\xi) \right]^{1/2}, \quad (2.2.11)$$

where  $\epsilon_x$  and  $\epsilon_y$  is called the *transverse thermal emittance* or root-mean-square emittance relative to the direction  $x$  and  $y$ , respectively. If the beam is moving in vacuo, it is possible to show that  $\epsilon_x$  and  $\epsilon_y$  are conserved during motion. Each of them has a geometric interpretation as an area conserved in the subspace of the Boltzmann phase space  $(x, p_x)$  and  $(y, p_y)$ , respectively.

Suppose, for simplicity, that  $\epsilon_x = \epsilon_y \equiv \epsilon_t$  (transverse thermal emittance). From Eqs. (2.2.10) and (2.2.11), it follows immediately that:

$$\sigma_x \sigma_{p_x} \geq \frac{\epsilon_t}{2}, \quad \sigma_y \sigma_{p_y} \geq \frac{\epsilon_t}{2}. \quad (2.2.12)$$

Equation (2.2.12) is a set of uncertainty relations similar to those valid in quantum or optical paraxial of EM radiation. They relate the uncertainty of the position  $\sigma_x$  and  $\sigma_y$  of the beams in the transverse plane with the slope of the corresponding  $\sigma_{p_x}$  and  $\sigma_{p_y}$ ,

respectively. In the case of a charged-particle beam with a Maxwellian distribution, it can be shown that under the conditions of minimum uncertainty, we have [58]:

$$\frac{\epsilon_t}{\sigma^*} = \sqrt{\frac{k_B T}{m_0 \gamma_0 c^2}} \equiv \sigma_p^*, \quad (2.2.13)$$

where, for simplicity, it was assumed that both the uncertainties in the conditions of the minimum temperatures in the two transverse directions were the same:  $\sigma_x^* = \sigma_y^* \equiv \sigma^*$ ,  $T_x = T_y \equiv T$ .

The thermal spreading, (*emittance spreading*) of the trajectories around the beam propagation causes a mixing of the trajectories with small deviation of slopes with respect to the propagation direction  $z$  in such a way to produce a picture fully similar to the one obtained with paraxial diffraction of the EM beams, provided to replace the particle trajectories (*electron rays*) with the light rays (*thermal paraxial dispersion*). In this case the transverse emittance plays the role analog to a diffraction parameter whilst the small deviation of the electron rays from the propagation direction represents a sort of paraxial approximation behind the particle beam optics. To this end, note that, in the limit  $\epsilon_t \rightarrow 0$ , the particle trajectories within the beam are not affected by the spreading and, therefore, one can recover the electron ray equation.

Recently, on the basis of the above analogy electron optics at thermal regime has been extended to the wave context in paraxial approximation. A new technique to derive an equation of motion for a thermal system, like a charged-particle beam at finite temperature, which is able to take into account the collective behavior of an ensemble, has been obtained. The starting point of this technique, called thermal wave quantization, is the single-particle Hamiltonian of the system. At this point, the formal analogy, manifested in the case of the transverse dynamics for relativistic charged particle beams with electromagnetic optics in the paraxial approximation and with two dimensional non relativistic quantum mechanics have been used. These suggests replacing the single-particle Hamiltonian with a differential operator, and the Hamilton equation with a Schrödinger-like equation, in which the particle's coordinate and momentum are replaced by a complex wave function, called beam wave function (BWF) whose squared modulus is proportional to the transverse beam density profile.

This technique, applied to the longitudinal and transverse beam dynamics, has led to the formulation of a quantum-like model, called the thermal wave model (TWM) for relativistic charged particle beam propagation [59]. It represents a useful quantum-like description of the total beam optics by using the thermal quantization rules, in

which Planck's constant  $\hbar$  and time are replaced by the transverse thermal beam emittance [60]  $\epsilon_t$  and the propagation coordinate, respectively. According to the TWM prescriptions [59, 61–63] we follow “the quantum analogy”, which suggests the following correspondence rules for Eq. (2.2.6):  $\mathcal{H} \rightarrow \hat{\mathcal{H}} = i\epsilon_t \partial / \partial \xi$ , and  $\mathcal{P}_\perp \rightarrow \hat{\mathcal{P}}_\perp - i\epsilon_t \nabla_\perp$ , and  $\mathcal{U} \rightarrow \hat{\mathcal{U}}$ . Then, one can write the following Schrödinger-like equation for the BWF  $\Psi$ , as

$$i\epsilon_t \frac{\partial \Psi}{\partial \xi} = -\frac{\epsilon_t^2}{2} \nabla_\perp^2 \Psi + \hat{\mathcal{U}} \Psi, \quad (2.2.14)$$

Note that Eq. (2.2.14) describes the transverse beam dynamics in terms of the BWF  $\Psi$ , which we assume to be related to the transverse linear beam number density  $\rho_b(x, y, \xi)$  through the following relationship:

$$\rho_b(x, y, \xi) = N |\Psi|^2, \quad (2.2.15)$$

where  $N$  is the total number of beam particles. According to the previous definitions,  $|\Psi|^2$  is proportional to the transverse beam density profile. In these conditions, from Eq. (2.2.15) it follows that the norm squared  $\mathcal{N}^2$  of the BWF, determined as

$$\mathcal{N}^2 = \int_{-\infty}^{+\infty} \int_{-\infty}^{+\infty} |\Psi|^2 dx dy, \quad (2.2.16)$$

is conserved ( $\mathcal{U}$  is assumed to be a real function). This result is compatible with the physical requirement that

$$\int_{-\infty}^{+\infty} \int_{-\infty}^{+\infty} \rho_b(x, y, \xi) dx dy = N. \quad (2.2.17)$$

Thus, we can determine the effective beam width  $\sigma_x$ ,  $\sigma_y$  and the expectation value of the momentum  $\sigma_{p_x}$ ,  $\sigma_{p_y}$  respectively, as follows being the radial-cylindrical coordinate)

$$\sigma_x \equiv \left[ \frac{1}{\mathcal{N}^2} \int_{-\infty}^{+\infty} \int_{-\infty}^{+\infty} (x - \langle x \rangle)^2 |\Psi|^2 dx dy \right]^{1/2}, \quad (2.2.18)$$

$$\sigma_y \equiv \left[ \frac{1}{\mathcal{N}^2} \int_{-\infty}^{+\infty} \int_{-\infty}^{+\infty} (y - \langle y \rangle)^2 |\Psi|^2 dx dy \right]^{1/2}, \quad (2.2.19)$$

$$\sigma_{p_x} \equiv \left[ \frac{1}{\mathcal{N}^2} \int_{-\infty}^{+\infty} \int_{-\infty}^{+\infty} \Psi^* (\hat{p}_x - \langle \hat{p}_x \rangle)^2 \Psi dx dy \right]^{1/2}, \quad (2.2.20)$$

$$\sigma_{p_y} \equiv \left[ \frac{1}{\mathcal{N}^2} \int_{-\infty}^{+\infty} \int_{-\infty}^{+\infty} \Psi^* (\hat{p}_y - \langle \hat{p}_y \rangle)^2 \Psi dx dy \right]^{1/2}. \quad (2.2.21)$$

Eqs. (2.2.18) - (2.2.21) satisfy the quantum-like uncertainty principle (2.2.12). TWM has already been successfully applied for estimating the effects of aberrations in accelerators [61–63], as well as for describing nonlinear beam plasma interaction [64, 65],

nonlinear longitudinal dynamics in accelerators [66–68], modulational instabilities and nonlocal effects in high-energy charged-particle beams [69,70], etc. It, indeed, extends successfully the geometrical electron optics to the wave electron optics providing a formalism that accounts for the thermal spreading as a diffraction-like effect.

### B. Quantum regime

In this section, we present the concept of *quantum paraxial diffraction* for a charged-particle beam taking into account the individual quantum nature of the particles (single-particle uncertainty principle and spin). To present the concept in a simple way, we disregard the overlapping of the particle wave functions. This assumption corresponds to precise physical conditions (in terms of density and temperature of the system) that will be presented later and in chapter 3.

We take into account the quantum nature of the beam particles provided by the Hamiltonian (2.2.6). First of all, let us consider the quantum nature of individual particles. By using the language of the electron optics, at each  $\xi$ , the uncertainty relation between the position and the momentum, which holds for a single particle, is translated as the uncertainty relation between the position and the slope of the individual electron ray in the transverse plane, namely,  $\langle x^2 \rangle^{1/2} \langle p_x^2 \rangle^{1/2} \geq \hbar/2$  and  $\langle y^2 \rangle^{1/2} \langle p_y^2 \rangle^{1/2} \geq \hbar/2$ . Here, for simplicity, we have assumed that  $\langle x \rangle = \langle y \rangle = \langle p_x \rangle = \langle p_y \rangle = 0$ . Then, the probability density to find an electron ray with the position  $(x, y)$  at the time  $\xi$  or the probability density to find an electron ray with the slopes  $p_x, p_y$  at the time  $\xi$  can be introduced naturally. For instance, the probability density to find an electron ray at position  $(x, y)$  at  $\xi$  is of course given by the square modulus of the wave function associated with the single particle in the transverse plane. This way, the standard paraxial ray picture of a charged particle beam is implemented by the quantum uncertainty. It may be expected that, due to the *quantum paraxial* behavior, the beam cannot have an arbitrarily small spot size. In fact, it can be reduced to a certain minimum value, according to the uncertainty principle. Note also that, each particle of the beam interacts with all the other particles of the beam. Thus, this collective interaction acts exactly as the mean field [71], which for the generic particle of the beam located at the generic Eulerian position  $(\mathbf{r}_\perp, \xi)$ , operates in that position as an external force on the particle.

Taking into account the spin and the uncertainty relation of each particles, we can now describe the transverse beam dynamics by correcting the paraxial geometric electron optics with the paraxial wave electron optics, given in terms of a single-particle wave function. In principle, the effective quantum description of the transverse motion of the beam, containing  $N$  charged particles, can be provided by the system of  $N$

two-dimensional Schrödinger equations whose Hamilton operator corresponds to the classical Hamiltonian  $\mathcal{H}$  defined in Eq. (2.2.6). According to the quantum mechanics prescriptions, to write the appropriate Schrödinger equation for a single particle of the beam, which includes also the spin, we have to introduce the Bohr correspondence rules into the classical Hamiltonian given by Eq. (2.2.6). Since our quantities  $\mathcal{H}$  and  $\mathcal{P}_\perp$  have been made dimensionless dividing by  $m_0\gamma_0c^2$  and  $m_0\gamma_0c$ , respectively, it is easy to see that the appropriate correspondence rules are  $\mathcal{H} \rightarrow \hat{\mathcal{H}} = i\epsilon_c\partial/\partial\xi$ ,  $\mathcal{P}_\perp \rightarrow \hat{\mathcal{P}}_\perp = -i\epsilon_c\nabla_\perp$ , and  $\mathcal{U} \rightarrow \hat{\mathcal{U}}$ , where  $\epsilon_c \equiv \hbar/m_0\gamma_0c = \lambda_c/\gamma_0$ . Note that  $\lambda_c$  is the Compton wavelength, and therefore, the quantity  $\epsilon_c$  plays the role of the relativistic Compton wavelength. Thus, following this quantization rule, one can write the following two-dimensional Schrödinger-like equations

$$i\epsilon_c\frac{\partial\Psi}{\partial\xi} = -\frac{\epsilon_c^2}{2}\nabla_\perp^2\Psi + \hat{\mathcal{U}}\Psi. \quad (2.2.22)$$

Note that, On the basis of these considerations, taking into account the spin and the uncertainty relation of each particles, by Hartrees mean field procedure our description can be given in terms of the spatio-temporal evolution of a *single-particle spinor*  $\vec{\Psi} = (\Psi_s)$  governing two-dimensional Schrödinger-like spinorial equations, where  $s$  corresponds to the “spin down” and “spin up” states of the spinor. However, they are like independent evolution equations for the BWF with different spin, since there is no coupling due to the absence of any external magnetic field. This aspect of the interaction between the intrinsic magnetic moment of spin and the magnetic field will be deepen in Chapter 3, where an external magnetic field has been taken into account.

We would like to emphasize the fact that quantum paraxial diffraction differs than the one described in the part **A.** of Section 2.2.2, which actually has the the thermal origin. In particular, we have assumed an idealized physical condition corresponding to the absence of overlapping of the particle wave functions. The overlapping among the single-particle wave functions manifests when the inter-particle distance  $\delta$  is comparable to, or smaller than the thermal de Broglie wavelength  $\lambda_T$ ,  $\delta \lesssim \lambda_T$ . This means that to take into account quantum paraxial diffraction, the inter-particle distance must be greater than the thermal de Broglie wavelength, viz.,  $\delta > \lambda_T$ . This aspect will be deepen in chapter 3.

## Chapter 3

### Self-consistent PWF Excitation

In this chapter, we summarize the results of our investigations [28, 29, 72–76] that have been carried out within the framework of the INFN collaboration SL (SPARC LAB) COMB (Coherent plasma Oscillations excitation by Multiple electron Bunches) as further development of the former collaboration between PLASMONX. The activities have been mainly constituted both "quantum-like" and "quantum" description of theory of the Plasma Wake Field (PWF) excitation. These researches have been also carried out within the framework of Fondo Affari Internazionali (FAI) of INFN, in collaboration with Professor Dusan Jovanović (Institute of Physics, University of Belgrade, Serbia) who visited our group several times in the last 3 years for longer periods, and with Dr. Sergio De Nicola (INO-CNR Pozzuoli (Napoli), Italy). We also had valuable seminal discussions with late Professor Padma Kant Shukla (Center of Advanced Studies in Physical Sciences, Ruhr-Universität Bochum, Germany) within exchange visit program between groups of Napoli and Bochum, during last 3 years.

In PWF excitation, due to the very strong nonlinear and collective beam-plasma interaction, the beam becomes the driver of a large amplitude plasma wave that follows the beam with almost the same speed (plasma wake) and carries the longitudinal and transverse fields (plasma wake fields). The electromagnetic (EM) field associated to the wake (wake field) has transverse as well as longitudinal components. Thus, a test particle experiences the effects of both the transverse (focusing/defocusing) and the longitudinal (acceleration/deceleration) components of the wake field. Depending on the regimes, the test particle can be the one of a secondary beam externally injected in phase locking with the wake (driven beam) or belonging to the driver. In the last circumstance, the driver experiences the effects of the wake field that itself produced. Taking into account all together the effects on each particle of the driver we can describe the collective self-interaction of the driver with the plasma. If the beam length

is much greater than the plasma wavelength (*long beam limit*), the entire beam experiences the effects of the wake fields that has been produced by it (*self interaction*).

In this Chapter, we carry out a theoretical investigation of the collective and non-local quantum effects that are generated when a relativistic charged particle beam is travelling in a cold, collisionless, strongly magnetized plasma [28,29]. We confine our analysis to the physical conditions that makes the beam the driver of the PWF excitation. The beam is supposed to be cold and sufficiently dilute to take into account the individual quantum nature of the beam particles. Three different nonlinear regimes of this analysis are considered: (i) the strictly local regime, where the beam spot size is much greater than the plasma wavelength; (ii) the moderately nonlocal regime where the beam spot size is comparable to the plasma wavelength; (iii) the strongly nonlocal regime where the beam spot size is much smaller than the plasma wavelength.

### 3.1 Plasma fluid model

We first of all assume that a relativistic electron/positron beam travelling initially along the  $z$ -axis (hereafter called the *longitudinal direction*) enters a collisionless cold magnetized plasma of unperturbed number density  $n_0$ . The beam has an initial (before entering the plasma) unperturbed number density  $n_b$  and unperturbed velocity  $\beta c$ . A strong, constant and uniform external magnetic field is assumed to be oriented along the propagation direction of the beam, viz.,  $\mathbf{B}_0 = B_0 \hat{z}$ . We assume that in the overdense condition ( $n_0 \gg n_b$ ) the ions are immobile and forming a uniform background of density  $n_0$ . Within these assumptions, it is well known that the beam excites both plasma wake field and density perturbation of the electrons. Under suitable physical conditions, the wake field may act on the beam itself producing the self-interaction.

We adopt a fluid plasma model, given by the following Lorentz-Maxwell (LM) system of equations, viz.,

$$\frac{\partial \mathbf{u}}{\partial t} + \mathbf{u} \cdot \nabla \mathbf{u} = -\frac{e}{m_0} \mathbf{E} - \frac{e}{m_0 c} \mathbf{u} \times \mathbf{B}, \quad (3.1.1)$$

$$\frac{\partial n}{\partial t} + \nabla \cdot (n \mathbf{u}) = 0, \quad (3.1.2)$$

$$\nabla \cdot \mathbf{E} = 4\pi [e(n_0 - n) + q\rho_b], \quad (3.1.3)$$

$$\nabla \cdot \mathbf{B} = 0, \quad (3.1.4)$$

$$\nabla \times \mathbf{E} = -\frac{1}{c} \frac{\partial \mathbf{B}}{\partial t}, \quad (3.1.5)$$

$$\nabla \times \mathbf{B} = \frac{4\pi}{c} (q\rho_b \mathbf{u}_b - en \mathbf{u}) + \frac{1}{c} \frac{\partial \mathbf{E}}{\partial t}, \quad (3.1.6)$$

where  $\mathbf{E}$  and  $\mathbf{B}$  are the electric field and the magnetic field of the system, respectively,  $\mathbf{u}$  is the electron fluid velocity,  $n$  is the electron number density,  $\rho_b$  is the beam number density,  $\mathbf{u}_b$  is the beam fluid velocity in the plasma,  $q(= -e$  for electrons;  $e$  for positrons) is the charge of the beam particles, and  $m_0$  is the rest mass of the electron/positron. The transverse and longitudinal components of  $\mathbf{u}_b$  are denoted by  $\mathbf{u}_{b\perp}$  and  $\mathbf{u}_{bz}$ , respectively.

To write the system of equations (3.1.1) - (3.1.3), we have assumed that during the interaction with the beam, the plasma electrons have a classical motion. We also assume that  $\rho_b$  is a function of position and time as a result of the interaction with plasma, i.e.,  $\rho_b = \rho_b(\mathbf{r}, t)$ . In principle, the plasma field spatio-temporal evolution depends on  $\rho_b$  and vice versa,  $\rho_b$  is affected by the plasma fields through their interactions with the beam particles. For the time being, we consider  $\rho_b$  as a given function for the purpose to determine its connection with the plasma wake fields.

### 3.1.1 Introducing perturbations and Gauge transformations

We next assume that, before interacting with the beam, the plasma fluid is in a stationary state determined by the following set of physical quantities:  $n = n_0$ ,  $\mathbf{u} = \mathbf{E} = 0$ , and  $\mathbf{B} = \mathbf{B}_0$ . Additionally, we assume that at the initial time ( $t = 0$ ) the beam enters the plasma at  $z = 0$  with  $\mathbf{u}_b = \beta c \hat{z}$  (i.e.,  $\mathbf{u}_{bz} = \beta c \hat{z}$  and  $\mathbf{u}_{b\perp} = 0$ ). Then, we introduce the small perturbations of all the physical quantities, such as  $n_1$  for the plasma electron number density,  $\mathbf{u}_{b\perp 1}$  and  $\mathbf{u}_{bz 1}$  for the transverse and longitudinal perturbation components of the beam velocity,  $\mathbf{u}_1$  for the plasma electron velocity,  $\mathbf{E}_1$  and  $\mathbf{B}_1$  for the electric and magnetic fields, respectively. We express the fields  $\mathbf{E}$  and  $\mathbf{B}$  in terms of the four-potential  $(\mathbf{A}, \phi)$ , viz.,

$$\mathbf{E} = -\nabla\phi - \frac{1}{c} \frac{\partial \mathbf{A}}{\partial t}, \quad (3.1.7)$$

$$\mathbf{B} = \nabla \times \mathbf{A}, \quad (3.1.8)$$

and apply the Lorentz gauge, viz.,

$$\nabla \cdot \mathbf{A} + \frac{1}{c} \frac{\partial \phi}{\partial t} = 0. \quad (3.1.9)$$

According to the above perturbations, Eqs. (3.1.7) and (3.1.8) become

$$\mathbf{E}_1 = -\nabla\phi_1 - \frac{1}{c} \frac{\partial \mathbf{A}_1}{\partial t}, \quad (3.1.10)$$

$$\mathbf{B}_0 + \mathbf{B}_1 = \nabla \times \mathbf{A}_0 + \nabla \times \mathbf{A}_1. \quad (3.1.11)$$

According to Eq. (3.1.11) we can express  $\mathbf{A}_0$  as  $\mathbf{A}_0(\mathbf{r}_\perp) = (\mathbf{B}_0 \times \mathbf{r}_\perp)/2$ , where  $\mathbf{r} = \mathbf{r}_\perp + \hat{z}z$  and  $\mathbf{r}_\perp = \hat{x}x + \hat{y}y$ . Correspondingly, the Lorentz gauge can be split into the

following conditions

$$\nabla \cdot \mathbf{A}_0 = 0, \quad (3.1.12)$$

$$\nabla \cdot \mathbf{A}_1 + \frac{1}{c} \frac{\partial \phi_1}{\partial t} = 0. \quad (3.1.13)$$

### 3.1.2 Introducing the self-similar variable

Next, we split the gradient operator  $\nabla$  into the longitudinal and transverse components, viz.,  $\nabla = \nabla_{\perp} + \hat{z}\partial/\partial z$ . Furthermore, we assume that the spatio-temporal evolution of the beam density is  $\rho_b(\mathbf{r}, t) = \rho_b(\mathbf{r}_{\perp}, \xi)$ , where the self-similar variable  $\xi = z - \beta ct \simeq z - ct$  ( $\beta \simeq 1$ ) plays the role of a time-like variable. Then we assume that all the physical quantities have such spatio-temporal dependence. Under these assumptions and notations we observe that  $\nabla = \nabla_{\perp} + \hat{z}\partial/\partial \xi$ ,  $\partial/\partial t = \beta c \partial/\partial \xi \simeq c \partial/\partial \xi$ , and the linearized system of equations (3.1.1) - (3.1.3) can be reduced to

$$\left(\nabla_{\perp}^2 - k_{pe}^2\right)(A_{1z} - \phi_1) = -4\pi en_1, \quad (3.1.14)$$

$$\nabla_{\perp}^2 \mathbf{A}_{1\perp} = \frac{4\pi en_0}{c} \mathbf{u}_{1\perp}, \quad (3.1.15)$$

$$\left(\frac{\partial^2}{\partial \xi^2} + k_{uh}^2\right)n_1 = \pm k_{pe}^2 \rho_b + \frac{en_0 k_{ce}^2}{m_0 c^2} (A_{1z} - \phi_1) - \frac{en_0 k_{ce}}{m_0 c^2} \hat{z} \cdot (\nabla_{\perp} \times \mathbf{A}_{1\perp}), \quad (3.1.16)$$

where in Eq. (3.1.16) “-” (“+”) sign is for the electron (positron) beam. Here,  $k_{uh} = \omega_{uh}/c$ ,  $k_{pe} = \omega_{pe}/c$  and  $k_{ce} = \omega_{ce}/c$ ; where  $\omega_{uh} = (\omega_{pe}^2 + \omega_{ce}^2)^{1/2}$  is the upper hybrid frequency,  $\omega_{pe} = (4\pi n_0 e^2/m_0)^{1/2}$  is the electron plasma frequency and  $\omega_{ce} = -eB_0/m_0 c$  is the electron cyclotron frequency, respectively.

Since  $n_b \ll n_0$ , we note that the transverse fields produced by the driving beam are first order quantities, whilst the longitudinal magnetic field appearing in Eq. (3.1.16), i.e.,  $B_{1z} = \hat{z} \cdot (\nabla_{\perp} \times \mathbf{A}_{1\perp})$ , is a second order quantity since it is determined by the transverse velocity field times  $\rho_b$ . Consequently, in Eq. (3.1.16) we can neglect the last term on the right hand side, therefore, Eq. (3.1.15) can be decoupled from Eq. (3.1.16). Then, we concentrate our analysis on the following pair of equations.

$$\left(\nabla_{\perp}^2 - k_{pe}^2\right) U_w = \pm \frac{k_{pe}^2}{\gamma_0} \frac{n_1}{n_0}, \quad (3.1.17)$$

$$\left(\frac{\partial^2}{\partial \xi^2} + k_{uh}^2\right) \frac{n_1}{n_0} = \pm \left(k_{pe}^2 \frac{\rho_b}{n_0} - k_{ce}^2 \gamma_0 U_w\right), \quad (3.1.18)$$

where we have introduced the dimensionless wake potential  $U_w(\mathbf{r}_{\perp}, \xi) = -q(A_{1z} - \phi_1)/m_0 \gamma_0 c^2$  and  $\gamma_0$  is the unperturbed relativistic factor. Combining Eqs. (3.1.17) and (3.1.18), we get an equation for wake potential in terms of beam density, viz.,

$$\left[\left(\frac{\partial^2}{\partial \xi^2} + k_{uh}^2\right)\left(\nabla_{\perp}^2 - k_{pe}^2\right) + k_{pe}^2 k_{ce}^2\right] U_w = k_{pe}^4 \frac{\rho_b}{\gamma_0 n_0}. \quad (3.1.19)$$

### 3.1.3 Long beam limit

Next, we assume the so called *long beam limit*, i.e., the beam length,  $\sigma_z$  is much greater than the electron plasma wavelength,  $\lambda_{pe}$ , (i.e.,  $\sigma_z \ll \lambda_{pe}$ ). Since,  $1/\sigma_z \sim \partial/\partial\xi$ , we easily get the condition that  $k_{pe}\sigma_z \gg 1$ , which implies  $k_{uh}\sigma_z \gg 1$ , as well. Consequently, in Eq. (3.1.19) the term corresponding to  $\partial^2/\partial\xi^2$  is much less than  $k_{uh}^2$ . Therefore, Eq. (3.1.19) reduces to the following equation

$$\left(\nabla_{\perp}^2 - \frac{k_{pe}^4}{k_{uh}^2}\right)U_w = \frac{k_{pe}^4}{k_{uh}^2} \frac{\rho_b}{n_0\gamma_0}. \quad (3.1.20)$$

## 3.2 Transverse beam dynamics

We describe the beam dynamics in the regime defined by the assumptions in the previous section. Ignoring the longitudinal dynamics, in order to get the governing equations for the transverse beam dynamics, we consider the relativistic classical Hamiltonian of a beam particle in the presence of the four-potential  $(\mathbf{A}, \phi)$ , acting in the beam-plasma system, viz.,

$$H = c \left[ (\mathbf{P} - \frac{q}{c}\mathbf{A})^2 + m_0^2 c^2 \right]^{1/2} + q\phi, \quad (3.2.1)$$

where  $\mathbf{P}$  is the canonical momentum of a single particle of the beam. We consider the paraxial approximation and use the same procedure described in Section 2.2.2 of Chapter 2. First we make Eq. (3.2.1) dimensionless of the form

$$\frac{H}{H_0} = \left[ (\mathcal{P} - \mathcal{A})^2 + \frac{1}{\gamma_0^2} \right]^{1/2} + \Phi, \quad (3.2.2)$$

where  $H_0 = c(P_0^2 + m_0^2 c^2)^{1/2} = m_0\gamma_0 c^2$  is the unperturbed energy of the single particle with associated momentum  $P_0 = m_0\gamma_0\beta c$ ,  $\mathcal{P} = \mathbf{P}/m_0\gamma_0 c$  is the dimensionless momentum,  $\mathcal{A} = q\mathbf{A}/m_0\gamma_0 c^2$  is the dimensionless vector potential, and  $\Phi = q\phi/m_0\gamma_0 c^2$  is the dimensionless scalar potential.

We split  $\mathcal{P}$  and  $\mathcal{A}$  into the longitudinal and transverse components, viz.,  $\mathcal{P} = \hat{z}\mathcal{P}_z + \mathcal{P}_{\perp}$ ,  $\mathcal{A} = \hat{z}\mathcal{A}_z + \mathcal{A}_{\perp}$ . We are interested in the transverse dynamics of the beam, so we set  $\mathcal{P}_z \equiv \mathcal{P}_0 = p_0/m_0\gamma_0 c = \beta \simeq 1$  for the entire duration of the beam motion. In order to be consistent with the paraxial approximation, the beam particles may have a relativistic motion along  $z$  (longitudinal motion) but the transverse component of the single particle motion must be non relativistic. This implies that our Hamiltonian can be expanded in  $\mathcal{P}_{\perp} - \mathcal{A}_{\perp}$ , up to the second power. We introduce small perturbations for the quantities  $\mathcal{A}_z$ ,  $\mathcal{A}_{\perp}$ , and  $\Phi$ , viz.,  $\mathcal{A}_z = \mathcal{A}_{1z}$ ,  $\mathcal{A}_{\perp} = \mathcal{A}_0 + \mathcal{A}_{1\perp}$ , and  $\Phi = \Phi_1$ .

Then, the combined action of the non relativistic expansion of the Hamiltonian (3.2.2) to the first order in the fluid quantities leads to the following effective dimensionless Hamiltonian, viz.,

$$\mathcal{H} = \frac{1}{2}\mathcal{P}_\perp^2 + \frac{1}{2}k_c\hat{z} \cdot (\mathbf{r}_\perp \times \mathcal{P}_\perp) + U_w(\mathbf{r}_\perp, \xi) + \frac{1}{2}Kr_\perp^2, \quad (3.2.3)$$

where  $\mathcal{H} = \Delta H/H_0 = (H - H_0)/H_0$ ,  $k_c = -qB_0/m_0\gamma_0c^2$ , and  $K \equiv (k_c/2)^2 = \omega_{ce}^2/4\gamma_0^2c^2$ . Note that  $\mathcal{H}$  is a function of the transverse canonical variables  $\mathbf{r}_\perp$ ,  $\mathcal{P}_\perp$ , and  $\xi$ , viz.,  $\mathcal{H} = \mathcal{H}(\mathbf{r}_\perp, \mathcal{P}_\perp, \xi)$  that describes the effective perturbed normalized ‘‘transverse’’ motion, where the interaction of the beam particles with the plasma is manifested through the wake potential  $U_w$ .

### 3.2.1 Hartree’s approximation

Note that, the interaction of the beam particles with the plasma is manifested through the wake potential  $U_w$  as a mean field effect (Hartree’s mean field approximation) [71]. In fact,  $U_w$  is proportional to the potential combination, i.e.  $(A_{1z} - \phi_1)$ , that in the configuration space  $(\mathbf{r}_\perp, \xi)$  acts as an electrostatic potential, whose gradient produces the force on the beam particles.  $U_w$  is generated by both the charges and the currents that are produced by the plasma as well as the beam particles. However, the particles of the beam play the role of the driver of the beam-plasma interaction. As the effects of  $U_w$  represent the self-interaction of the particle beam, it turns out that each particle of the beam interacts finally with all the other particles of the beam. Thus, this collective interaction acts exactly as the mean field, which for the generic particle of the beam located at the generic Eulerian position  $(\mathbf{r}_\perp, \xi)$ , operates in that position as an external force on the particle.

In the next sections, we give a wave description to Eq. (3.2.3) in terms of a complex wave function, viz., the beam wave function (BWF) following the quantization procedure that has been already described elaborately in Chapter 2.

### 3.2.2 Quantum-like description: thermal regime

The quantization procedure to describe the propagation of charged particle beams taking into account the thermal spreading among the electron rays are described elaborately in Section 2.2.2 of Chapter 2. We can give the same ‘‘quantum-like’’ description to the charged particle beam of our current consideration by using the Thermal Wave Model (TWM) [59].

The paraxial approximation that is usually taken into account in the classical theory of electron optics has a thermal origin (thermal spreading of the electron rays). It

takes into account the envelope equation (rms beam description) through the thermal beam emittance [58, 60]. This *thermal paraxial* behavior is also the basic ingredient of the *quantum-like* description provided by the Thermal Wave Model (TWM) [59, 61–65, 67–70, 77, 78]. This is done by assuming that the paraxial transverse motion of a relativistic charged-particle beam is described in terms of a complex wave function, called beam wave function (BWF), whose squared modulus is proportional to the transverse beam density profile. The spatio-temporal evolution of the BWF is governed by a Schrödinger-like equation when the Planck's constant is replaced by transverse beam emittance (more details description of TWM is provided Section 2.2.2 of Chapter 2).

In this particular case, the BWF  $\Psi$ , whose squared modulus is proportional to the beam density, i.e.,  $\rho_b \propto |\Psi|^2$ , and Eq. (3.2.3) can be quantized using the appropriate correspondence rules as:  $\mathcal{H} \rightarrow \hat{\mathcal{H}} = i\epsilon_t \partial / \partial \xi$ ,  $\mathcal{P}_\perp \rightarrow \hat{\mathcal{P}}_\perp = -i\epsilon_t \nabla_\perp$ , and consequently can be written as.

$$i\epsilon_t \frac{\partial \Psi}{\partial \xi} = -\frac{\epsilon_t^2}{2} \nabla_\perp^2 \Psi - \frac{i\epsilon_t k_c}{2} \hat{z} \cdot (\mathbf{r}_\perp \times \nabla_\perp) \Psi + U_w[|\Psi^2|] \Psi + \frac{1}{2} K r_\perp^2 \Psi, \quad (3.2.4)$$

Note that, since  $\rho_b \propto |\Psi|^2$ , recalling Eq. (3.1.20),  $U_w$  becomes also a function of  $|\Psi^2|$ , viz.,  $U_w[|\Psi^2|]$ . In cylindrical coordinates, Eq. (3.2.4) can be reduced to the following one

$$i\epsilon_t \frac{\partial \Psi}{\partial \xi} = -\frac{\epsilon_t^2}{2} \frac{1}{r_\perp} \frac{\partial}{\partial r_\perp} \left( r_\perp \frac{\partial \Psi}{\partial r_\perp} \right) - \frac{\epsilon_t^2}{2} \frac{1}{r_\perp^2} \frac{\partial^2 \Psi}{\partial \varphi^2} - \frac{i\epsilon_t k_c}{2} \frac{\partial \Psi}{\partial \varphi} + U_w[|\Psi^2|] \Psi + \frac{1}{2} K r_\perp^2 \Psi. \quad (3.2.5)$$

### 3.2.3 Quantum description: quantum regime

To give the quantum description, we use the same quantization procedure, described as *quantum paraxial diffraction*, in Section 2.2.2 of Chapter 2 by taking into account the individual quantum nature of the beam particles (single-particle uncertainty principle and spin) and disregarding the overlapping of the particle wave functions. Former contributions to the electron wave optics fall into this quantum paraxial approximation [79–81].

We want to elucidate also the role played by the collective quantum nature of the beam particles that is manifested when there is a non-negligible overlapping among the single-particle wave functions, i.e., when the inter-particle distance is comparable to, or smaller than the thermal de Broglie wavelength  $\lambda_T$ , viz.,  $\delta \lesssim \lambda_T$ . Since the particle motion is relativistic in the  $z$ -direction, the latter is given by  $\lambda_T = h/m_0 \gamma_0 v_T$ , where

$v_T = \sqrt{k_B T / m_0 \gamma_0}$  is the thermal velocity ( $k_B$  and  $T$  being the Boltzmann constant and the transverse beam temperature, respectively). Then, we easily get the following condition that relates the beam density and the beam temperature:

$$T \lesssim \frac{m_0 c^2}{\gamma_0 k_B} (n_b \lambda_c^3)^{2/3}, \quad (3.2.6)$$

where  $n_b$  is the beam density and  $\lambda_c$  the electron Compton wavelength. This leads to a temperature threshold, viz.  $T_{th} = (m_0 c^2 / \gamma_0 k_B) (n_b \lambda_c^3)^{2/3} \propto n_b^{2/3} / \gamma_0$ . In the typical range of the beam densities,  $n_b \sim 10^{13} - 10^{15} \text{ cm}^{-3}$  and energies  $\gamma_0 \sim 10^2 - 10^4$ , the temperature threshold would vary in the range of  $T_{th} \sim (10^{-5} - 10^{-2}) \text{ K}$ , which is much lower than the typical temperatures of the beams employed in the high-energy accelerators. Therefore, for the typical electron/positron beams that are employed in the high-energy accelerators (conventional as well as non-conventional), we can ignore the collective quantum nature (overlapping of the wave functions) of the particles and take into account only the individual quantum nature, i.e., the uncertainty principle and the spin. This can be effectively possible by choosing the above typical ranges of densities and energies in such a way that we may choose the temperatures in the range:  $10^{-2} \ll T \ll 10^4 \text{ K}$ . The above assumptions (i.e., to take into account the spin and the uncertainty relation of each particles, but disregarding the overlapping of the particle wave functions) were sufficient to describe the transverse beam dynamics by correcting the paraxial geometric electron optics with the paraxial wave electron optics, given in terms of a single-particle wave function in the presence of external electromagnetic fields (i.e., no self-consistent collective effects due to the electromagnetic interaction was taken into account) [79,81]. This will suffice also to describe the quantum particle beam behavior in the presence of classical collective effects (f.i., the PWF excitation) that are typically leading to the formation of coherent structures. This aspect is very important because it shows that the individual quantum nature of the particles can be exhibited at the macroscopic level if it is suitably coupled with a macroscopic collective effect such as in Sokolov-Ternov effect [82–85], quantum excitation [86–88], quantum FEL [89–91], etc.

Thus, to write the appropriate Schrödinger equation for a single particle of the beam, that includes also the spin, Eq. (3.2.3) can be quantized using the appropriate correspondence rules as:  $\mathcal{H} \rightarrow \hat{\mathcal{H}} = i\epsilon_c \partial / \partial \xi$ ,  $\mathcal{P}_\perp \rightarrow \hat{\mathcal{P}}_\perp = -i\epsilon_c \nabla_\perp$ . Note that, here, the Hamiltonian operator  $\hat{\mathcal{H}}$  includes also the potential energy operator  $\hat{U}_M = -\hat{\mu}_s \cdot \mathbf{B}_0 / m_0 \gamma_0 c^2$  associated with the interaction between the intrinsic magnetic moment of spin and the magnetic field. Here  $\hat{\mu}_s = q\epsilon_c \hat{s}$ , where  $\hat{s}$  is the electron/positron spin operator. Therefore,  $\hat{U}_M = \hat{U}_M(\hat{s}_z)$ , where  $\hat{s}_z$  is the projection of  $\hat{s}$  along  $z$ . Since the spin of an elementary particle is a purely quantum property, there is no classical

term in the classical Hamiltonian (3.2.3) that corresponds to  $\hat{U}_M$ . In fact, the *quantized Hamiltonian* (Hamiltonian operator) has the form:

$$\hat{\mathcal{H}} = \frac{1}{2}\hat{\mathcal{P}}_{\perp}^2 + \frac{1}{2}k_c\hat{z} \cdot (\mathbf{r}_{\perp} \times \hat{\mathcal{P}}_{\perp}) + U_w(\mathbf{r}_{\perp}, \xi) + \frac{1}{2}Kr_{\perp}^2 + \hat{U}_M(\hat{s}_z). \quad (3.2.7)$$

Note that in eq. (3.2.7) the term  $U_w(\mathbf{r}_{\perp}, \xi) + Kr_{\perp}^2/2$  plays the role of a multiplication operator. On the basis of these considerations, it is easy to see that the application of the *Hartree's mean field procedure* [71] allows us to reduce our description to finding a *single-particle spinor*  $\vec{\Psi} = (\Psi_s)$ , whose spatio-temporal evolution is governed by the following two-dimensional Schrödinger equations

$$i\epsilon_c \frac{\partial \vec{\Psi}}{\partial \xi} = -\frac{\epsilon_c^2}{2} \nabla_{\perp}^2 \vec{\Psi} - \frac{i\epsilon_c k_c}{2} \hat{z} \cdot (\mathbf{r}_{\perp} \times \nabla_{\perp}) \vec{\Psi} + U_w \vec{\Psi} + \frac{1}{2} Kr_{\perp}^2 \vec{\Psi} + \epsilon_c k_c \hat{s}_z \cdot \vec{\Psi}, \quad (3.2.8)$$

where  $s$  is ranging in the set  $\{-1/2, 1/2\}$  of eigenvalues of  $\hat{s}_z$  corresponding to the “spin down” and “spin up” states, respectively. Consequently, Eq. (3.2.8) can be decomposed into two scalar equations, one for  $\Psi_{-1/2}$  and another one for  $\Psi_{1/2}$ , respectively, viz.,

$$i\epsilon_c \frac{\partial \Psi_{-1/2}}{\partial \xi} = -\frac{\epsilon_c^2}{2} \nabla_{\perp}^2 \Psi_{-1/2} - \frac{i\epsilon_c k_c}{2} \hat{z} \cdot (\mathbf{r}_{\perp} \times \nabla_{\perp}) \Psi_{-1/2} + U_w \Psi_{-1/2} + \frac{1}{2} Kr_{\perp}^2 \Psi_{-1/2} + \epsilon_c k_c \hat{s}_z \Psi_{-1/2}, \quad (3.2.9)$$

$$i\epsilon_c \frac{\partial \Psi_{1/2}}{\partial \xi} = -\frac{\epsilon_c^2}{2} \nabla_{\perp}^2 \Psi_{1/2} - \frac{i\epsilon_c k_c}{2} \hat{z} \cdot (\mathbf{r}_{\perp} \times \nabla_{\perp}) \Psi_{1/2} + U_w \Psi_{1/2} + \frac{1}{2} Kr_{\perp}^2 \Psi_{1/2} + \epsilon_c k_c \hat{s}_z \cdot \Psi_{1/2}. \quad (3.2.10)$$

Since the beam is composed of only two kinds of electrons, according to the Hartree's approach [71], the beam density is given by  $\rho_b(\mathbf{r}_{\perp}, \xi) = (N/2\sigma_z)|\vec{\Psi}|^2 = (N/2\sigma_z)(|\Psi_{-1/2}|^2 + |\Psi_{1/2}|^2)$ , where we have assumed that statistically the beam population is equipartite into “down” and “up” spin states and  $\sigma_z$  is the beam length. Here, we assumed that each  $\Psi_s$  is normalized.

In cylindrical coordinates, the above Eqs. (3.2.9) and (3.2.10) can be reduced to the following one

$$i\epsilon_c \frac{\partial \Psi_s}{\partial \xi} = -\frac{\epsilon_c^2}{2} \frac{1}{r_{\perp}} \frac{\partial}{\partial r_{\perp}} \left( r_{\perp} \frac{\partial \Psi_s}{\partial r_{\perp}} \right) - \frac{\epsilon_c^2}{2} \frac{1}{r_{\perp}^2} \frac{\partial^2 \Psi_s}{\partial \varphi^2} - \frac{i\epsilon_c k_c}{2} \frac{\partial \Psi_s}{\partial \varphi} + \left( U_w [|\Psi_{-1/2}|^2] + U_w [|\Psi_{1/2}|^2] \right) \Psi_s + \frac{1}{2} Kr_{\perp}^2 \Psi_s + \epsilon_c k_c \hat{s}_z \Psi_s, \quad (3.2.11)$$

where  $s = -1/2, 1/2$  [corresponding to Eqs. (3.2.9) and (3.2.10), respectively].

### 3.3 The self-consistent system

The ‘‘quantum-like’’ and ‘‘quantum’’ approach that have been presented in the previous sections to describe the beam dynamics, can be given a unified description seeking proper solutions for the BWF. In the case of the solutions of Eq. (3.2.5) with the form  $\Psi(r_\perp, \xi, \varphi) = \psi_m(r_\perp, \xi) \exp\{i[m(\varphi - k_c/2)\xi]\}$ , where  $m$  is integer,  $U_w[|\psi_m|^2]$  becomes cylindrically symmetric. Then the system can be cast in the following form

$$i\epsilon_t \frac{\partial \psi_m}{\partial \xi} = -\frac{\epsilon_t^2}{2} \frac{1}{r_\perp} \frac{\partial}{\partial r_\perp} \left( r_\perp \frac{\partial \psi_m}{\partial r_\perp} \right) + U_w[|\psi_m|^2] \psi_m + \left( \frac{1}{2} K r_\perp^2 + \frac{m^2 \epsilon_t^2}{2 r_\perp^2} \right) \psi_m, \quad (3.3.1)$$

Similarly, for solutions of the form  $\Psi_s(r_\perp, \xi, \varphi) = \psi_m(r_\perp, \xi) \exp\{i[m\varphi - (k_c/2)(m+2s)\xi]\}$ ,  $U_w[|\psi_m|^2]$  becomes cylindrically symmetric and the system Eq. (3.2.11) can be cast in the following spin-independent form

$$i\epsilon_c \frac{\partial \psi_m}{\partial \xi} = -\frac{\epsilon_c^2}{2} \frac{1}{r_\perp} \frac{\partial}{\partial r_\perp} \left( r_\perp \frac{\partial \psi_m}{\partial r_\perp} \right) + U_w[|\psi_m|^2] \psi_m + \left( \frac{1}{2} K r_\perp^2 + \frac{m^2 \epsilon_c^2}{2 r_\perp^2} \right) \psi_m, \quad (3.3.2)$$

Equations (3.3.1) and (3.3.2) have the same structure thus coinciding the quantum-like and quantum approach. Consequently for both the approaches,  $\rho_b$  also becomes proportional to  $|\psi_m|^2$ , viz.,  $\rho_b(\mathbf{r}_\perp, \xi) = (N/2\sigma_z)|\psi_m|^2$ . Therefore self-consistent beam-plasma interaction that accounts for the PWF excitations and the paraxial beam diffraction (for both thermal and quantum regimes) is governed by the system of equations (3.3.1) or (3.3.2) coupled with Eq. (3.1.20). Once the above expression for  $\rho_b$  is substituted in Eq. (3.1.20), we obtain the self-consistent coupled system as

$$i\epsilon \frac{\partial \psi_m}{\partial \xi} = -\frac{\epsilon^2}{2} \frac{1}{r_\perp} \frac{\partial}{\partial r_\perp} \left( r_\perp \frac{\partial \psi_m}{\partial r_\perp} \right) + U_w[|\psi_m|^2] \psi_m + \left( \frac{1}{2} K r_\perp^2 + \frac{m^2 \epsilon^2}{2 r_\perp^2} \right) \psi_m, \quad (3.3.3)$$

$$\frac{1}{r_\perp} \frac{\partial}{\partial r_\perp} \left( r_\perp \frac{\partial U_w}{\partial r_\perp} \right) - \frac{k_{pe}^4}{k_{uh}^2} U_w = \frac{k_{pe}^4}{k_{uh}^2} \frac{N}{n_0 \gamma_0 \sigma_z} |\psi_m|^2, \quad (3.3.4)$$

where, for the convenience of further analytical and numerical analysis, in Eq. (3.3.3), we use  $\epsilon$  instead of  $\epsilon_t$  and  $\epsilon_c$  of Eq. (3.3.1) and (3.3.2), respectively. This is the pair of governing equations that we are going to solve, both in linear and nonlinear regimes, in order to show the existence of nonlocal coherent structures associated with the vortex states of the beam.

### 3.4 Envelope description of the beam

In this section, we implement the above description given by Eqs. (3.3.3) and (3.3.4) along with the envelope description that is provided by the virial equations (for details,

see Appendix D). Let us assume, for simplicity, that  $\psi_m$  is normalized and introduce the quantum average of the generic operator  $\hat{f}(\mathbf{r}_\perp, \xi)$  as

$$\langle \hat{f} \rangle_m = \int_0^\infty \psi_m^*(r_\perp, \xi) \hat{f}(\mathbf{r}_\perp, \xi) \psi_m(r_\perp, \xi) d^2 r_\perp. \quad (3.4.1)$$

Then, we assume that  $\langle r_\perp \rangle_m = 0$  and introduce the effective beam spot size  $\sigma_m(\xi)$  and the total energy  $\mathcal{E}_m(\xi)$  as

$$\sigma_m(\xi) = [\langle r_\perp^2 \rangle_m]^{1/2} = \left[ \int_0^\infty \psi_m^* r_\perp^2 \psi_m d^2 r_\perp \right]^{1/2}, \quad (3.4.2)$$

$$\mathcal{E}_m(\xi) = \left\langle i\epsilon \frac{\partial}{\partial \xi} \right\rangle_m = i\epsilon \int_0^\infty \psi_m^* \frac{\partial \psi_m}{\partial \xi} d^2 r_\perp. \quad (3.4.3)$$

Taking the second order derivative, with respect to  $\xi$ , of  $\sigma_m^2(\xi)$  and the first order derivative of  $\mathcal{E}_m(\xi)$  and, using Eq. (3.3.3), we get the following pair of equations, viz.,

$$\frac{d^2 \sigma_m^2}{d\xi^2} = 4\mathcal{E}_m - 4\langle U_w \rangle_m - 4K\sigma_m^2 - 2\langle \mathbf{r}_\perp \cdot \nabla_\perp U_w \rangle_m. \quad (3.4.4)$$

$$\frac{d\mathcal{E}_m}{d\xi} = \int |\psi_m|^2 \frac{\partial U_w}{\partial \xi} d^2 r_\perp. \quad (3.4.5)$$

Note that, once the governing pair of equations (3.3.3) and (3.3.4) is solved, the envelope description is provided by Eqs. (3.4.4) and (3.4.5). Additionally, note also that the quantity  $4[\mathcal{E}_m - \langle U_w \rangle_m]$  is equal to four times the average kinetic energy  $\mathcal{T}$  associated with Eq. (3.3.3), viz.,

$$\mathcal{T} = 2\pi \int_0^\infty \frac{\epsilon^2}{2} \left[ \left| \frac{\partial \psi_m}{\partial r_\perp} \right|^2 + \frac{m^2}{r_\perp^2} |\psi_m|^2 \right] r_\perp dr_\perp,$$

which, when  $m \neq 0$ , accounts for the *centrifugal potential* term, viz.,  $m^2/2r_\perp^2$ , due to the orbital angular momentum.

### 3.5 Linear regime

In this section, we describe the beam behavior in the limiting case of negligible collective effects. Then, the effects of the plasma is supposed to be so small that we have to solve Eq. (3.3.3) for  $U_w \approx 0$ , yielding the following linear Schrödinger equation

$$i\epsilon \frac{\partial \psi_m}{\partial \xi} = -\frac{\epsilon^2}{2} \frac{1}{r_\perp} \frac{\partial}{\partial r_\perp} \left( r_\perp \frac{\partial \psi_m}{\partial r_\perp} \right) + \left( \frac{1}{2} K r_\perp^2 + \frac{m^2 \epsilon^2}{2 r_\perp^2} \right) \psi_m. \quad (3.5.1)$$

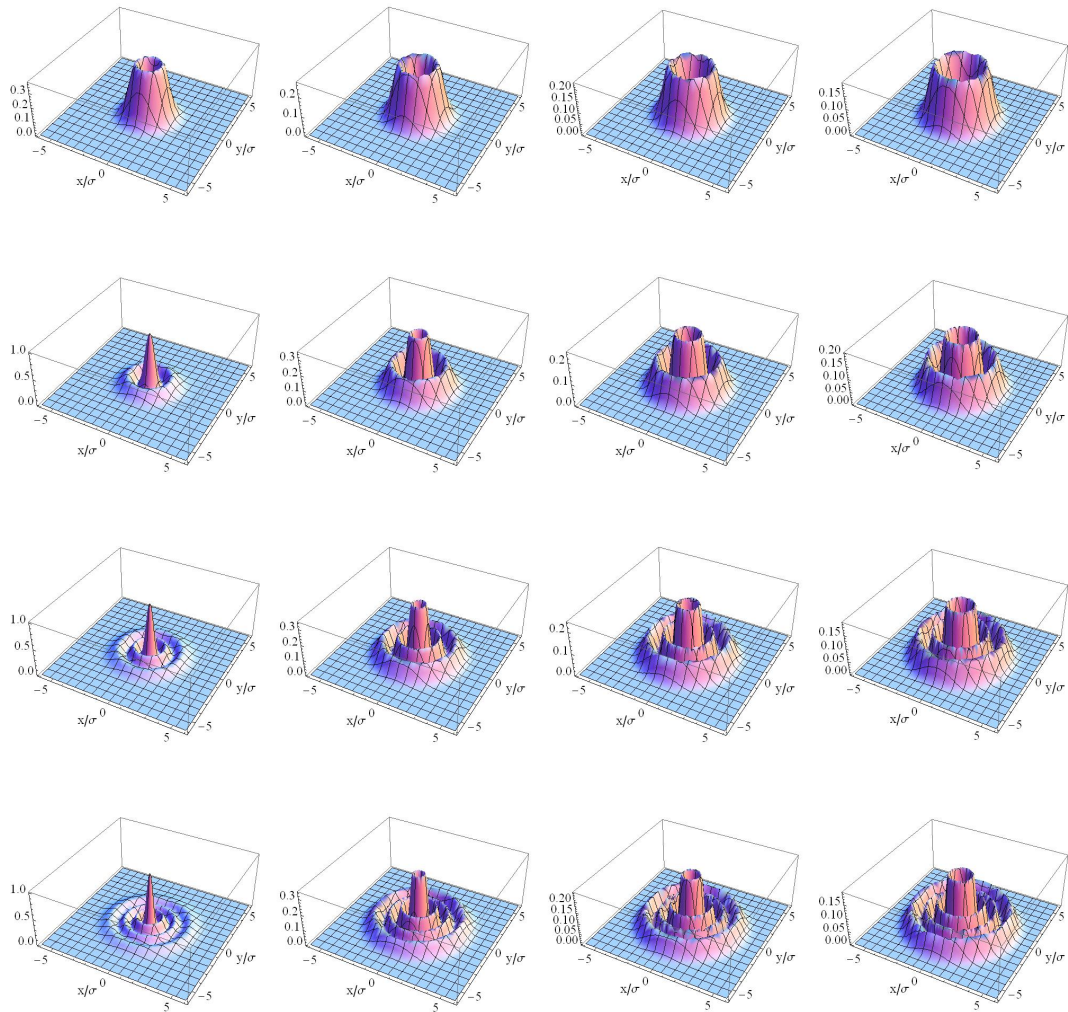


Figure 3.1:  $|\psi_{p,m}|^2$  as a function of  $x/\sigma$  and  $y/\sigma$  for several combinations of  $p$  and  $m$  ( $p, m = 0, 1, 2, 3$ ). Note that, for a given  $m$ , the number of the “lateral” maxima increases as  $p$  increases. For a given  $p$ , the peaks corresponding to  $m \neq 0$  are shifted with respect to those with  $m = 0$ ; the shift increases as  $m$  increases.

It can be shown that the complete set of normalized solutions for Eq. (3.5.1) is

$$\psi_{m,p}(r_{\perp}, \xi) = \sqrt{\frac{1}{\pi\sigma^2} \frac{p!}{(p+m)!}} \exp\left(-\frac{r_{\perp}^2}{2\sigma^2} + \frac{ir_{\perp}^2}{2\epsilon\rho} + i\phi_{m,p}\right) \left(\frac{r_{\perp}}{\sigma}\right)^m L_p^m\left(\frac{r_{\perp}^2}{\sigma^2}\right), \quad (3.5.2)$$

where  $m$  and  $p$  are positive integers,  $\sigma = \sigma(\xi)$ ,  $\rho = \rho(\xi)$  is the curvature radius, and  $\phi_{m,p} = \phi_{m,p}(\xi)$  satisfy the following differential equations

$$\frac{1}{\rho} = \frac{1}{\sigma} \frac{d\sigma}{d\xi}, \quad (3.5.3)$$

$$-\frac{\sigma^2}{2\epsilon} \frac{d\phi_{m,p}}{d\xi} = p + \frac{1}{2} + \frac{m}{2}, \quad (3.5.4)$$

$$\frac{d^2\sigma}{d\xi^2} + K\sigma - \frac{\epsilon^2}{\sigma^3} = 0. \quad (3.5.5)$$

Furthermore, using the solutions of Eq. (3.5.2) in Eqs. (3.4.4) and (3.4.5), we immediately get

$$\frac{d^2\sigma_{m,p}^2}{d\xi^2} + 4K\sigma_{m,p}^2 = 4\mathcal{E}_{m,p}, \quad (3.5.6)$$

$$\frac{d\mathcal{E}_{m,p}}{d\xi} = 0, \quad (3.5.7)$$

where

$$\sigma_{m,p}(\xi) \equiv \left[\langle r_{\perp}^2 \rangle_{m,p}\right]^{1/2} = (2p + m + 1)^{1/2} \sigma(\xi). \quad (3.5.8)$$

From Eq. (3.5.7) it results that  $\mathcal{E}_{m,p}$  is a constant of motion. Thus, for the initial conditions  $\sigma_{m,p}(0) = (2p + m + 1)^{1/2} \sigma(0) \equiv (2p + m + 1)^{1/2} \sigma_0$  and  $\sigma'_{m,p}(0) = (2p + m + 1)^{1/2} \sigma'(0) \equiv (2p + m + 1)^{1/2} \sigma'_0$  (where the primes denote the differentiation with respect to  $\xi$ ), we have

$$\mathcal{E}_{m,p} = \frac{\sigma_0'^2}{2} + \frac{\epsilon^2}{2\sigma_0^2} + \frac{1}{2}K\sigma_0^2 + \frac{(2p+m)}{(2p+m+1)} \frac{\epsilon^2}{2\sigma_0^2} \equiv \mathcal{E}_{0,0} + \frac{(2p+m)}{(2p+m+1)} \frac{\epsilon^2}{2\sigma_0^2}, \quad (3.5.9)$$

where

$$\mathcal{E}_{0,0} = \frac{\sigma_0'^2}{2} + \frac{\epsilon^2}{2\sigma_0^2} + \frac{1}{2}K\sigma_0^2.$$

It is worth to observe that, substituting Eq. (3.5.8) into (3.5.6), we easily reobtain the Ermakov-Pinney equation (3.5.5). Using the above initial conditions for  $\sigma$  and  $\sigma'$ , Eq. (3.5.5) is solved as

$$\sigma(\xi) = \sqrt{a + b \cos(2\sqrt{K}\xi) + c \sin(2\sqrt{K}\xi)}, \quad (3.5.10)$$

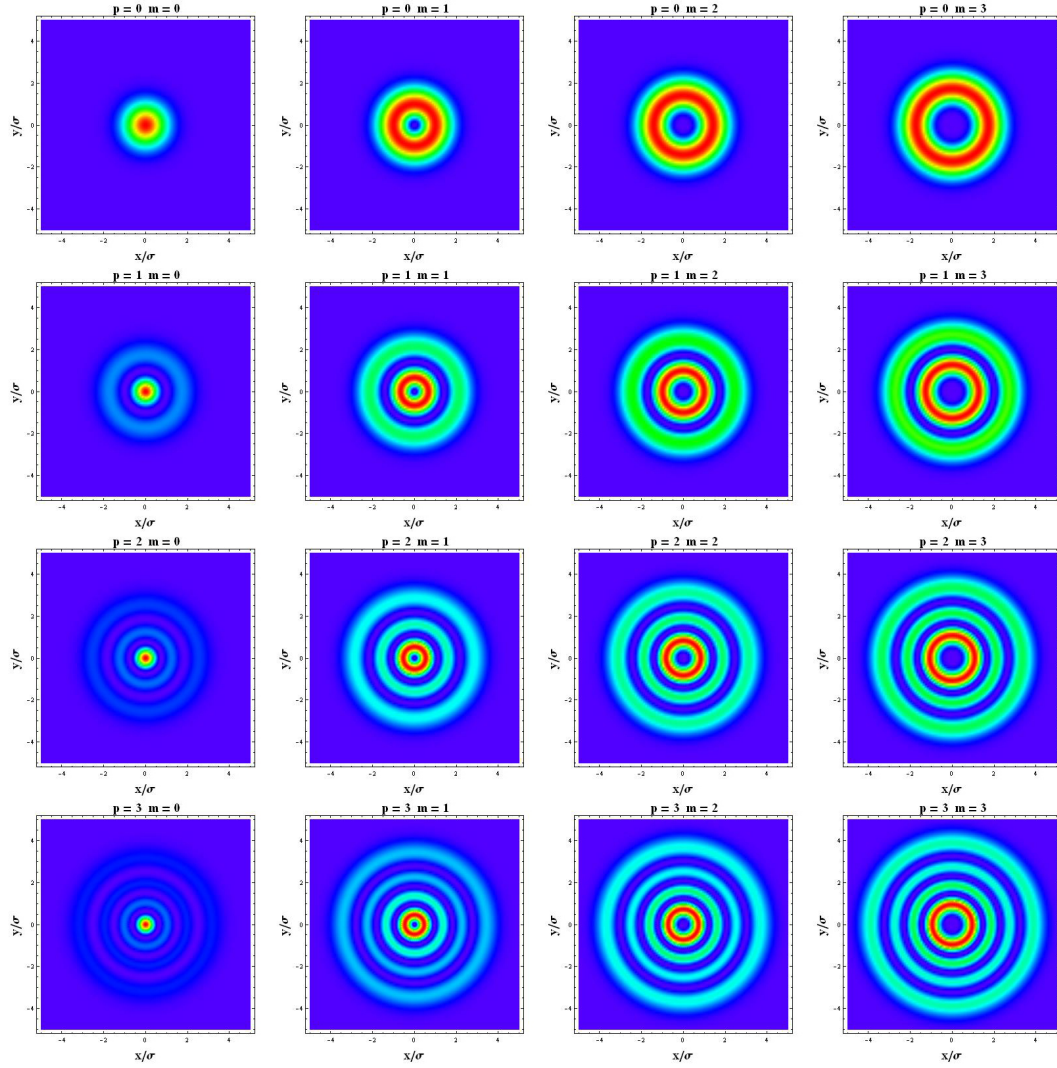


Figure 3.2: Density plot for  $|\psi_{p,m}|^2$  in the transverse  $x - y$  plane normalized by  $\sigma$ . The combinations of  $p$  and  $m$  are the same as Figure 3.1. Note that, for given  $m$ , the number of rings increases as  $p$  (number of "lateral" maxima in Figure 3.1 increases). In particular, when  $m = 0$ , the structure of the density plots is always constituted by a central core plus  $p$  rings. When  $m \neq 0$ , due to the shift of the peaks (see Figure 1), the density plots appear without core (hollow beam corresponding to Figure 1). For the given value of  $p$ , the ring radii increase as  $m$  increases.

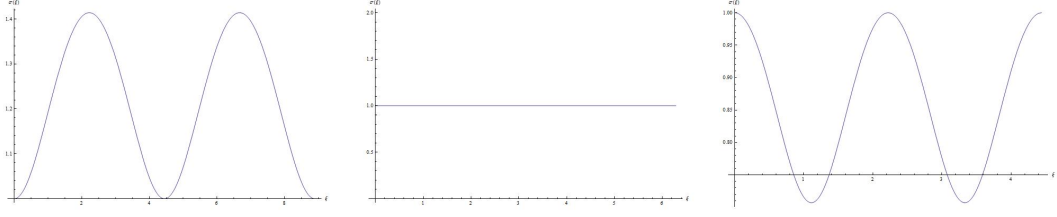


Figure 3.3:  $\sigma$ , as the function of  $\xi$ , for three different values of  $K_b$ . Left plot:  $K_b = 0.5$  ( $\sigma_0 < \mathcal{E}_{0,0}/K$ ); middle plot:  $K_b = 1.0$  ( $\sigma_0 = \mathcal{E}_{0,0}/K$ ); right plot:  $K_b = 2.0$  ( $\sigma_0 > \mathcal{E}_{0,0}/K$ ). The plots account for the periodic transverse breathing of the beam that is not visible in Figures 3.1 and 3.2, due to the use of the normalized variables  $x/\sigma$  and  $y/\sigma$ .

where  $a = \mathcal{E}_{00}/K$ ,  $b = \sigma_0^2 - \mathcal{E}_{00}/K$ , and  $c = \sigma_0 \sigma'_0 / \sqrt{K}$ . Consequently, Eqs. (3.5.3) and (3.5.4) have the following solutions

$$\rho(\xi) = \frac{1}{\sqrt{K}} \frac{a + b \cos(2\sqrt{K}\xi) + c \sin(2\sqrt{K}\xi)}{c \cos(2\sqrt{K}\xi) - b \sin(2\sqrt{K}\xi)}, \quad (3.5.11)$$

$$\phi = \phi_{m,p}(\xi) = -(2p + m + 1) \arctan \left[ \left( \frac{\sigma_0^2}{\epsilon \sqrt{K} \rho_0^2} + \frac{\epsilon}{\sqrt{K} \sigma_0^2} \right) \tan(\sqrt{K}\xi) + \frac{\sigma_0^2}{\epsilon \rho_0} \right] \quad (3.5.12)$$

where  $\rho_0 \equiv \rho(0) = \sigma_0/\sigma'_0$ . If the region in which the magnetic field is present is sufficiently long, Eq. (3.5.8) describes a transverse *sausage-like* beam modulation along the propagation direction (betatron oscillations). The assumption that the individual wave functions do not overlap, imposes a constraint for the range of the values of  $\sigma$ . The present description is valid only if the values of the waist of the sausage shape are sufficiently far from  $\lambda_T$ . Then, it is clear that this condition can be satisfied if the focusing effects provided by  $K$  is suitably moderate.

Figure 3.1 represents the 3D representation of  $|\psi_{p,m}|^2$  given by Eq. (3.5.2) as the function of the normalized transverse coordinates  $x/\sigma$  and  $y/\sigma$  for several combinations of  $p$  and  $m$  ( $p, m = 0, 1, 2, 3$ ). The 3D plots exhibit a central structure surrounded by  $p$  circular ripples. This structure is a Gaussian beam for  $m = 0$  and a hollow beam for  $m \neq 0$ . Furthermore, for a given value of  $p$ , the radii of the central structure and of the ripples increase as  $m$  increases.

Figure 3.2 displays the probability density plot corresponding to the solution given by Eq. (3.5.2) in the normalized transverse plane  $x/\sigma - y/\sigma$ . For  $m = 0$ , the structure of the plots shows a core at the origin ( $x = y = 0$ ) and  $p$  rings. When  $m \neq 0$ , there is no core at the origin (hollow beam). For the given value of  $p$ , the ring radii increase as  $m$  increases. All structures related to  $m \neq 0$  describe the vortex states associated with the given eigenvalues of the orbital angular momentum. Remarkably,  $m$  plays the role of vortex charge. They describe the vortices in terms of the probability density

associated with the corresponding states, viz.,  $|\psi_m(r_\perp, \xi)|^2$ . In addition, the counterpart of these effects is exhibited by the phase factor viz.,  $\exp\{i[m\varphi - (k_c/2)(m+2s)\xi]\}$ . Note that the helicity character of the phase is associated not only with the orbital angular momentum but also with the spin angular momentum.

It should be noted that the probability density structures displayed in Figures 3.1 and 3.2 appear stationary because they are represented in the normalized plane  $x/\sigma - y/\sigma$ . However, according to the temporal dependence of  $\sigma$  given by Eq. (3.5.10), the Gaussian/hollow beam as well as the ripples experience the time-modulation (or breathing) of their radii, if we represent their profiles as a function of the non-normalized spatial variables  $x, y$ . In fact, Figure 3.3 displays  $\sigma$  as the function of  $\xi$ . Here, the quantities have been normalized as:  $\sigma \rightarrow \sigma/\sigma_0$ ,  $\xi \rightarrow \xi\epsilon/\sigma_0^2$  and  $K \rightarrow K_b \equiv K\sigma_0^4/\epsilon$ . The plots are displayed for  $K_b = 0.5, 1.0, 2.0$ , respectively (from left to right). We have chosen the initial condition for  $\sigma'_0 = 0$  (here the normalized initial  $\sigma$  is automatically fixed to 1). The plot on the left-hand side corresponds to the initial value  $\sigma_0 < \mathcal{E}_{0,0}/K$ ; the middle plot corresponds to the equilibrium condition in which the diffraction is balanced by the restoring force due to the external magnetic field ( $\sigma_0 = \mathcal{E}_{0,0}/K$ ); and the plot on the right-hand side corresponds to the initial condition  $\sigma_0 > \mathcal{E}_{0,0}/K$ .

## 3.6 Nonlinear regime

In this section, we describe the beam behavior taking into account collective effects via PWF excitations. Three different nonlinear regimes of this analysis are considered:

- (i) *Strictly local regime*, where, roughly, the beam spot size is much greater than the plasma wavelength corresponding to  $\nabla_\perp^2 U_w \ll (k_{pe}^4/k_{uh}^2) U_w$ .
- (ii) *Moderately nonlocal regime*, where, roughly, the beam spot size is comparable to the plasma wavelength corresponding to  $\nabla_\perp^2 U_w \sim (k_{pe}^4/k_{uh}^2) U_w$ .
- (iii) *Strongly nonlocal regime*, where, roughly, the beam spot size is much smaller than the plasma wavelength corresponding to  $\nabla_\perp^2 U_w \gg (k_{pe}^4/k_{uh}^2) U_w$ .

### 3.6.1 Strictly local regime

In this section, we assume that the relation between the wake potential and the beam density is *strictly local*. This is obtained by assuming in Eq. (3.3.4) that the beam spot size is roughly much greater than the plasma wavelength viz.,  $\nabla_\perp^2 U_w \ll (k_{pe}^4/k_{uh}^2) U_w$ . Then, we have

$$U_w = -\frac{N}{\sigma_z n_0 \gamma_0} |\psi_m|^2. \quad (3.6.1)$$

Consequently, Eq. (3.3.3) becomes

$$i\epsilon \frac{\partial \psi_m}{\partial \xi} = -\frac{\epsilon^2}{2} \frac{1}{r_\perp} \frac{\partial}{\partial r_\perp} \left( r_\perp \frac{\partial \psi_m}{\partial r_\perp} \right) - \frac{N}{\sigma_z n_0 \gamma_0} |\psi_m|^2 \psi_m + \left( \frac{1}{2} K r_\perp^2 + \frac{m^2 \epsilon^2}{2 r_\perp^2} \right) \psi_m. \quad (3.6.2)$$

Equation (3.6.2) is a 2D cubic nonlinear Schrödinger equation in the form of the 2D Gross-Pitaevskii equation (GPE) for a Bose Einstein condensate [92, 93] in the presence of the cylindrically symmetric external potential well  $(K r_\perp^2 + m^2 \epsilon^2 / r_\perp^2) / 2$ . Substituting Eq. (3.6.1) in Eqs. (3.4.4) and (3.4.5), we easily get the following pair of equations

$$\frac{d^2 \sigma_m^2}{d\xi^2} + 4K \sigma_m^2 = 4\mathcal{A}_m, \quad (3.6.3)$$

$$\frac{d\mathcal{A}_m}{d\xi} = 0, \quad (3.6.4)$$

where

$$\mathcal{A}_m = 2\pi \int \frac{\epsilon^2}{2} \left[ \left| \frac{\partial \psi_m}{\partial r_\perp} \right|^2 + \frac{m^2}{r_\perp^2} |\psi_m|^2 \right] r_\perp dr_\perp - \frac{N}{2\sigma_z n_0 \gamma_0} 2\pi \int |\psi_m|^4 r_\perp dr_\perp + \frac{1}{2} K \sigma_m^2. \quad (3.6.5)$$

Consequently,  $\mathcal{A}_m$  is the new constant of motion that plays the same role as the conserved energy  $\mathcal{E}_m$  in the linear case. Note that, although we are in the nonlinear case, the envelope equation (3.6.3) is a linear equation of a harmonic oscillator in  $\sigma_m^2$ , as it has been the case in the linear limit. The only difference here is that the constant of motion  $\mathcal{A}_m$  replaces the total averaged energy  $\mathcal{E}_{m,p}$ , which is a conserved quantity in the linear case. The main new feature comes from the possibility that  $\mathcal{A}_m$  takes negative values, whilst, in the linear case,  $\mathcal{E}_{m,p}$  is positive definite. Moreover, provided that  $\mathcal{E}_{m,p}$  is replaced by  $\mathcal{A}_m$ , the analytical solution of Eq. (3.6.3) is formally identical to the one of the linear case, viz.,

$$\sigma_m(\xi) = \sqrt{\frac{\mathcal{A}_m}{K} + \left( \sigma_{0m}^2 - \frac{\mathcal{A}_m}{K} \right) \cos(2\sqrt{K}\xi) + \frac{\sigma_{0m}\sigma'_{0m}}{\sqrt{K}} \sin(2\sqrt{K}\xi)}, \quad (3.6.6)$$

where  $\sigma_{0m}$  and  $\sigma'_{0m}$  are the initial condition for  $\sigma_m(\xi)$  and  $\sigma'_m(\xi)$ , respectively. Finally, we observe that, from Eq. (3.6.3) or from the above solution, the matching condition corresponding to the self-equilibrium state of the beam is  $\sigma_m = \sigma_m^{eq}$  is:  $K (\sigma_m^{eq})^2 = \mathcal{A}_m$ .

Equation (3.6.2) has been solved numerically, assuming a beam with the initial wave function of the form

$$\psi_m(r_\perp, 0) = \frac{1}{\sqrt{\pi m! \sigma_0^2}} \left( \frac{r_\perp}{\sigma_0} \right)^m \exp\left(-\frac{r_\perp^2}{2\sigma_0^2}\right).$$

It is easy to see that such initial condition fixes automatically  $\langle r_\perp^2 \rangle_m(\xi = 0) \equiv \sigma_{0m} = (m+1)\sigma_0$  and  $\langle r_\perp^2 \rangle'_m(\xi = 0) \equiv \sigma'_{0m} = (m+1)\sigma'_0 = 0$ . In order to present the numerical results, we conveniently introduce the following dimensionless quantities:

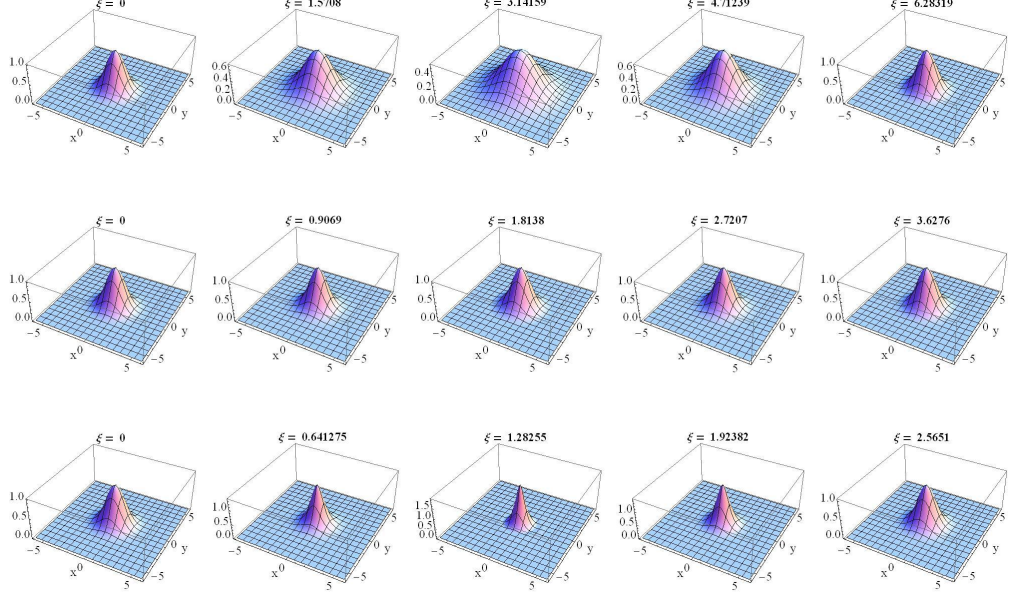


Figure 3.4: 3D plots of  $|\psi_m|^2$  as the function of  $x/\sigma$  and  $y/\sigma$  for different values of the dimensionless time  $\xi$  for  $m = 0$ :  $K_b = 0.25$ ;  $\delta = 0.5$ ;  $\tilde{\mathcal{A}}_m = 0.5$  (first row);  $K_b = 0.5$ ;  $\delta = 1.0$ ;  $\tilde{\mathcal{A}}_m = 0.5$  (second row);  $K_b = 1.0$ ;  $\delta = 1.3$ ;  $\tilde{\mathcal{A}}_m = 0.675$  (third row).

$\xi \rightarrow \xi/\beta_0$ ,  $r_\perp \rightarrow r_\perp/\sigma_0$ ,  $\psi_m(r_\perp, \xi) \rightarrow \sqrt{\pi m! \sigma_0^2} \psi_m(r_\perp, \xi)$ ,  $\sigma_m \rightarrow \sqrt{m!} \sigma_m/\sigma_0$  and  $\tilde{\mathcal{A}}_m \rightarrow (m! \sigma_0^2/\epsilon^2) \mathcal{A}_m = (m+1)! 2(1+K_b) - (\delta/m!) (2m)! 2^{-2(m+1)}$ , where  $\beta_0 = \sigma_0^2/\epsilon$ ,  $K_b = K\sigma_0^4/\epsilon^2$  and  $\delta = n_b\sigma_0^2/n_0\gamma_0\epsilon^2$ .

The spatio-temporal evolution of  $|\psi_m|^2$  has been investigated for different values of  $m$ ,  $K_b$  and  $\delta$ , at  $\xi = 0, 0.25T, 0.5T, 0.75T, T$ , where  $T = \pi/\sqrt{K_b}$  is the time period. For  $m = 0$ ,  $m = 1$ , and  $m = 2$ , when the matching condition of the envelope equation is satisfied, the profile is practically unchanged (see the second row of Figures 3.4 - 3.6, respectively). This predicts the existence of nonlinear coherent states (sometimes called 2D solitons). Due to the interplay between the strong transverse effects of the plasma wake field (collective and nonlinear effects) and the external magnetic field, envelope oscillations with weak and relatively strong focusing and defocusing have been observed for  $m = 0$ ,  $m = 1$ , and  $m = 2$  (see the first and the third row of Figures 3.4 - 3.6, respectively). Those oscillations are in full agreement with the analytical solution (3.6.6) of the envelope equation (3.6.3) for the above initial conditions.

The parameter ranges used for our numerical investigation are such that  $\mathcal{A}_m$  is

always positive. This choice has been taken to avoid the instability conditions due to the collapse. In fact, for the family of cubic nonlinear Schrödinger equations given by Eq. (3.6.2), it results that [see Eq. (3.6.3)] the beam would always be unstable for  $\mathcal{A}_m < 0$  or  $0 < \mathcal{A}_m < (\sigma_0'^2 + K\sigma_0^2)/2$ , approaching the collapse. Conversely, the beam is stable when  $0 < (\sigma_0'^2 + K\sigma_0^2)/2 < \mathcal{A}_m$ . However, one should be cautious in the study of the unstable regime, because our assumptions of the strictly local regime and of the absence of overlapping of the wave functions are violated when the collapse takes place. Finally, Figures 3.4 - 3.6 show the beam structures similar to those

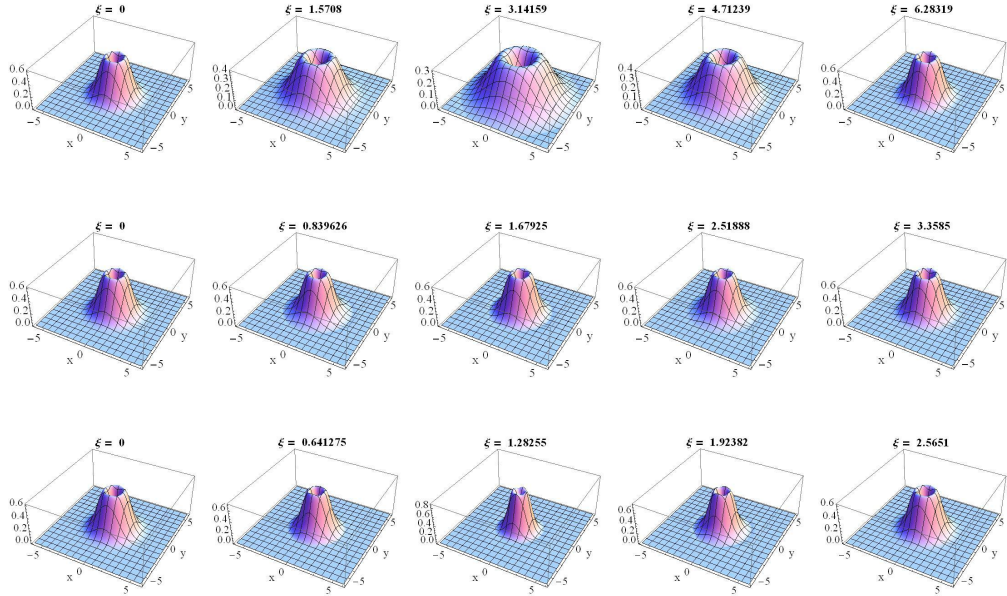


Figure 3.5: 3D plots of  $|\psi_m|^2$  as the function of  $x/\sigma$  and  $y/\sigma$  for different values of the dimensionless time  $\xi$  for  $m = 1$ :  $K_b = 0.25$ ;  $\delta = 0.25$ ;  $\tilde{\mathcal{A}}_m = 1.21875$  (first row);  $K_b = 0.9375$ ;  $\delta = 0.5$ ;  $\tilde{\mathcal{A}}_m = 1.875$  (second row);  $K_b = 1.7$ ;  $\delta = 1.5$ ;  $\tilde{\mathcal{A}}_m = 2.5125$  (third row).

found in the linear case (Figures 3.1 and 3.2, especially for  $p = 0$ ) with a central Gaussian-like core for  $m = 0$  (Figure 3.4) and a hollow structure for  $m \neq 0$  (Figures 3.5 and 3.6), that would appear as ring structures in the density plot. Consequently, the beam structures for non zero vortex charge ( $m \neq 0$ ) are physically related to the orbital angular momentum and they can be associated with nonlinear vortex states. We emphasize here that such vortex effects due to the angular momentum, as in the linear case, are present also in the phase, which accounts also for the spin (not displayed in

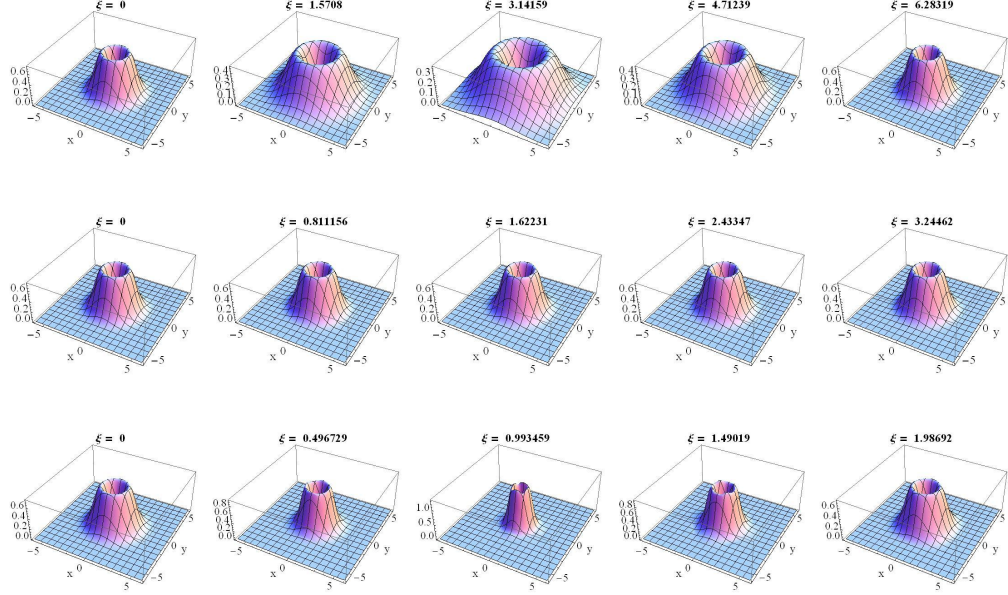


Figure 3.6: 3D plots of  $|\psi_m|^2$  as the function of  $x/\sigma$  and  $y/\sigma$  for different values of the dimensionless time  $\xi$  for  $m = 2$ :  $K_b = 0.25$ ;  $\delta = 0.25$ ;  $\tilde{\mathcal{A}}_m = 3.70313$  (first row);  $K_b = 0.953125$ ;  $\delta = 0.75$ ;  $\tilde{\mathcal{A}}_m = 5.71875$  (second row);  $K_b = 2.5$ ;  $\delta = 2.7$ ;  $\tilde{\mathcal{A}}_m = 9.99375$  (third row).

the figures).

### 3.6.2 Moderately nonlocal regime

We now assume that the relation between the wake potential and the beam density is *moderately nonlocal*. This corresponds, through Eq. (3.3.4), to assuming that roughly the beam spot size is comparable to the plasma wavelength, viz.,

$$\nabla_{\perp}^2 U_w \sim (k_{pe}^4/k_{uh}^2) U_w.$$

Then, in this regime, we solve numerically the full system of governing equations (3.3.3) and (3.3.4). For the numerical solution it is convenient to use the following

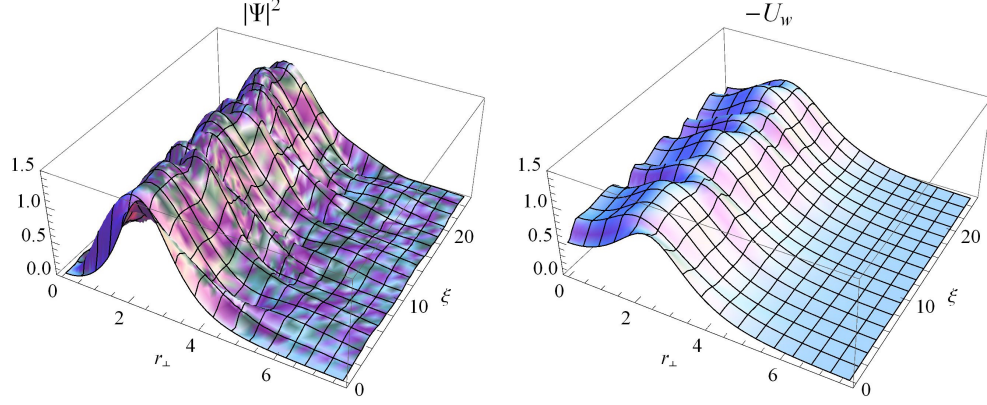


Figure 3.7: Ring soliton of a moderate beam. The evolution of the wave function (left) and of the wake potential (right). The initial wave function was adopted as a slab soliton [Eq. (3.6.11)] with the amplitude  $a = 1.5$  and with the velocity equal to zero,  $b = 0$ . The azimuthal wavenumber is adopted as  $m = 2$ , and the coefficient of the restoring force is  $K = 0.1$ . All normalizations are given in Eq. (3.6.7).

normalizations

$$r'_\perp = r \frac{k_{pe}^2}{k_{uh}}, \quad \xi' = \xi \epsilon \frac{k_{pe}^4}{k_{uh}^2}, \quad (3.6.7)$$

$$\psi'_m = \frac{\psi_m k_{uh}}{\epsilon k_{pe}^2} \sqrt{\frac{N}{n_0 \gamma_0 \sigma_z}}, \quad U'_w = \frac{U_w k_{uh}^2}{\epsilon^2 k_{pe}^4}, \quad K' = \frac{K k_{uh}^4}{\epsilon^2 k_{pe}^8}, \quad (3.6.8)$$

which permits us to rewrite our basic system (3.3.3) and (3.3.4) in a dimensionless form, with only one physical parameter,  $K$ , (hereafter, the primes are omitted for simplicity) viz.,

$$i \frac{\partial \psi_m}{\partial \xi} = -\frac{1}{2r_\perp} \frac{\partial}{\partial r_\perp} \left( r_\perp \frac{\partial \psi_m}{\partial r_\perp} \right) + U_w \psi_m + \left( \frac{1}{2} K r_\perp^2 + \frac{m^2}{2r_\perp^2} \right) \psi_m, \quad (3.6.9)$$

$$\frac{1}{r_\perp} \frac{\partial}{\partial r_\perp} \left( r_\perp \frac{\partial U_w}{\partial r_\perp} \right) - U_w = |\psi_m|^2. \quad (3.6.10)$$

Obviously, in the absence of the external potential, curvature, and nonlocality effects,  $K \rightarrow 0$ ,  $1/r_\perp \ll \partial/\partial r_\perp$  and  $\partial^2 U_w / \partial r_\perp^2 \ll U_w$ , Eqs. (3.6.9) and (3.6.10) reduce to a cubic nonlinear Schrödinger equation, which possesses the well known envelope soliton solution

$$\psi_S(r_\perp, \xi) = a \exp \left\{ i \left[ b r_\perp + (a^2 - b^2) \xi / 2 \right] \right\} \operatorname{sech} [a(r_\perp - b\xi)], \quad (3.6.11)$$

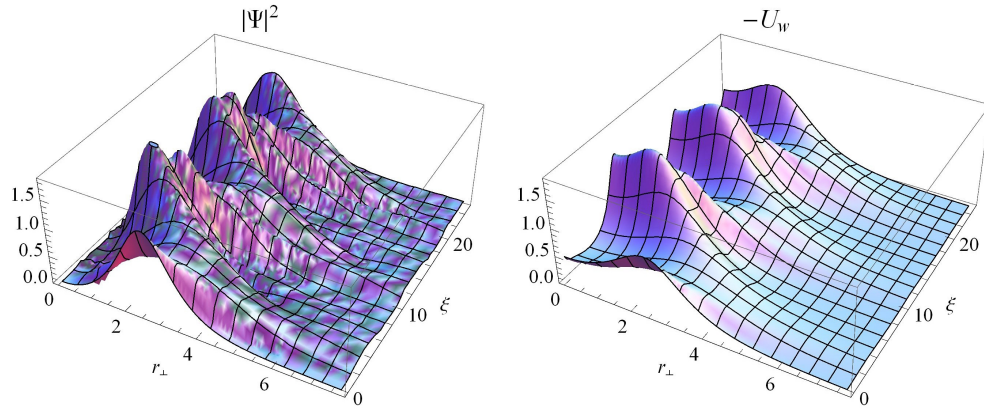


Figure 3.8: The evolution of the wave function (left) and of the wake potential (right). All parameters are the same as in Figure 3.7, except a finite initial velocity of the structure,  $b = 0.7$ .

where  $a$  and  $b$  are arbitrary real constants. We solved numerically Eqs. (3.6.9) and (3.6.10), using the initial condition of the form  $\psi_m(r_\perp, 0) = \psi_S(r_\perp - r_0, 0) \exp[(i\xi/2)(Kr_0^2 - m^2/r_0^2)] \tanh(r_\perp^m/L^m)$ , where  $L \gg r_0$  and the initial position  $r_0$  is adopted at the bottom of the potential well, viz.,

$$\frac{\partial}{\partial r_0} \left( \frac{1}{2} Kr_0^2 + \frac{m^2}{2r_0^2} \right) = 0. \quad (3.6.12)$$

The above initial wave function is weighed so that at  $r_\perp \rightarrow 0$  it behaves as  $O(r_\perp^m)$ .

First, we looked for a solution whose initial velocity was equal to zero. We adopted  $K = 0.1$ ,  $m = 2$ , and the following parameters of the initial condition  $a = 1.5$ ,  $b = 0$ . The numerical solution is displayed in Figure 3.7. The solution remained remarkably stable for a long time,  $\xi_{max} \geq 25$ . During this period, periodic ‘‘breathing’’ was observed, with a relatively small amplitude, similar to that found in the preceding section, for the local regime.

Next, we looked for a solution with a finite initial velocity and we adopted the same parameters as in Fig. 3.7, except  $b = 0.7$ . The solution is displayed in Figure 3.8. It also remained stable for a long time,  $\xi_{max} \geq 25$ , but it exhibited violent oscillations in the radial direction, as well as the ‘breathing’ and the periodic variation of the amplitude. Using this procedure, we were able to obtain stable solutions only in the weak and moderately nonlocal regimes. In the cases of very narrow initial wave function,  $a \gtrsim 2$ , the numerical solutions were unstable.

### 3.6.3 Strongly nonlocal regime

Here we describe the evolution of the beam in the regime of *strong nonlocality*. Assuming roughly that the beam spot size is much smaller than the plasma wavelength, when in Eq. (3.3.4) we can take the approximation  $\nabla_{\perp}^2 U_w \gg (k_{pe}^4/k_{uh}^2) U_w$ , the attraction among the beam particles takes place in such a way that the beam may exhibit a strong self-focusing [74]. Then, we have

$$\frac{1}{r_{\perp}} \frac{\partial}{\partial r_{\perp}} \left( r_{\perp} \frac{\partial U_w}{\partial r_{\perp}} \right) = \frac{k_{pe}^4}{k_{uh}^2} \frac{N}{2\pi n_0 \gamma_0 \sigma_z} |\psi_m|^2. \quad (3.6.13)$$

An approximate analytical solution of this regime and the scheme of quantum plasma lens would be provided by in Chapter 5.

# Chapter 4

## Self-consistent LWF excitation

In this chapter, we summarize the main results of investigations [30, 94] carried out within INFN collaboration of SPARC LAB (SL) SITE (Self Injection Test Experiment) as a development of the former collaboration PLASMONX, devoted to the Laser Wake Field (LWF) acceleration by means of the laser FLAME (Frascati Laser for Acceleration and Multidisciplinary Experiments). This research has been developed within FAI (Fondo Affari Internazionale) of INFN and very much supported by Prof. Dusan Jovanović (Institute of Physics, University of Belgrade, Serbia), the long term visits he had in the last three years in Napoli, working in our group.

The broad problem of the LWF excitation involves two families of processes that are subordinated to each other. The first concerns the nonlinear modifications of the plasma induced by an EM pulse and the subsequent feedback of the plasma on the pulse itself. This pair of concomitant processes constitute the self-consistent interaction of the laser pulse during its propagation in the plasma, which may assume a nonlocal character. When the wave amplitudes become extremely large, the nonlinear and nonlocal response may lead to the nonlinearity saturation that, in turn, may work as a stabilizing factor for the localized structures. The subordinated family of processes is the manipulation of an electron bunch, suitably injected into the plasma (external injection) and subsequently accelerated by the ultra-intense plasma fields (laser wake fields) [95], or violently created by the laser ponderomotive action that accelerates directly the plasma electrons to a very high energy within a very short distance (self-injection) [96].

### 4.1 Basic assumptions

In this section, we formulate the main assumptions used to develop the appropriate mathematical model, such as the plasma and laser characteristics, the geometry of the

propagation, and the model adopted for the *plasma + laser* system. In order to take into account different experimental conditions, we define three different intensity regimes that actually, for a given maximum laser power, depend on the transverse beam spot size,  $L_{\perp}$ . In particular, we follow the evolution of a laser pulse in the form of pancake, i.e. we take that the effective longitudinal pulse length,  $L_z$ , is much smaller than  $L_{\perp}$  (i.e.,  $L_z \ll L_{\perp}$ ).

Our basic assumptions of the laser are mainly formulated on the basis of the principal characteristics of the Ti:Sa laser FLAME [97]. In particular, the laser pulse carries the energy  $E = 7$  J before compression, which for a compression efficiency of 70% gives a pulse energy of approximately 5 J. The minimum pulse duration is  $\tau \geq 23$  fs and the maximum power is therefore  $W_{max} \sim 220$  TW, at the wavelength  $\lambda = 0.8 \mu\text{m}$ , (which corresponds to  $\omega = 2.36 \times 10^{15} \text{ s}^{-1}$ ), and repetition rate is  $\nu_{rep} = 10$  Hz. It is worth noting that  $\tau = 25 \times 10^{-15} \text{ s}$  corresponds to the pulse length  $L_z = 7.5 \mu\text{m}$ , i.e. there are around 10 wavelengths of the laser light within the pulse. According to references [98, 99], the plasma density in different experiments where FLAME is employed ranges as  $n_e = (0.6 - 1) \times 10^{19} \text{ cm}^{-3}$ , and even  $4 \times 10^{19} \text{ cm}^{-3}$ . The electron density  $n_e = \times 10^{19} \text{ cm}^{-3}$  corresponds to the plasma frequency  $\omega_{pe} = 1.78 \times 10^{14} \text{ s}^{-1}$ . Thus, the pulse duration is roughly  $\tau = 0.7 T_p$ , where  $T_p$  is the plasma period  $T_p = 2\pi/\omega_{pe} = 35.22 \times 10^{-15} \text{ s}$ , while the collisionless skin depth (which is the wavelength of the natural oscillation mode of the plasma),  $d_e = 2\pi c/\omega_{pe} = 10.56 \mu\text{m}$  is one order of magnitude longer than the laser wavelength ( $\lambda = 0.8 \mu\text{m}$ ) and close to the pulse length ( $L_z = 7.5 \mu\text{m}$ ). Ranging from weak to strong laser intensities, we can take into account the diverse physical conditions of the pancake ( $L_z \ll L_{\perp}$ ) propagation that correspond to different experimental conditions. We take that the electric field of the laser light is sufficiently strong for the electrons to achieve relativistic jitter velocities. In particular, for the maximum laser power of the order of 220 TW, we consider three different regimes that are extrapolated from the various experiment proposals available in literature. Namely:

- (i) *Weak Intensity Regime* (WIR), where the maximum intensity  $I_{max}$  is roughly ranging from  $2.5 \times 10^{14}$  to  $2.5 \times 10^{16} \text{ W/cm}^2$  [100–102].
- (ii) *Moderate Intensity Regime* (MIR), where the maximum intensity  $I_{max}$  is roughly ranging from  $1.5 \times 10^{18}$  to  $3 \times 10^{19} \text{ W/cm}^2$  [102, 103];
- (iii) *Strong Intensity Regime* (SIR), where the maximum intensity  $I_{max}$  is roughly ranging from  $10^{20}$  to  $2.5 \times 10^{22} \text{ W/cm}^2$  [98, 102]. This very high intensity regime will be accessible with FLAME only by means of the phase front correction, that

is planned in the near future, and using very fast focusing optics in order to reach a  $1 \mu\text{m}$  diameter focal spot.

Note that:  $L_{\perp}$  ranges roughly from 0.1 to 1 cm for WIR; from 30 to 130  $\mu\text{m}$  for MIR; from 1 to 16  $\mu\text{m}$  for SIR. However, in the physical conditions of SIR it turns out that  $L_{\perp}$  and  $L_z$  (typically,  $\sim 7.5 \mu\text{m}$ ) would be of the same order of magnitudes, against the assumption of a pancake geometry. Actually, to reach the SIR within the same assumption we have to assume that  $L_z$  be reduced to 1/3 of its typical value, i.e.  $L_z \sim 2.5 \mu\text{m}$ .

In the FLAME plasma-based accelerator scheme, the plasma is created in a helium gas jet by the laser ionization. A qualitative assessment of the ionization process can be obtained from the value of the Keldysh parameter  $\Gamma = \sqrt{U_i/\mathcal{E}}$ , where  $U_i$  is the ionization potential and  $\mathcal{E}$  is the kinetic energy of the electron quiver motion in the laser field,  $\mathcal{E} = \alpha^2 e^2 E_0^2 / 2m_e \omega^2$ . Here  $-e$  and  $m_e$  are the electron charge and mass, respectively,  $E_0$  and  $\omega$  are the laser electric field amplitude and angular frequency, and  $\alpha^2 = 1$  for a linear polarization,  $\alpha^2 = 2$  for a circular polarization. For small values of the Keldysh parameter,  $\Gamma \ll 1$ , the optical field ionization leads to an almost instantaneous freeing of the electron and plasma formation, while in the opposite case  $\Gamma \gg 1$ , the multi-photon ionization dominates (see Ref. [104]). For helium, the potentials of the first and the second ionization are  $U_{i1} = 24.5874 \text{ eV}$  and  $U_{i2} = 54.416 \text{ eV}$ , respectively. Thus, the Keldysh parameter for a double ionization of He, in the MIR (moderate intensity regime) scales as  $0.01/\alpha \lesssim \Gamma \lesssim 0.003/\alpha$  and in the WIR (weak intensity regime) as  $0.1/\alpha \lesssim \Gamma \lesssim 1/\alpha$ . For such large electric fields, as in the MIR, the ionization occurs instantaneously. This can be seen in the simple quasi-classical picture of the optical field ionization [104, 105], when the laser field (regarded as quasi-static) is described by an electrostatic potential  $-rE$  that is additive to the Coulomb potential of the nucleus. When the potential of the laser field is sufficiently strong, so that the total potential barrier lies below the electron energy level  $-U_i$ , the electron is free. The minimum laser intensity for which such barrier suppression ionization (BSI) occurs is easily calculated as

$$I_{BSI}[\text{W/cm}^2] = 4.00 \times 10^9 Z^{-2} U_i^4 [\text{eV}],$$

where  $Z$  is the nucleus charge. For helium, the BSI threshold is found to be  $I_{BSI} = 8.77 \times 10^{15} \text{ W/cm}^2$ , which is three to four orders of magnitude smaller than the laser intensity in MIR, and comparable with that in WIR. However, a high level of ionization occurs also in WIR, since the quantum distribution function of the electron allows it to tunnel under the barrier and leave the atom even if the intensity is below the threshold. Terawatt-power laser systems of moderate size can have the electric

field strength above  $10^{10}$  V cm $^{-1}$ . In such intense fields, the over-barrier ionization of atoms occurs in atomic time on the order of  $10^{-17}$  s [106]. The experiments on propagation of a laser pulse of moderate relativistic intensity in He of density suitable for electron acceleration [107], confirmed also by simulations [102], have shown a rather stable propagation with weak refractive effects associated with the different degrees of ionization. In the focal region, ionization driven effects were limited to the lateral wings of the pulse. The precursors of the pulse were observed to pre-ionize the focal region, but they did not trigger propagation instabilities. As a result, an intermediate range of intensities was established, in which the ionization was too fast to perturb the propagating pulse, the relativistic effects were weak, and the ponderomotive effects appeared to be slow. Finally, we assume that the above laser pump is traveling in an initially-homogeneous, unmagnetized plasma, where the ions are regarded as infinitely massive, forming therefore a background of positive uniform charge with number density  $n_0$ . Within the fluid theory, the system *plasma + laser* is described by the Lorentz-Maxwell system of equations in the fully relativistic regime. Given the above laser intensities, the radiation pressure (ponderomotive effect) is much greater than the kinetic pressure. Therefore, to the ends of the present investigation, the plasma can be regarded as a cold fluid [108].

## 4.2 Governing equations

According to Section 4.1, starting from the Lorentz-Maxwell system, it is the most convenient to write the wave equation, i.e., the equation for the electromagnetic field, expressing the electric and magnetic fields via the electrostatic potential  $\phi$  and the vector potential  $\mathbf{A}$ , using the Coulomb gauge,  $\nabla \cdot \mathbf{A} = 0$ . Then, the Ampere's law (in SI units)

$$\nabla \times \mathbf{B} = \frac{1}{c} \left( \frac{\partial \mathbf{E}}{\partial t} + \frac{4\pi}{c} \mathbf{J} \right), \quad (4.2.1)$$

is readily rewritten as

$$\frac{\partial^2 \mathbf{A}}{\partial t^2} - c^2 \nabla^2 \mathbf{A} + \nabla \frac{\partial \phi}{\partial t} = \frac{4\pi}{c} \mathbf{J}, \quad (4.2.2)$$

where  $\mathbf{J}$  is the current density. For our purposes, it is more convenient to use only the component of equation (4.2.2) that is perpendicular to the direction of propagation of the laser beam (which is taken to be along the  $z$ -axis), and the divergence of equation

(4.2.2) (i.e., the Poissons equation), viz.,

$$\frac{\partial^2 \mathbf{A}_\perp}{\partial t^2} - c^2 \left( \nabla_\perp^2 + \frac{\partial^2}{\partial z^2} \right) \mathbf{A}_\perp + \nabla_\perp \frac{\partial \phi}{\partial t} = \frac{\mathbf{J}_\perp}{\epsilon_0}, \quad (4.2.3)$$

$$\left( \nabla_\perp^2 + \frac{\partial^2}{\partial z^2} \right) \phi = -\frac{\rho}{\epsilon_0}, \quad (4.2.4)$$

where  $\rho$  is the charge density that satisfies the continuity equation  $\partial \rho / \partial t + \nabla \cdot \mathbf{J} = 0$ . The current and the charge density are calculated as

$$\rho = \sum_\alpha q_\alpha n_\alpha, \quad \mathbf{J} = \sum_\alpha q_\alpha n_\alpha \mathbf{v}_\alpha, \quad (4.2.5)$$

where  $q_\alpha$  is the charge of the particle species  $\alpha$ , and the hydrodynamic densities  $n_\alpha$  and velocities  $\mathbf{v}_\alpha$  are calculated from the appropriate hydrodynamic equations. For simplicity, we take that the characteristic frequency of the laser light and of the other processes involved is so high, compared to the plasma frequency, that the ions are essentially immobile. This justifies the assumption taken above of infinitely massive ions, constituting a neutralizing background for the electrons, i.e.  $n_i = n_0$ . In other words, we consider the interaction of high frequency electromagnetic and Langmuir waves, while the acoustic phenomena are disregarded. The electrons are regarded as cold, i.e., the phase velocity of the nonlinear modes involved are assumed to be much higher than the electron thermal velocity. The same regime is studied also in the standard literature, see e.g., Refs. [4, 5, 14–16, 109–111]. Then, the electron continuity and momentum equations take the form

$$\frac{\partial n}{\partial t} + \nabla \cdot (n\mathbf{v}) = 0, \quad (4.2.6)$$

$$\left( \frac{\partial}{\partial t} + \mathbf{v} \cdot \nabla \right) \mathbf{p} = q \left[ -\nabla \phi - \frac{\partial \mathbf{A}}{\partial t} + \mathbf{v} \times (\nabla \times \mathbf{A}) \right], \quad (4.2.7)$$

where, for simplicity, the subscript for electrons has been omitted and  $q = -e$ . Here  $\mathbf{p}$  is the electron momentum, which is related with the electron velocity  $\mathbf{v}$  through the standard relativistic relation  $\mathbf{v} = \mathbf{p}/m_0\gamma$ , where  $m_0$  is the electron rest mass,  $\gamma = (1 + p^2/m_0^2c^2)^{1/2}$  is the relativistic factor, and  $c$  is the speed of light. Using the identities

$$(\mathbf{v} \cdot \nabla) \mathbf{p} = \mathbf{v} \times (\nabla \times \mathbf{p}) + (\nabla \mathbf{p}) \cdot \mathbf{v}, \quad \text{and} \quad (\nabla \mathbf{p}) \cdot \mathbf{v} = m_0 c^2 \nabla \gamma, \quad (4.2.8)$$

the electron momentum equation (4.2.7) is rewritten as

$$\frac{\partial}{\partial t} (\mathbf{p} + q\mathbf{A}) - \mathbf{v} \times [\nabla \times (\mathbf{p} + q\mathbf{A})] + \nabla (m_0 c^2 \gamma + q\phi) = 0. \quad (4.2.9)$$

For later purposes, we write explicitly the transverse and the longitudinal components of equation (4.2.9), viz.,

$$\left(\frac{\partial}{\partial t} + \mathbf{v}_\perp \cdot \nabla_\perp + v_z \frac{\partial}{\partial z}\right)(\mathbf{p}_\perp + q\mathbf{A}_\perp) - v_i \nabla_\perp (\mathbf{p}_i + q\mathbf{A}_i) + \nabla_\perp (m_0 c^2 \gamma + q\phi) = 0, \quad (4.2.10)$$

$$\left(\frac{\partial}{\partial t} + \mathbf{v}_\perp \cdot \nabla_\perp\right)(p_z + qA_z) - \mathbf{v}_\perp \frac{\partial}{\partial z} (\mathbf{p}_\perp + q\mathbf{A}_\perp) + \frac{\partial}{\partial z} (m_0 c^2 \gamma + q\phi) = 0, \quad (4.2.11)$$

### 4.2.1 Dimensionless equations in the moving frame

Following references [4, 5, 14–16, 109–111] we consider the solution that is slowly varying in the reference frame that is moving with the velocity  $u$  in the direction of the  $z$ -axis. Using the dimensionless quantities

$$\begin{aligned} \mathbf{p}' &= \frac{\mathbf{p}}{m_0 c}, & \mathbf{v}' &= \frac{\mathbf{v}}{c}, & \phi' &= \frac{q\phi}{m_0 c^2}, \\ \mathbf{A}' &= \frac{q\mathbf{A}}{m_0 c}, & n' &= \frac{n}{n_0}, & u' &= \frac{u}{c}, \\ t' &= \omega_{pe} t, & \mathbf{r}' &= \frac{\omega_{pe}}{c} (\mathbf{r} - \mathbf{e}_z u t), \end{aligned} \quad (4.2.12)$$

where  $\omega_{pe}$  is the plasma frequency of stationary electrons,  $\omega_{pe} = (n_0 q^2 / m_0 \epsilon_0)^{1/2}$ , and making use of equation (4.2.5), we rewrite equations (4.2.3), (4.2.4), (4.2.6), (4.2.10), and (4.2.11) in the moving frame, viz.,

$$\left[\frac{\partial^2}{\partial t'^2} - 2u' \frac{\partial^2}{\partial z' \partial t'} - (1 - u'^2) \frac{\partial^2}{\partial z'^2} - \nabla_\perp'^2\right] \mathbf{A}'_\perp + \nabla_\perp' \left(\frac{\partial}{\partial t'} - u' \frac{\partial}{\partial z'}\right) \phi = \mathbf{v}'_\perp n, \quad (4.2.13)$$

$$\left(\nabla_\perp'^2 + \frac{\partial^2}{\partial z'^2}\right) \phi = 1 - n, \quad (4.2.14)$$

$$\left(\frac{\partial}{\partial t'} - u' \frac{\partial}{\partial z'}\right) n + \nabla' \cdot (n \mathbf{v}') = 0, \quad (4.2.15)$$

$$\left(\frac{\partial}{\partial t'} - u' \frac{\partial}{\partial z'} + \mathbf{v}'_\perp \cdot \nabla_\perp'\right) (p_z + A_z) - \mathbf{v}'_\perp \frac{\partial}{\partial z'} (\mathbf{p}'_\perp + \mathbf{A}'_\perp) + \frac{\partial}{\partial z'} (\gamma + \phi) = 0, \quad (4.2.16)$$

$$\left[\frac{\partial}{\partial t'} + (v_z' - u') \frac{\partial}{\partial z'} + \mathbf{v}'_\perp \cdot \nabla_\perp'\right] (\mathbf{p}'_\perp + \mathbf{A}'_\perp) - v_i' \nabla_\perp' (p_i + A_i) + \nabla_\perp' (\gamma + \phi) = 0, \quad (4.2.17)$$

Usually, the solution of the hydrodynamic equations (4.2.15) - (4.2.17) is sought in the quasistatic regime, i.e., when the solution is slowly varying in the moving reference frame,  $\partial/\partial t \ll u \partial/\partial z$ . The hydrodynamic equations (4.2.15) - (4.2.17) remain very complicated and in the classical works [4, 5, 14–16, 109, 111]. They are further simplified by taking  $u$  to be very close to the speed of light viz.,

$$1 - u \ll 1, \quad (4.2.18)$$

and assuming an almost 1D (one dimensional) regime, viz.,

$$\nabla_{\perp} \ll \frac{\partial}{\partial z}. \quad (4.2.19)$$

Note that, in Refs. [4, 5, 14, 15] the equations are written in a reference frame moving with the speed of light ( $u = 1$  in dimensionless units). However, with such a choice, an important dispersive term  $\propto (1 - u^2)\partial^2 \mathbf{A}_{\perp} / \partial z^2$  is lost in the wave equation, which makes the further analysis and ordering more difficult. Following Ref. [109] we take  $u$  which is equal to the group velocity of an electromagnetic wave. For the FLAME laser frequency and plasma density, the latter is sufficiently close to the speed of light and one may apply the ordering (4.2.18).

Note also that, this 1D assumption (4.2.19) is valid for the perpendicular momentum equation (4.2.17) under the FLAME conditions and for all spot sizes. Conversely, it will be shown below that the quantities associated with the electrostatic components, viz.  $\phi, n, \mathbf{v}_z, \mathbf{p}_z$  and  $\mathbf{A}_z$ , scale with the envelope of the laser pulse rather than with the electromagnetic wave. Thus, the 1D assumption (4.2.19) is appropriate for the continuity and the parallel momentum equations (4.2.15) and (4.2.16), only when  $L_z \ll L_{\perp}$  (i.e., in the pancake regime).

For a stationary 1D solution propagating with the speed of light, setting  $\partial/\partial t = \nabla_{\perp} = 1 - u = 0$ , the leading order parts of equations (4.2.15) - (4.2.17) are obtained in the simple form

$$\frac{\partial}{\partial z} [(v_z - 1)n] = 0, \quad (4.2.20)$$

$$\frac{\partial}{\partial z} (-p_z + \gamma + \phi) = 0, \quad (4.2.21)$$

$$\frac{\partial}{\partial z} (\mathbf{p}_{\perp} + \mathbf{A}_{\perp}) = 0, \quad (4.2.22)$$

while from  $\nabla \cdot \mathbf{A} = 0$ , within the same accuracy, we have

$$\frac{\partial A_z}{\partial z} = 0. \quad (4.2.23)$$

Noting that for  $z \rightarrow \pm\infty$  we have  $\phi = \mathbf{A} = \mathbf{v} = \mathbf{p} = 0$  and  $\gamma = n = 1$ , and using  $\gamma = (1 + p_z^2 + \mathbf{p}_{\perp}^2)^{1/2}$ , equations (4.2.20) - (4.2.23) are readily integrated, yielding

$$(v_z - 1)n + 1 = 0, \quad (4.2.24)$$

$$-p_z + \gamma + 1 + \phi = 0, \quad (4.2.25)$$

$$\mathbf{p}_{\perp} + \mathbf{A}_{\perp} = 0, \quad (4.2.26)$$

$$A_z = 0. \quad (4.2.27)$$

Then, using the definition for  $\gamma$  and equations (4.2.24) - (4.2.26), and after some straightforward algebra, we obtain the dimensionless charge and current densities as

$$n = \frac{(\phi - 1)^2 + \mathbf{A}_\perp^2 + 1}{2(\phi - 1)^2}, \quad (4.2.28)$$

$$\mathbf{v}_\perp n = \frac{\mathbf{A}_\perp}{\phi - 1}, \quad (4.2.29)$$

which permits us to rewrite our basic equations as

$$\left[ \frac{\partial^2}{\partial t^2} - 2u \frac{\partial^2}{\partial t \partial z} - (1 - u^2) \frac{\partial^2}{\partial z^2} - \nabla_\perp^2 + \frac{1}{1 - \phi} \right] \mathbf{A}_\perp = - \left( \frac{\partial}{\partial t} - u \frac{\partial}{\partial z} \right) \nabla_\perp \phi, \quad (4.2.30)$$

$$\frac{\partial^2 \phi}{\partial z^2} = \frac{(\phi - 1)^2 - 1 + \mathbf{A}_\perp^2}{2(\phi - 1)^2}. \quad (4.2.31)$$

Equations (4.2.30) and (4.2.31) constitute a system of coupled nonlinear equations that describe the spatio-temporal evolution of a modulated electromagnetic wave, in the form of a pancake, interacting with a Langmuir wave via the nonlocal nonlinearities that arise from the relativistic effects, beyond the slowly varying amplitude approximation and for an arbitrary intensity regime. They can not be simply regarded as the pair of Zakharov-like equations, but nevertheless they appropriately describe the parametric processes involved. Thus, besides the standard nonrelativistic three-wave coupling phenomena (the Raman scattering), in the relativistic case, in principle, they may provide also the description of the four-wave processes, directly related to the modulational instability, soliton formation, etc. However, the actual nonlinear dynamics of the pulse strongly depends on the physical conditions in each particular device and can not be generalized.

We note that the nonlinear term in the wave equation (4.2.30),  $\mathbf{A}_\perp/(1 - \phi)$ , tends to zero for very large Langmuir electrostatic potential. Thus, essentially different behavior is expected in the moderate and large intensity regimes,  $\phi \ll 1$  and  $\phi \gg 1$ , respectively. Intuitively, we expect that this condition coincides with the similar condition for the laser intensity,  $\mathbf{A}_\perp^2 \ll 1$  and  $\mathbf{A}_\perp^2 \gg 1$ . It will be shown below that with the present power of FLAME, in most experimental setups we have  $\mathbf{A}_\perp^2 < 1$ , and we can take the pulse to have a moderate intensity. Only in the case of strong focusing, the condition of large intensity ( $\mathbf{A}_\perp^2 \gg 1$ ) is satisfied, but such small spot size is not used in the accelerator scheme that is of our primary interest here. Furthermore, as we have already mentioned, in the latter case the longitudinal and transverse scales of the pulse are comparable, and the simple 1D approximation, equations (4.2.19) - (4.2.23) are not applicable.

### 4.3 Modulational representation and scalings

In the case of moderate intensities, we seek the solution of the wave equation in the moving frame (4.2.13) in the form of a modulated electromagnetic wave, viz.,

$$\mathbf{A}_\perp = \mathbf{A}_{\perp 0} e^{-i[\omega' t - k'(z+ut)]} + c.c., \quad (4.3.1)$$

where the dimensionless frequency  $\omega'$  and the dimensionless wavenumber  $k'$  are defined as

$$\omega' = \frac{\omega}{\omega_{pe}}, \quad k' = \frac{ck}{\omega_{pe}} = \frac{d_e}{\lambda}, \quad (4.3.2)$$

where  $\omega$ ,  $k$ , and  $\lambda$  are the frequency, wavenumber, and wavelength of the electromagnetic laser wave, respectively. They satisfy the linear dispersion relation of electromagnetic waves,  $\omega = (c^2 k^2 + \omega_{pe}^2)^{1/2}$ , whose dimensionless version has the form  $\omega = (k^2 + 1)^{1/2}$ . For simplicity, hereafter, we drop the primes. We adopt  $u$  to be equal to the group velocity of the electromagnetic wave  $u = d\omega/dk = k/\omega$ , which permits us to rewrite the wave equation (4.2.13) and the Poissons equation (4.2.14) as

$$\begin{aligned} 2\text{Re} \left\{ e^{-i(t/\omega - kz)} \left[ 2i\omega \frac{\partial}{\partial t} - \omega^2 \frac{\partial^2}{\partial t^2} + \left( k \frac{\partial}{\partial t} + \frac{1}{\omega} \frac{\partial}{\partial z} \right)^2 + \nabla_\perp^2 - \frac{\phi}{1-\phi} \right] \mathbf{A}_{\perp 0} \right\} \\ = \left( \frac{\partial}{\partial t} - \frac{k}{\omega} \frac{\partial}{\partial z} \right) \nabla_\perp \phi, \end{aligned} \quad (4.3.3)$$

$$\frac{\partial^2 \phi}{\partial z^2} = \frac{(\phi - 1)^2 - 1 - \mathbf{A}_\perp^2}{2(\phi - 1)^2}. \quad (4.3.4)$$

The pair of equations (4.3.3) and (4.3.4) can be regarded as a sort of generalized Zakharov system governing the envelope evolution of the laser for the pancake geometry beyond the slowly varying amplitude approximation. Under the typical laser-plasma acceleration conditions under investigation with the FLAME laser, the dimensionless frequency and wavenumber of the laser light are relatively large, i.e.,  $\omega \approx k \gtrsim 12$ . Likewise, the spatial derivative in the direction of propagation is estimated as  $\partial \mathbf{A}_{\perp 0} / \partial z \sim \mathbf{A}_{\perp 0} / L_z$ , where  $L_z = \tau c = 7.5 \mu\text{m}$  is the pulse length, whose dimensionless value [see equation (4.2.12)], is  $L'_z = \tau \omega_{pe} = 4.46$ . In the numerical simulations for MIR [98], a plasma density almost 50 times smaller than the plasma density was used ( $n_e = 1.5 - 2.5 \times 10^{17} \text{ cm}^{-3}$ ), which corresponds to  $L'_z = 0.7$  and  $\omega' = 100$ .

With such small plasma density (i.e., with such large value of the parameter  $\omega$ ), the laser pulse tends to self-organize into a standard NLS (nonlinear Schrödinger) soliton with a linear phase, while the effects of a parabolic phase (often referred to as “the chirp”) could be observed only for much larger laser intensities.

Requesting that, in the wave equation (4.3.3), the terms describing the temporal evolution of the envelope  $\mathbf{A}_{\perp 0}$  and its spatial evolution in the direction of propagation are of the same order, we have [in dimensionless quantities (4.2.12)]

$$\begin{aligned} \omega \frac{\partial \mathbf{A}_{\perp 0}}{\partial t} &\sim \frac{1}{\omega^2} \frac{\partial^2 \mathbf{A}_{\perp 0}}{\partial z^2} \sim 4 \times 10^{-4} \mathbf{A}_{\perp 0} \\ &\gg \frac{k}{\omega} \frac{\partial^2 \mathbf{A}_{\perp 0}}{\partial t \partial z} \sim 8 \times 10^{-6} \mathbf{A}_{\perp 0} \gg \omega^2 \frac{\partial^2 \mathbf{A}_{\perp 0}}{\partial t^2} \sim 16 \times 10^{-8} \mathbf{A}_{\perp 0}. \end{aligned} \quad (4.3.5)$$

Under these conditions, the 1D approximation in the hydrodynamic equations (4.2.15) - (4.2.17) is also justified. Likewise, from the first three terms in equation (4.3.5) we find that the envelope is slowly varying in time

$$\frac{\partial \mathbf{A}_{\perp 0}}{\partial t} \sim \frac{\mathbf{A}_{\perp 0}}{\omega^3 L_z^2} \sim 2.42 \times 10^{-6} \omega \mathbf{A}_{\perp 0} \ll \omega \mathbf{A}_{\perp 0}. \quad (4.3.6)$$

The second derivative in time in equation (4.3.3) becomes relevant only in the case of a collapse, i.e., if the longitudinal size of the pulse becomes comparable to the laser wavelength,  $\partial \mathbf{A}_{\perp 0} / \partial z \sim k \mathbf{A}_{\perp 0}$ . We also note that, under the same conditions, the regimes of intensity defined in the Section 4.1 can now be expressed in terms of the following mathematical conditions:

- (i)  $\nabla_{\perp}^2 \mathbf{A}_{\perp 0} \ll (1/\omega^2) \partial^2 \mathbf{A}_{\perp 0} / \partial z^2$  corresponds to WIR;
- (ii)  $\nabla_{\perp}^2 \mathbf{A}_{\perp 0} \sim (1/\omega^2) \partial^2 \mathbf{A}_{\perp 0} / \partial z^2$  corresponds to MIR;
- (iii)  $\nabla_{\perp}^2 \mathbf{A}_{\perp 0} \gg (1/\omega^2) \partial^2 \mathbf{A}_{\perp 0} / \partial z^2$  corresponds to SIR.

However, for a fully 3D pulse, realized in the SIR, our equations (4.3.3) and (4.3.4) are applicable only if  $L_z$  is reduced in such a way to satisfy the pancake condition, i.e.,  $L_z \ll L_{\perp}$ .

From the Poisson's equation (4.3.4), one can easily see that for a modulated electromagnetic wave (4.3.1), due to the presence of the term  $\mathbf{A}_{\perp 0}^2$ , the electrostatic potential contains a slowly varying component and a second harmonic,  $\propto \exp[-2i(t/\omega - kz)]$ . Thus, for a slowly varying amplitude [see condition (4.3.6)], the right-hand-side of the wave equation (4.3.3) is nonresonant and can be neglected, except in the case of a collapse, when both  $\partial \mathbf{A}_{\perp 0} / \partial z \sim k \mathbf{A}_{\perp 0}$  and  $\partial \mathbf{A}_{\perp 0} / \partial t \sim \omega \mathbf{A}_{\perp 0}$ . However, in the case of a collapse, it is not possible to use the 1D approximation (4.2.19) in the hydrodynamic equations (4.2.15) - (4.2.17), and the relatively simple model equations (4.3.3) and (4.3.4) are not applicable. For the same reason, we can neglect the second harmonic

as non-resonant, also in the Poissons equation (4.3.4). Particularly simple case is that of a circularly polarized wave

$$\mathbf{A}_\perp = A_{\perp 0} \frac{\mathbf{e}_x + i\mathbf{e}_y}{\sqrt{2}} e^{-i[\omega't - k'(z+ut)]} + c.c., \quad (4.3.7)$$

when we have  $\mathbf{A}_\perp^2 = |A_{\perp 0}|^2$ , i.e., the second harmonic is absent. Thus, in the absence of a collapse, our basic equation are simplified to

$$\left[ 2i\omega \frac{\partial}{\partial t} + \frac{1}{\omega^2} \frac{\partial^2}{\partial z^2} + \nabla_\perp^2 - \frac{\phi}{1-\phi} \right] A_{\perp 0} = 0, \quad (4.3.8)$$

$$\frac{\partial^2 \phi}{\partial z^2} = \frac{(\phi - 1)^2 - 1 - |A_{\perp 0}|^2}{2(\phi - 1)^2}, \quad (4.3.9)$$

where for a circularly and a linearly polarized wave we have  $\mathbf{A}_{\perp 0} = (A_{\perp 0}/\sqrt{2})(\mathbf{e}_x + \mathbf{e}_y)$  and  $\mathbf{A}_{\perp 0} = A_{\perp 0}\mathbf{e}_x$ , respectively. Then, denoting the maximum amplitude of  $A_{\perp 0}$  by  $A_{max}$ , it is easy to see that, for circularly polarized waves, the maximum quiver velocity  $v_{max} = A_{max}/\sqrt{2}$  is given by

$$v_{max} = \frac{e}{m_0 c^2 \sqrt{2\pi^3 \epsilon_0}} \frac{\sqrt{W_{max}}}{L_\perp} \sim \frac{6 \times 10^{-5}}{L_\perp}, \quad (4.3.10)$$

where  $L_\perp$  is in meters. According to the definitions given in Section 4.1:  $v_{max} \sim 6.3 \times 10^{-2} - 6.3 \times 10^{-3}$  for WIR;  $v_{max} \sim 2.1 - 0.5$  for MIR;  $v_{max} \sim 63 - 4$  for SIR.

## 4.4 Weak and moderate laser intensities

For WIR and MIR, it is justified to assume (at least qualitatively) a small electrostatic potential,  $\phi \ll 1$  (which in dimensional quantities corresponds to  $\phi \ll m_0 c^2/e = 0.51 \times 10^6$  V), and expand the nonlinear terms in equations (4.3.8) and (4.3.9). Thus, for a weak and moderate intensity regimes, we have the following simplified equations

$$\left( 2i\omega \frac{\partial}{\partial t} + \frac{1}{\omega^2} \frac{\partial^2}{\partial z^2} + \nabla_\perp^2 - \phi \right) A_{\perp 0} = 0, \quad (4.4.1)$$

$$\left( \frac{\partial^2}{\partial z^2} + 1 \right) \phi = -\frac{|A_{\perp 0}|^2}{2}. \quad (4.4.2)$$

for the pancake structures, as the perturbation of the electron density can be expressed from the Poisson's equation as  $n-1 = -\partial^2 \phi / \partial z^2 \ll 1$ , we note that, owing to such small density perturbation, both the WIR and MIR can be attributed as "linear regimes". In this regime our "quasistatic approximation" holds and a very detailed description

of the nonlinear dynamics can be achieved within the applied semi-analytic model [4, 5, 14–16, 109–113].

For the laser pulses that are much longer than the collisionless skin depth,  $d_e$ , one might set  $\partial^2\phi/\partial z^2 \rightarrow 0$  in the Poisson's equation (4.3.9), which after the substitution in equation (4.4.1) gives rise to a standard cubic nonlinear Schrödinger equation. Such regime was studied extensively in reference [109]. However, under the plasma acceleration conditions under consideration here [97, 107], the normalized pulse length, which is here defined as ratio between  $L_z$  and  $d_e$ , is  $\sim 1$ , and consequently  $\partial^2\phi/\partial z^2 \sim \phi/L_z^2 \sim \phi$ . This is particularly true for the *moderate intensity regime* [98]. Under such ordering, it is convenient to introduce the rescaled quantities  $t \rightarrow \omega^3 t$ ,  $\mathbf{r}_\perp \rightarrow \omega \mathbf{r}_\perp$ ,  $\phi \rightarrow \phi/\omega^2$ , and  $A_{\perp 0} \rightarrow A_{\perp 0}/\omega$ . Then the above equations are rewritten as

$$\left(2i\frac{\partial}{\partial t} + \frac{\partial^2}{\partial z^2} + \nabla_\perp^2 - \phi\right)A_{\perp 0} = 0, \quad (4.4.3)$$

$$\left(\frac{\partial^2}{\partial z^2} + 1\right)\phi = -\frac{|A_{\perp 0}|^2}{2}. \quad (4.4.4)$$

The inhomogeneous linear equation (4.4.2) is easily solved in the form of a convolution, viz.,

$$\phi(z, t) = \frac{\cos z}{2} \int_{z_1}^z dz' \sin z' |A_{\perp 0}(z', t)|^2 - \frac{\sin z}{2} \int_{z_2}^z dz' \cos z' |A_{\perp 0}(z', t)|^2, \quad (4.4.5)$$

where  $z_1$  and  $z_2$  are arbitrary initial positions.

First, we note that there exists a symmetric solution, which can be cast in the standard form of a *nonlocal response*, viz.,

$$\phi(z, t) = \int d^3\mathbf{r}' R(|\mathbf{r} - \mathbf{r}'|) |A_{\perp 0}(\mathbf{r}', t)|^2, \quad (4.4.6)$$

where

$$R(|\mathbf{r} - \mathbf{r}'|) = -\frac{1}{4} \delta|x - x'| \delta|y - y'| \sin|z - z'|,$$

and the integration is performed for the entire space. It is interesting to note that, in the above, the nonlocality function  $R$  is not localized, in contrast to the standard examples of the nonlocal response.

Obviously, the solution (4.4.6), that can be conveniently rewritten as

$$\phi(z, t) = -\frac{1}{4} \int dz' \sin|z - z'| |A_{\perp 0}(z', t)|^2, \quad (4.4.7)$$

is symmetric if  $|A_{\perp 0}|$  is an even function of  $z$ , i.e.,  $|A_{\perp 0}(z, t)| = |A_{\perp 0}(-z, t)| \Rightarrow \phi(z, t) = \phi(-z, t)$ .

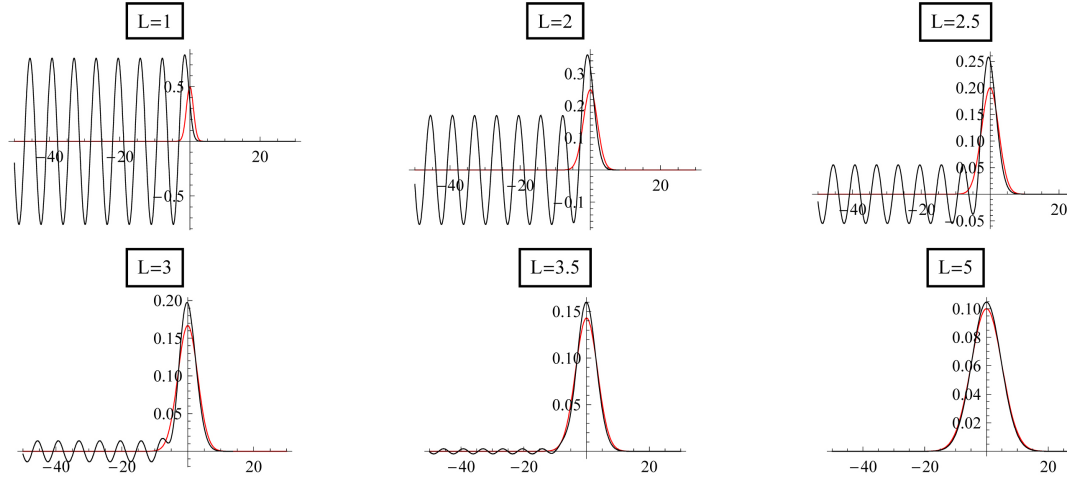


Figure 4.1: The electrostatic potential  $-\phi$  (black line), found as the solution of Eq. (4.4.4) driven by a laser pulse with the Gaussian shape. The square amplitude of the vector potential (red line) is taken as  $|A_{\perp 0}(z)|^2 = (1/2L) \exp(-z^2/2L^2)$ , with different dimensionless pulse widths ranging from 1 to 5.

#### 4.4.1 1D longitudinal evolution of the pulse

It is worth noting that our equation (4.4.6) features the nonlocality only in the direction of propagation (i.e. in the direction of the  $z$ -axis), which is due to the effective 1D nature of the hydrodynamic equations in the regime when the perpendicular spot size is larger than the pulse length. Conversely, in the SIR, the hydrodynamic equations are much more difficult to solve and, apart from other complications, one may expect a full 3D nonlocal response of the pancake.

However, such nonlocality analyses are not relevant for our problem of propagation of a laser pulse in a nonlinear medium. Our problem is strongly asymmetric, i.e., virtually no response is expected to occur *in front* of the pulse. The solution (4.4.5) that is *driven by the laser pulse*, i.e., the one that is equal to zero in front of the pulse, has the form

$$\phi(z, t) = \frac{1}{2} \int_z^{\infty} dz' \sin(z - z') |A_{\perp 0}(z', t)|^2. \quad (4.4.8)$$

For a localized pulse in the vector potential, the solution (4.4.8) has the form of an oscillating wake. The amplitudes of the leading pulse-like structure and of the wake in the electrostatic potential, are determined by the width of the laser pulse. As a simple model, we have calculated the non-selfconsistent electrostatic response  $\phi$  to Gaussian wavepackets, in the form  $|A_{\perp 0}(z)|^2 = (1/2L) \exp(-z^2/2L^2)$ , neglecting the feedback of the potential  $\phi$  to the laser propagation. The solutions are displayed in Figure 4.1. We note that the electrostatic response (i.e., the form of the oscillating wake) strongly

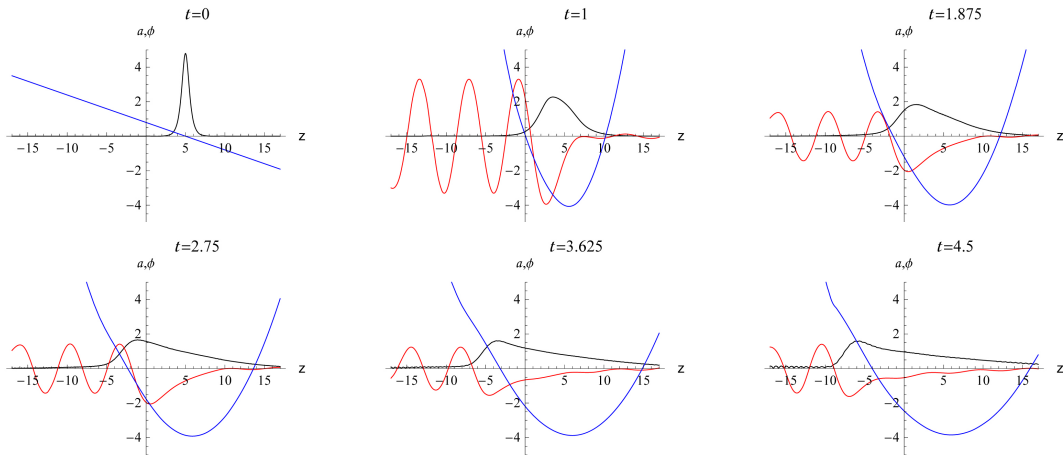


Figure 4.2: The evolution of a moderately focused laser pulse. The laser amplitude  $a = |A_{\perp 0}|$  (black), the phase  $\theta = \arg A_{\perp 0}$  (blue) and the electrostatic potential  $\phi$  (red) are obtained as the numerical solutions of Eqs. (4.4.3) and (4.4.4) in the 1D regime  $\nabla_{\perp} \rightarrow 0$ . The initial condition is solitonlike, i.e.  $A_{\perp 0}(z, 0) = 2\sqrt{C_1} \exp(i\delta kz) \operatorname{sech}(\sqrt{C_1}z)$ , with  $\delta k = -0.5$  and with a larger amplitude,  $C_1 = 5.75$ .

depends on the width of the laser pulse. If the width of the pulse is comparable to, or smaller than, the wavelength of the wake,  $L \leq 1$ , the wake is an almost purely sinusoidal function, existing only behind the laser pulse. If the laser pulse is somewhat larger than the wavelength,  $L > 3.5$ , the wake almost disappears and the electrostatic response is a single potential maximum that (almost) coincides with the envelope of the laser pulse. Already in the early paper [114] a nice study of the excitation of an oscillating tail was presented.

Obviously, in the strongly nonlinear regime when in equation (4.3.8) we have  $\phi \sim 1$ , the solution must be self-consistent. In other words, one must account for the feedback from the electrostatic wake (which is a spatially extended structure) to the electromagnetic pulse (which is localized in the direction of propagation). The conditions for the coexistence of such localized and extended components will be studied below.

The self-consistent nonlinear response in the moderate intensity regime and in the 1D limit was found by a numerical solution of equations (4.4.1) and (4.4.2), taking  $\nabla_{\perp} = 0$ . The results are displayed in Figure 4.2, in which we follow the temporal evolution of a pulse with the moderate intensity and with the initial solitonlike profile  $A_{\perp 0}(z, 0) = 2\sqrt{C_1} \exp(i\delta kz) \operatorname{sech}(\sqrt{C_1}z)$ , with  $C_1 = 5.5$ . The observed behavior was considerably different than that of the *weak intensity* pulses. The amplitude very

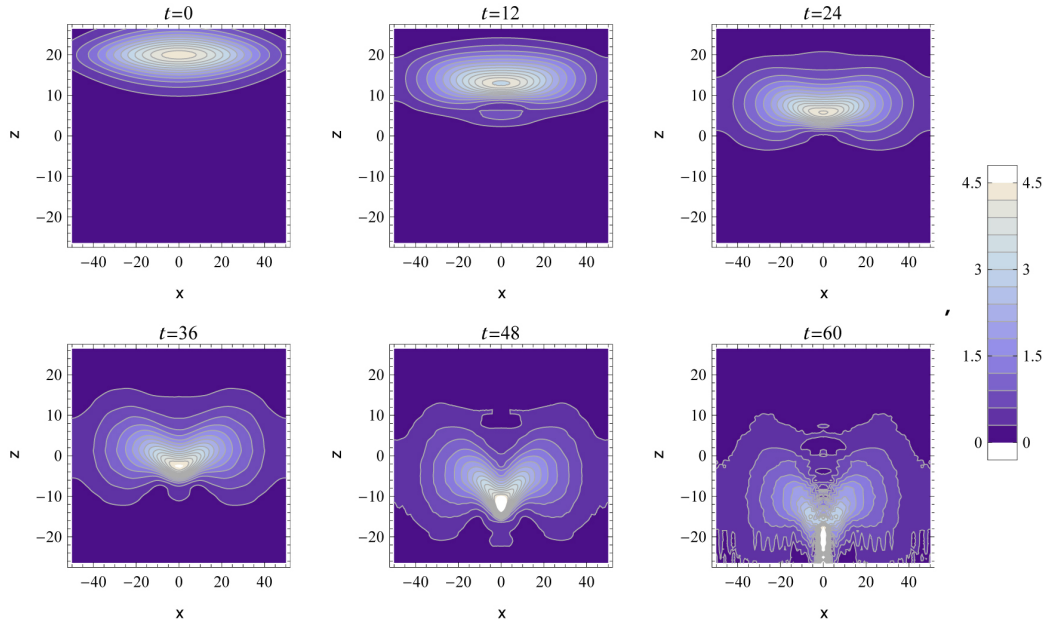


Figure 4.3: The evolution of the envelope of a weak intensity regime FLAME laser pulse, found as the numerical solution of Eqs. (4.4.3) and (4.4.4) in the 2D regime  $\nabla_{\perp}^2 \ll \partial^2/\partial x^2$ . The initial condition was adopted in the form of an unchirped NLS soliton, that is modulated in the perpendicular direction by a Gaussian,  $A_{\perp 0}(z, 0) = 2\sqrt{C_1} \exp(i\delta k z) \operatorname{sech}(\sqrt{C_1}z)$ , with  $L_x = 25$ ,  $C_1 = 0.07$ , and  $\delta k = -0.5$ . The initial electrostatic potential was adopted to be zero,  $\phi(x, z, 0) = 0$ .

rapidly dropped to less than 1/2 of its initial value and continued to reduce, longitudinal direction and obtained a highly asymmetric shape - steep on the rear side and very gentle on the front side. The maximum of the pulse propagated backwards, as governed by our choice of a negative parameter  $\delta k = -0.5$ , but it was spreading so fast that its rear edge was actually moving forward. The phase of the laser amplitude,  $\arg A_{\perp 0}$ , was found to be an approximately quadratic function of  $z$  that did not propagate (in the moving frame) along  $z$ . Instead, it was spreading for larger times. Such behavior is typical for the *chirped solitons*. As the soliton velocity, in the case of linear phase, is proportional to the gradient of the phase, the observed spatial spreading of the chirped structures can be attributed to the change of sign of  $d\theta/dz$  at  $z \sim 6$ .

In general, we may say that the solutions described here and in the preceding section are characterized by a chirp proportional to their peak power. Such chirp dependence was observed earlier for the pulses in optical fibers near linear resonances [115].

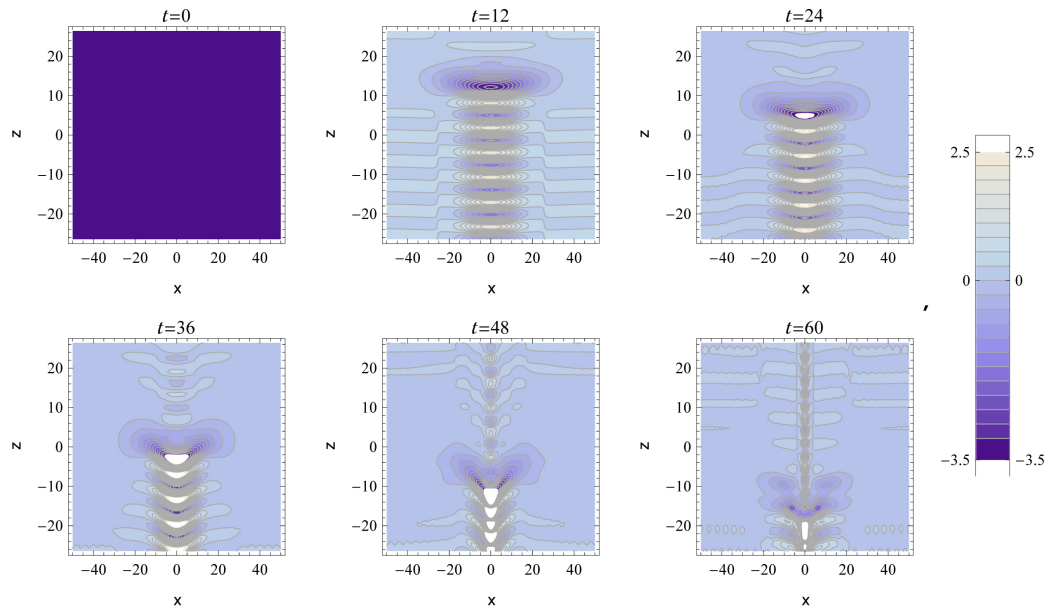


Figure 4.4: The evolution of the electrostatic potential produced by a weak intensity regime displayed in Figure 4.3.

#### 4.4.2 Evolution of the pulse in two dimensions: self focusing

First, we have studied the 2D evolution of the coupled laser pulse/wakefield structure in the weak intensity regime, using the small-amplitude 1D solution as the initial condition. In the perpendicular direction, we artificially introduced a Gaussian shape of the pulse, whose characteristic spatial scale was adopted to be roughly 6 – 8 time longer than the pulse length in the  $z$ - direction. For simplicity, we sought the solution in Cartesian coordinates,  $\nabla_{\perp}^2 = \partial^2/\partial x^2$ . These calculations were performed on a standard personal computer, using the numerical method of lines with  $64 \times 64$  points. Such, relatively small, resolution was sufficient to reveal the main features of the 2D evolution and to follow the pulse for times longer than  $t = 60$  in normalized units, during which the pulse travels approximately 17 cm in the laboratory frame. This is almost two times longer than the plasma length of 9.88 cm, quoted in Ref. [98]. The results are displayed in Figures 4.3 and 4.4. We found that a weak intensity structure is unstable in 2D, but the collapse is not very fast. We observed only a relatively slow transverse contraction for  $t > 48$ , which was different from what one expected intuitively. The simulations revealed that the velocity of propagation has the minimum in the centre. This is contrary to the expectation that a very strong laser pulse would push out all the electrons, so that the pulse, in the centre, propagate almost in a vacuum, by the speed of light. Instead, we have observed that the initial pancake folds, with the

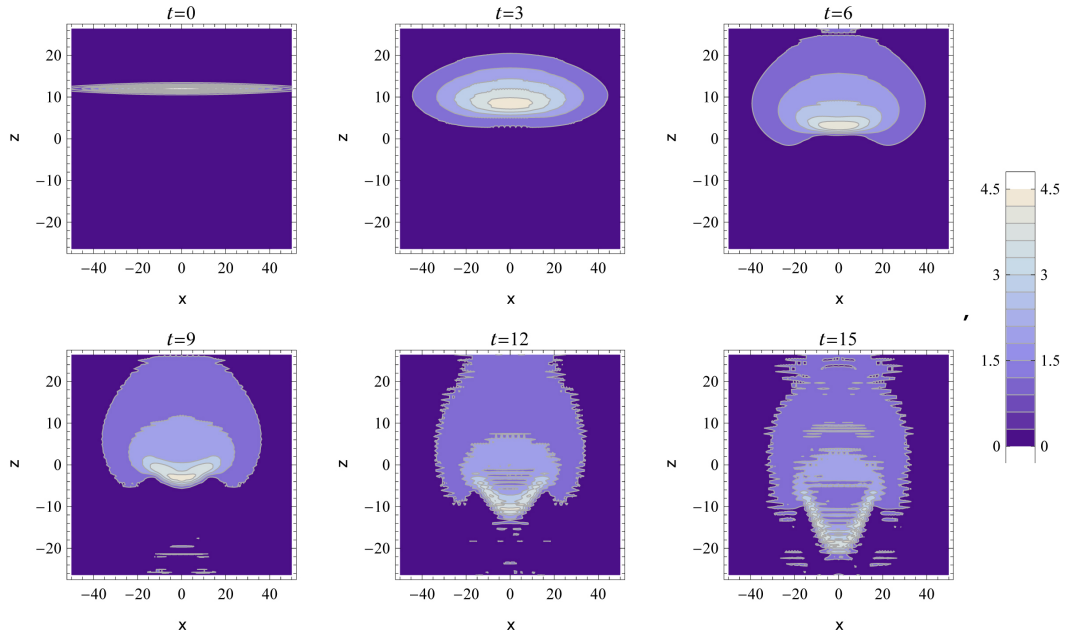


Figure 4.5: The evolution of the envelope of a laser pulse with the amplitude typical for the accelerator scheme under investigation here (referred to in the text as a moderate intensity regime). All parameters are the same as in Figure 4.3 except the amplitude, which is adopted as  $C_1 = 5.5$ .

wings moving forward while the central part is falling back, obtaining a V-shape at the time  $t \sim 24$ . For very large times, the oscillating wake of the structure collapsed and disintegrated into a sequence of filaments in the  $z$  direction, whose longitudinal and transverse dimensions were of the same order and considerably smaller than the initial length of the pulse.

We studied also the 2D evolution in a moderate intensity regime, adopting the initial condition in the form of a unchirped NLS soliton with  $C_1 = 5.5$ , that is propagating backwards with  $\delta k = -0.5$  (i.e., the same parameters as in the 1D case displayed in Figure 4.2). We followed its evolution for a longer time than in the 1D case, until  $t \gtrsim 15$ . During this time, the pulse travels approximately 4.5 cm, which is about half the length of the interaction chamber. The results are displayed in Figures 4.5 and 4.6. The folding of the pancake-like pulse and the creation of a V-shape was observed after  $t \sim 9$ , which is considerably earlier than in the weak intensity regime. Virtually no perpendicular contraction was observed for  $t \leq 15$ , while the longitudinal stretching due to the negative chirp was similar to that observed in the 1D case. The related diminishment affected mostly the laser envelope, while the electrostatic potential still featured a sizable amplitude; the depth of its first minimum was more than 50% of its

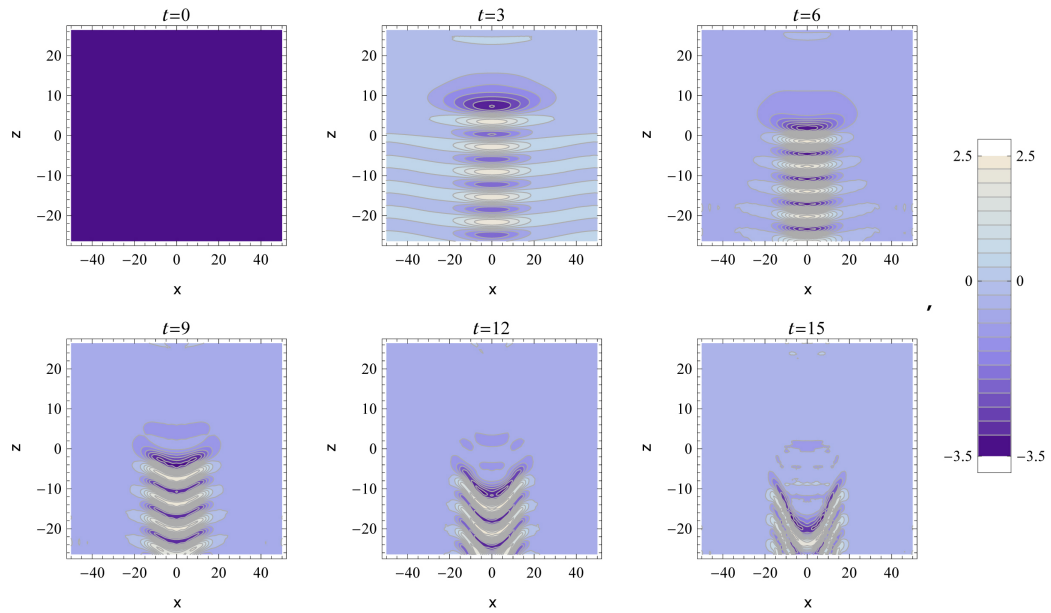


Figure 4.6: The evolution of the electrostatic potential produced by a moderate intensity regime displayed in Figure 4.5.

largest value, achieved shortly after the launch of the pulse. The potential minimum obtained a V-shape in the  $x - z$  plane, but its cusp was somewhat broader than that of the weak intensity structures.

## 4.5 Regime of very large intensities

Here we want to outline some important aspects relevant for the near-future LWF-based experiments.

First of all, we observe that it is possible to reach the high intensity regime keeping satisfied the condition  $L_z \ll L_\perp$ , i.e., preserving the applicability of the pancake approximation. (see Section 4.2.1). We expect that, in the near future, it might be technologically feasible to reduce the “pancake thickness”  $L_z$  to  $\sim 1/3$  of its present value reached in high-power lasers. In the case of FLAME, this corresponds to the reduction of  $L_z$  from almost  $10 \mu\text{m}$  to  $2 - 3 \mu\text{m}$ . Then, keeping the same maximum laser power  $W_{max}$  (for FLAME it is  $\sim 220 \text{ TW}$ ), we may also focus the beam to  $\sim 1/3$  of the spot size that is presently used in the wake field acceleration schemes with moderate laser intensities (for FLAME, this corresponds to the reduction of  $L$  from  $L_\perp$  from  $30 \mu\text{m}$  to  $10 \mu\text{m}$ ). In such a way, we reach the strong intensity regime with a pancake-shaped

pulse (i.e., the pulse length is still much smaller than its width). Within such ordering of the laser power and pancake geometry, our equations (4.3.8) and (4.3.9) can be applied also in the *strong intensity regime*.

Another important aspect is related to the saturation of the nonlinearity in the non-local response and the subsequent stabilization of localized structures. We readily note that in the regime  $|\phi| \gtrsim 1$  the nonlinear term is saturated. However, for such large amplitudes, using the representation of a modulated wave, equation (4.3.1), we find that the relative scaling of the terms on the left-hand-side of equation (4.3.3) is fundamentally different than in the case of moderate amplitudes. Obviously, the nonlinear term on the right-hand-side of equation (4.3.8) appears to be much larger than the linear terms, viz.,  $\phi/(1 - \phi) \gtrsim 1 \gg \omega/(\partial/\partial t) \sim (1/\omega^2)(\partial^2/\partial z^2)$ . In other words, the ordering (4.3.5) that is the basic assumption used in the derivation of the model equation (4.3.1) breaks down in the large amplitude regime. An appropriate scaling is obtained if we take the velocity  $u$  to be equal to the speed of light,  $u = 1$ , and that the frequency and the wavenumber satisfy the dispersion relation of the electromagnetic waves in vacuum,  $\omega = k$ . Then, from equations (4.2.30) and (4.2.31), dropping the nonresonant (second harmonic) terms, we readily obtain:

$$\left[ \frac{\partial}{\partial t} \left( 2i\omega + \frac{\partial}{\partial t} - 2\frac{\partial}{\partial z} \right) + \nabla_{\perp}^2 - \frac{1}{1 - \phi} \right] A_{\perp 0} \approx \left( 2i\omega \frac{\partial}{\partial t} + \nabla_{\perp}^2 + \frac{1}{\phi} \right) A_{\perp 0} = 0, \quad (4.5.1)$$

$$\frac{\partial^2 \phi}{\partial z^2} = \frac{(\phi - 1)^2 - 1 - |A_{\perp 0}|^2}{2(\phi - 1)^2} \approx \frac{\phi^2 - |A_{\perp 0}|^2}{2\phi^2}, \quad (4.5.2)$$

where we have expanded the nonlinear terms in the small quantity  $1/\phi \ll 1$  and used the assumption of the weak modulation  $\omega \gg \max(\partial/\partial t, \partial/\partial z)$ .

We note from equation (4.5.1) that the regime of very large intensities is physically different from that of the moderate intensities. The wave equation (4.5.1) describes an electromagnetic wave propagating in vacuum, with a “small” nonlinear term  $\propto 1/\phi$  added. This is due to the fact that the electron density perturbation, according to equation (4.2.28), is very large  $\delta n = n - 1 = \mathcal{O}(1)$ . This corresponds to the creation of *vacuum channels* in the plasma, that is well known from numerical simulations. However, for a 2D or a full 3D picture in the large amplitude regime, one needs to use the general equation (4.3.3), since the intensity  $\phi$  decreases radially, and close to the edges of the beam we are back to the  $\phi \ll 1$  regime. Obviously, such task is numerically more demanding, and it will be considered separately, in a forthcoming publication. Furthermore, huge electric fields arising from such electron density perturbation, may affect also the ions, whose dynamics also needs to be taken into account.

# Chapter 5

## Applications Towards Focusing: Quantum Plasma Lenses

In this Chapter, we have carried out a preliminary investigation to conceive a quantum plasma lens. We have applied the theory of ‘quantum’ description of the relativistic electron or positron beam propagation via self-consistent PWF excitation provided in Chapter 3. The transverse effects experienced by the beam is investigated and the scheme of the plasma lens in the overdense regime has been reviewed as possible application to design new final focusing devices for the compact generation of a linear collider.

### 5.1 Basic concept of plasma lens

The plasma lens is a thin plasma slab that is used to focus charged particle beams as well as laser pulses. Due to the electromechanical actions that electromagnetic (e.m.) or charged particle beams can experience, the plasma can produce acceleration or focusing on a beam traveling through it. By making use of a thin plasma lens, it is possible to compress and focus a laser or charged particle beam outside of the plasma in the vacuum region. Historically, plasmas had been used to focus a continuous low-energy electron beam by beam-ionized gas within a cathode ray tube way back in 1922 [116]. In 1987 Chen first proposed the concept that plasma lenses could form an immensely strong final focusing system for a linear collider [117]. At that time, the analog focusing of e.m. radiation beams by means of a plasma was already well developed. However, it became more popular just when the first proposals of large amplitude plasma wave excitation driven by e.m. wavepackets or very short e.m. pulses with a transverse profile appeared in literature. Then, the compression and focusing of

relativistic charged particle beams or high e.m. intensity laser beams through Laser-driven [4, 5, 14–16] or charged particle beam-driven [25–27] excitations have been of great interest during the last two decades.

In PWF-based plasma lens, when a relativistic electron (positron) beam passes through a plasma slab with a thickness of few of  $c/\omega_p$  ( $\omega_p$  is the plasma frequency), since the time of beam-plasma interaction is rather small, the radial component of the wake fields produces a bending of the trajectories inward to the propagation axis. Once the particles are again in vacuum, the wake fields are off. The repulsive electric force between the particles due to the beam space charge is initially almost balanced by the attractive magnetic force and then they will converge to a minimum spot (focus) [117–120].

Several analytical, numerical, as well as experimental investigations have been carried out to describe the behavior of the plasma lens characterized in the two regimes depending on the ratio of plasma density  $n_p$  to beam density  $n_b$ . In an overdense plasma lens where  $n_p \gg n_b$ , the space charge of the electron beam is fully neutralized by the plasma through the displacement of plasma electrons by the beam electrons, resulting in beam self-focusing through its own magnetic field [121–125]. In the underdense lens, where  $n_p \lesssim n_b$ , all plasma electrons are displaced by the beam electrons, and the focusing force is due to the remaining plasma ions [119, 126].

## 5.2 Thin plasma lens approximation

With a plasma slab of very small thickness, the so called *thin plasma lens approximation* [117, 119, 120] corresponds to a *kick approximation*, the beam wave function remains almost unchanged except for the appearance of a finite value of a chirping phase factor. Thus the transverse beam spot size remains almost unchanged inside the plasma lens. For instance, a beam with an initial  $\sigma_0 = \sigma(z=0)$  and  $\sigma'_0 \equiv (d\sigma/dz)_{z=0} = 0$  [ $\sigma(z)$  being the transverse beam spot size] enters a thin plasma slab of thickness  $l$ , according to the *thin plasma lens approximation*

$$\sqrt{Kl} \ll 1,$$

where  $K$  is the focusing strength. In this approximation, the focal length of the lens becomes

$$f = |\rho(z=l)| = \frac{1}{Kl} \left( 1 - \frac{\epsilon_r^2}{K\sigma_0^4} \right)^{-1}, \quad (5.2.1)$$

where  $\rho(z) = \sigma(z)/\sigma'(z)$  can be interpreted as the bending or curvature radius of the surface normal to envelope trajectory that intersects the longitudinal axis at location  $z$

and  $\epsilon_t$  is the transverse thermal emittance of the beam. Typically, in a strong plasma lens the focusing effect dominates the emittance spreading, i.e.,  $\epsilon_t^2/K\sigma_0^4 \ll 1$  is satisfied. Thus, with this approximation, Eq. (5.2.1) becomes

$$f \simeq \frac{1}{KI}. \quad (5.2.2)$$

In this Chapter, on the basis of the theory developed in Chapter 3, we propose a plasma lens to describe the transverse effect on a cold relativistic electron/positron beam traveling along  $z$ -axis through a magnetized thin plasma slab in the regime of *strong nonlocality*. We describe the beam wave function  $\psi_m$  in terms of the beam density  $\rho_b$ , i.e.,  $\psi_m = \sqrt{\rho_b} e^{i\theta}$ , where  $\theta$  is the eikonal. According to the picture of surface normal to the envelope trajectories given above,  $\rho(z)$  is the bending radius, at each  $z$ , of the locus of the points of constant phase  $\theta$  provided by the beam wave function. A preliminary analysis to investigate the transverse effect of the beam spot size to reach the nano scales in the final focus is carried out in the aberration-less approximation.

We investigate the transverse dynamics of an electron/positron beam, whose initial distribution is purely Gaussian. We also assume that the beam is traveling through a plasma slab (plasma lens), along the external magnetic field  $\mathbf{B}_0$  and subsequently in a vacuum (where the external magnetic field is present as well). By adopting the quantum model of charged particle beam described in Chapter 5, we study the physical conditions that allow the beam to experience a strong focusing outside the plasma lens. The latter, indeed, considered here, is sufficiently thin to provide a strong transverse kick to the beam particles that changes suddenly their momentum distribution but leaves their space distribution practically unchanged within the lens.

### 5.3 Governing equations

We recall the quantum description of the self-consistent system of equations (3.3.3) and (3.3.4) from Chapter 3. For strongly nonlocal nonlinear regime, assuming that  $m$  is fixed to 0, the wave-like description of the electron/positron transport within a lens of length  $l$  and subsequently *in vacuo* is provided by the following pair of governing equations

$$i\epsilon_c \frac{\partial \psi}{\partial \xi} = -\frac{\epsilon_c^2}{2} \frac{1}{r_\perp} \frac{\partial}{\partial r_\perp} \left( r_\perp \frac{\partial \psi}{\partial r_\perp} \right) + U [ |\psi|^2 ] \psi + \frac{1}{2} K r_\perp^2 \psi \quad (5.3.1)$$

$$\frac{1}{r_\perp} \frac{\partial}{\partial r_\perp} \left( r_\perp \frac{\partial U}{\partial r_\perp} \right) = \chi |\psi|^2, \quad (5.3.2)$$

where  $U(r_{\perp}, \xi)$  is the potential energy in plasma or in vacuo, respectively, depending on the constant

$$\chi = \begin{cases} (k_{pe}^4/k_{uh}^2)(N/2\pi n_0\gamma_0\sigma_z) \equiv \chi_w, & \text{for } 0 \leq \xi \leq l \\ -2q^2N/\sigma_z m_0\gamma_0^3 c^2 \equiv \chi_{sp}, & \text{for } \xi > l \end{cases}$$

### 5.3.1 Aberration-less approximation

Note that the strongly nonlocal regime we have assumed is compatible with the physical condition of strong beam focusing. Then, according to Ref. [127], we can assume that the beam density is sufficiently picked around the propagation direction, that  $U(r_{\perp}, \xi)$  can be expanded in power of  $r_{\perp}$ , around  $r_{\perp} = 0$ , up to the second one. Therefore,

$$U = \frac{1}{2} \frac{\chi}{\sigma^2(\xi)} r_{\perp}^2, \quad (5.3.3)$$

where  $\sigma(\xi)$  is the beam spot size. In fact, the collective effects that  $U(r_{\perp}, \xi)$  accounts for depends on the beam scale. A complete set of eigenfunctions of Eq. (5.3.2) consistent with Eq. (5.3.3) are given by the Laguerre-Gauss solutions. For sake of simplicity, among them we take the fundamental mode (aberration-less solution), i.e.

$$\psi(r_{\perp}, \xi) = \frac{1}{\sqrt{\pi}\sigma_c(\xi)} \exp\left(-\frac{r_{\perp}^2}{2\sigma_c^2(\xi)} + \frac{ir_{\perp}^2}{2\epsilon_c\rho_c(\xi)}\right) \exp[i\phi_c(\xi)], \quad (5.3.4)$$

where  $\sigma_c$  is the transverse rms of the quantum single-particle wave function (i.e., single quantum electron ray). Note that  $\sigma_c(\xi) \ll \sigma(\xi)$ . Furthermore, it is easily seen that the quantities  $\sigma_c$ ,  $\rho_c$  and  $\phi_c$  satisfy the following set of coupled ordinary differential equations, viz.

$$\frac{1}{\rho_c} = \frac{1}{\sigma_c} \frac{d\sigma_c}{d\xi}, \quad (5.3.5)$$

$$\frac{d\phi_c}{d\xi} = -\frac{\epsilon_c}{\sigma_c^2}, \quad (5.3.6)$$

$$\frac{d^2\sigma_c}{d\xi^2} + \bar{K}\sigma_c - \frac{\epsilon_c^2}{\sigma_c^3} = 0, \quad (5.3.7)$$

where  $\bar{K}(\xi) = K + \alpha/\sigma^2(\xi)$ . According to Ref. [127], the evolution of the quantum single-particle spot size contains the same information carried out by an evolution equation for the beam spot size (description of the beam as a whole constituted by Fermions). Such an evolution equation exhibits, through the collective interaction, an

amplification of the single-particle quantum effects. In fact, the evolution equation for the single-particle spot size, say  $\sigma_c$ , contains the fundamental emittance  $\epsilon_c$ . Then, the assumption  $\sigma \approx \sqrt{N_\perp} \sigma_c$  and  $\epsilon \approx N_\perp \epsilon_c$  define transverse beam spot size and emittance of the lowest quantum state compatible with the condition of *non overlapping* of the Fermions. Here  $N_\perp$  is the number of quantum electron rays that are intersecting the transverse plane (i.e., number of particles distributed in a single transverse plane). Therefore, we easily obtain (Sacherer equation) [128]

$$\frac{d^2\sigma}{d\xi^2} + K\sigma + \frac{\chi}{\sigma} - \frac{\epsilon^2}{\sigma^3} = 0. \quad (5.3.8)$$

Note that this macroscopic equation, written for the beam spot size at the lowest quantum state, is fully equivalent to the one for the quantum single-particle averaged motion in the presence of collective effects (for details, see Ref. [127]). This provides a macroscopic manifestation of the single-particle quantum effects.

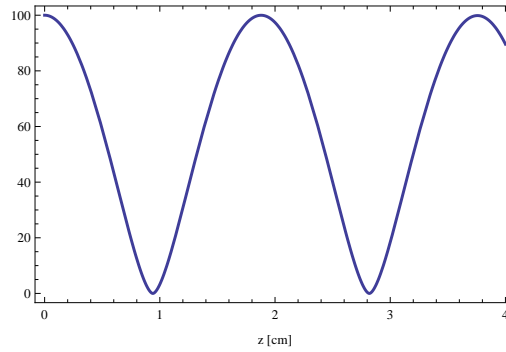


Figure 5.1: Periodic Breathing of  $\sigma^2$  [in  $\mu\text{m}^2$ ] as a function of  $z$  [in cm] inside the plasma with the initial condition of  $\sigma(0) = \sigma_0$  and  $\sigma'(0) = 0$ .

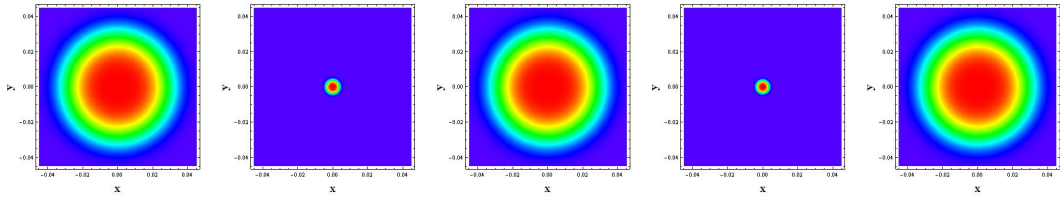


Figure 5.2: Density plot of  $|\psi^2|$  in transverse  $x - y$  plane corresponding to FIG. 1. The focusing and defocusing of the profile indicates the periodicity of  $\sigma$  inside the plasma

### 5.3.2 Inside the slab

We consider that the beam enters a thin plasma slab (plasma lens) of thickness  $l$ . According to both the conventional and the quantum theories, i.e., [117, 119, 120] as

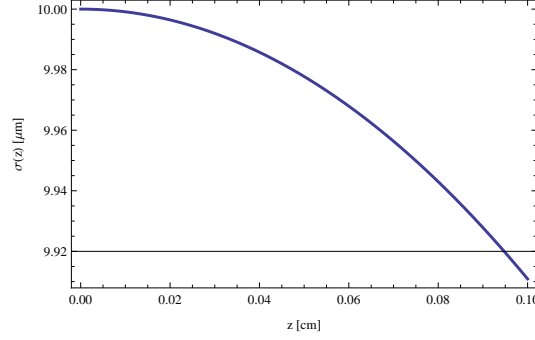


Figure 5.3: Variation of  $\sigma$  [in  $\mu\text{m}$ ] as a function of  $z$  [in cm] inside the lens with the initial condition of  $\sigma(0) = \sigma_0$  and  $\sigma'(0) = 0$ . For a lens of thickness  $l = 1$  mm, it has been found that  $\sigma(l) = 9.91 \mu\text{m}$  and  $f = 5.55$  cm.

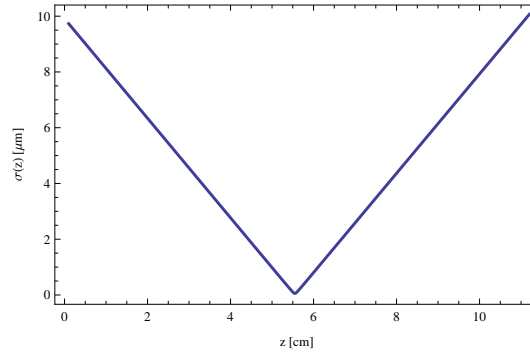


Figure 5.4: Variation of  $\sigma$  as a function of  $z$  in the vacuum with initial condition  $\sigma(0) = \sigma(l)$  and  $\sigma'(0) = \sigma(l)/\rho(l)$ .  $\sigma$  experiences strong focusing due to the dominance of the magnetic field term  $K$ . When  $\sigma$  becomes very small near the final focus, the space charge effects becomes dominant compared magnetic field and it blows up. The beam spot size in the interaction point is  $\sigma^* = 56$  nm.

well as wave description, the beam spot size remains almost unchanged inside the slab, i.e.,  $\sigma(l) \simeq \sigma_0$ , where  $\sigma_0$  is the initial (while entering the plasma) transverse beam spot size. Consequently, the focusing strength becomes almost constant, i.e.,  $\bar{K} = \bar{K}(\sigma_0) \simeq K + \chi_w/\sigma_0^2$ . Thus, with the approximation of thin lens, i.e.,  $\sqrt{\bar{K}l} \ll 1$  and strong focusing case, i.e.,  $\epsilon^2/\bar{K}\sigma_0^4 \ll 1$ , the focal length is

$$f = |\rho(\xi = l)| \simeq \frac{1}{\bar{K}l}. \quad (5.3.9)$$

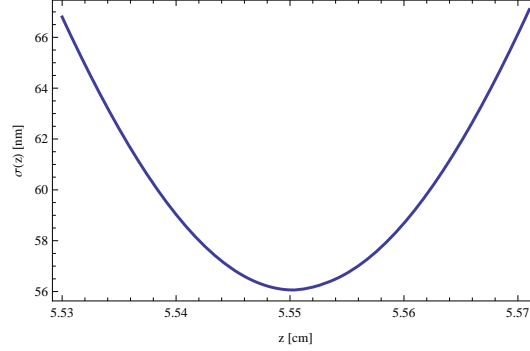


Figure 5.5: A closer look on the variation of  $\sigma$  around the interaction point. It shows the hyperbolic structure of  $\sigma$

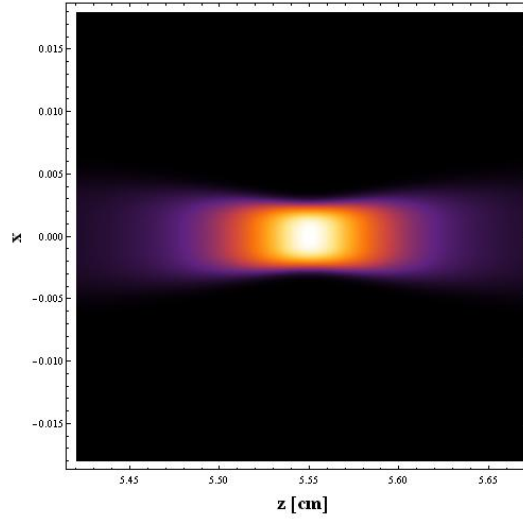


Figure 5.6: The cross section of  $\sigma$  with continuous  $z$  around the interaction point corresponding to Figure 5.5, showing the hyperbolic shape

### 5.3.3 In vacuo

Now, specializing the expansion (5.3.3) for the case of motion in vacuo, the effective focusing strength is now  $\bar{K}(\sigma) = K + \chi_{sp}/\sigma^2(\xi)$ , so that Eq. (5.3.8) becomes

$$\frac{d^2\sigma}{d\xi^2} + K\sigma + \frac{\chi_{sp}}{\sigma} - \frac{\epsilon^2}{\sigma^3} = 0. \quad (5.3.10)$$

Note that during the evolution in vacuo the effective focusing strength  $\bar{K}$  is no longer constant as inside the lens. Note also, since  $\chi_{sp}$  is a negative quantity, there is an interplay among the focusing term  $K\sigma$ , the space charge blow up  $\chi_{sp}/\sigma$  and the beam spreading term  $\epsilon^2/\sigma^3$ . As  $\sigma$  becomes smaller and smaller, during the process of focusing, the last two terms become greater and greater. For suitable choices of the

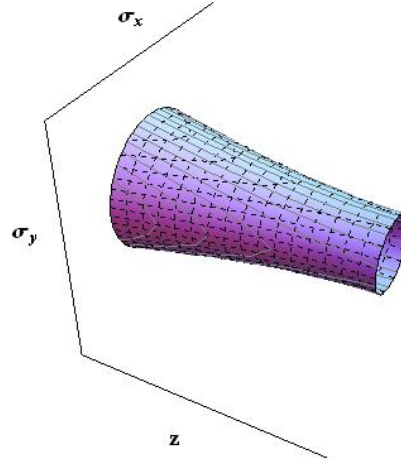


Figure 5.7: The focusing of  $\sigma$  with continuous  $z$  till the interaction point shows the trumpet structure

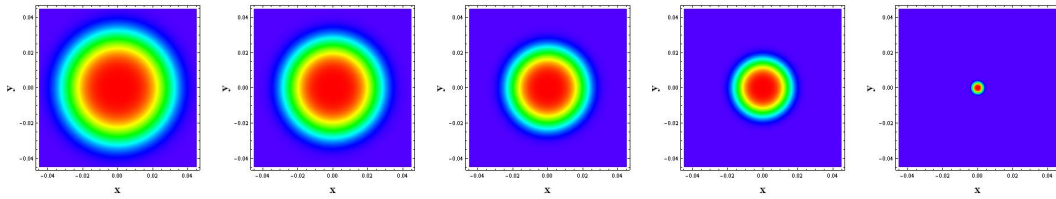


Figure 5.8: Density plot of  $|\psi|^2$  in the transverse  $x - y$  plane at the final focus corresponding to Figures 5.5 and 5.6

parameters, one may expect that  $\sigma$  reaches a minimum value for some  $\xi$ .

## 5.4 Numerical evaluation

We consider the quantum regime such that the overlapping of the single-particle wave functions is absent and the quantum paraxial beam behavior takes into account the individual quantum nature of the particles (uncertainty principle and spin). This implies that the inter-particle distance is much greater than the thermal de Broglie wavelength. For instance, this condition is attainable for a typical range of the beam densities  $n_b \sim 10^{13} - 10^{16} \text{ cm}^{-3}$ , energies  $\gamma_0 \sim 10^2 - 10^4$ , and relativistic transverse temperature  $T_{\perp} \sim 10^2 - 10^3 \text{ K}$ . Thus, we can show that in the region of the interaction point (final focusing stage of a linear collider), our beam can reach spotsizes that are roughly ranging from a few 0.1 to a few 10 nm *nanobeams*. We chose  $n_0 = 10^{17} \text{ cm}^{-3}$ ,  $n_b = 10^{16} \text{ cm}^{-3}$ ,  $\sigma_0 = 10 \mu\text{m}$ ,  $\sigma_z = 1 \text{ mm}$ ,  $\epsilon = 10^{-9} \text{ cm rad}$ ,  $\gamma_0 = 10^4$ , and  $B_0 = 10^4 \text{ Gauss}$ .

### 5.4.1 Inside the lens

We numerically solved Eq. (5.3.8) for the above set of parameters with the initial condition of  $\sigma(0) = \sigma_0$  and  $\sigma'(0) = 0$ . For a thick plasma as medium, the periodic transverse breathing of  $\sigma^2$  as a function  $z$  is observed with a maximum value of  $\sigma_0$  shown in Figure 5.1. The corresponding density plot of  $|\psi|^2$  also represents the periodic focusing and defocusing with  $z$  as shown in Figure 5.2. When the thick plasma medium is replaced by a slab of thickness  $l = 1$  mm, the periodic breathing of  $\sigma$  is no longer existing, rather it shows a slight bending of few fractions of  $\mu\text{m}$  keeping the value of  $\sigma$  almost unchanged inside the slab, as shown in Figure 5.3. For a lens of thickness  $l = 1$  mm, we numerically found that  $\sigma(l) = 9.91\mu\text{m}$ , which is almost the same as  $\sigma_0$  and in accordance with the prediction of thin plasma lens theory. The focal length is calculated numerically as  $f = 5.55$  cm, which is also in accordance with the theoretical approximation  $f \simeq 1/\bar{K}l$ .

### 5.4.2 In vacuo

When the beam leaves the lens and goes into the vacuum,  $\sigma$  is now governed by Eq. (5.3.10). We numerically solved Eq. (5.3.10) for the same set of parameters with the initial condition that we get at the end of the plasma slab, i.e.,  $\sigma(0) = \sigma(l)$  and  $\sigma'(0) = \sigma'(l) = \sigma(l)/\rho(l)$ . A strong focusing of  $\sigma$  until  $f$  is observed due to the dominance of the magnetic field term  $K\sigma$  over the space charge term  $\chi/\sigma$ , as shown in Figure 5.3. When  $\sigma$  becomes much smaller reaching  $f$ , the term  $\chi/\sigma$  becomes dominant over  $K\sigma$ , and it blows up afterwards. A closer look on the variation of  $\sigma$  around the interaction point and the corresponding cross section with continuous  $z$  are shown in Figures 5.5 and 5.6, respectively. Both show the hyperbolic structure of  $\sigma$  around the interaction point. Thus the focusing of the beam till the interaction point has a trumpet structure, as shown in Figure 5.7. The corresponding density plot of  $|\psi|^2$  till the final focus in the transverse  $x - y$  plane is shown in Figure 5.8. We found the beam spot size at the final focus is  $\sigma^* \simeq 56$  nm which is three order smaller than the initial beam spot size.

We would like to point out that the analysis has been carried out in the aberration-less approximation. Due to the feature of the medium (namely, the plasma), the linear focusing cannot be provided for all the values of the radial coordinate. In fact, distortions more or less important come into play during the focusing process. They cause the enhancement of the minimum beam spot size (aberrations). If the lens is conceived to be used at the final focusing stage of a linear collider, then such an enhancement of the minimum spot size causes the reduction of the luminosity at the interaction point.

In addition, collective effects on the classical and quantum scale such as beam-beam interaction and exchange interaction of a fermion system affect the luminosity. On the other hand, these two aspects come into play with special importance because our spot sizes are reduced to the nanoscales.

On the basis of the above considerations, a more careful analysis is under way. It takes into account both aberrations and collective effects related to both beamstrahlung and superposition of the single particle wave functions that we have disregarded in the present analysis.

Finally, we would like to emphasize that the transverse beam geometry encountered in conventional compact linear colliders differs from the cylindrically symmetric one that has been assumed here. This makes not easy the comparison of the two cases.

# Conclusion

In this PhD thesis work, we have provided a self-consistent description of the three-dimensional effects produced by the wake field excitation of ultra-intense charged-particle beams and e.m. radiation pulses, respectively.

## Charged-particle beams

We have analyzed the nonlocal effects that take place when a cold relativistic electron/positron beam is travelling in a cold, collisionless, magnetized plasma in overdense regime. This has been done by adopting a wave description in paraxial approximation for two different regimes, i.e., “quantum” and “thermal”. The collective effects have been included by the Hartree’s mean field approximation.

In the limit of sufficiently long beam, we have restricted our analysis to study the transverse dynamics of the beam and neglect its variations in the direction of propagation. In the quantum regime, the model has been further simplified by considering typical range of densities, energies and temperatures of the particles that allow us to disregard the quantum collective nature of the beam that is associated with the overlapping of the single particle wave functions. Under these physical conditions, the collective nature of the beam manifests only through the self-consistent macroscopic electromagnetic field (PWF), created by the charge density and the current density of the beam. It is worth noting that the interplay with the collective action of the wake field excitation permits the quantum nature of a single particle to manifest on the macroscopic level. Additionally, the effects of the orbital and spin angular momenta are involved in the mechanism for the beam vortex states with or without the wake field collective effect. The use of the Hartree’s mean field procedure, allowed us to describe the beam by the single-particle spinor, whose dynamics is governed by the appropriate two-dimensional spinorial Schrödinger equations, coupled with the Poisson’s equation for the wake potential. In cylindrical symmetry, we have reduced the above system of equations into a pair of coupled governing equations in scalar form. Then, our description has been reduced to a wave function whose squared modulus is proportional to the beam density. We have solved the pair of governing equations,

analytically as well as numerically for linear and nonlinear regimes.

Several interesting phenomena have been described:

- We have demonstrated the possibility of coherent, stable hollow linear and nonlinear solutions that are rotating ( $m \neq 0$ ).
- In linear regime, we have found quantum vortex states in the form of Laguerre-Gauss beams with a central structure surrounded by circular ripples associated with the given eigenvalues of the orbital angular momentum. The beam also exhibits a periodic breathing of the spot size described by the Ermakov-Pinney equation (3.5.5). These oscillations are the beam betatron oscillations in the presence of the focusing effects provided by the external magnetic field. When the diffraction is balanced by the restoring force due to the external magnetic field these oscillations have not been observed and the system is in equilibrium condition.
- In nonlinear regime, such rotating structures ( $m \neq 0$ ) which possess such topology are often called *the ring solitons* in the literature. In the local regime, a vortex soliton can be heuristically explained as a standard slab NLS soliton, somewhat modified by the curvature effects, that is trapped in the minimum of the effective external potential  $V(r)$  in Eq. (3.3.3), where  $V(r) = (1/2)(Kr_{\perp}^2 + m^2\epsilon^2/r_{\perp}^2)$ . From numerical and laboratory experiments (e.g. with Bose-Einstein condensates), it is known that in the presence of an external potential, the solitons often behave as quasiparticles. Their coherence properties and the shape are not much affected, but their propagation becomes determined by the external potential. In a potential well, a soliton remains trapped and exhibits a periodic (bouncing, or wiggling) motion. Conversely, the stationary structures that lie at the bottom of the potential well and do not move back and forth, may acquire a 'breathing' behavior due to the partial loss of coherence. Namely, the soliton tends to achieve coherence by shedding some of its excess content, but the latter gets reflected back in the potential well, and the whole structure appears to be periodically swelling and contracting. However, this simple heuristic explanation is not applicable to the fundamental ( $m = 0$ ) 2D solitons, for which the curvature effects are strong at the bottom of the potential well,  $r_{\perp} = 0$ , and a slab NLS soliton is not a good approximation for the trapped structures. As it has been argued in sec. 3.6.1, the appropriate envelope description on which our analytic solutions are based, Eqs. (3.6.3) - (3.6.5), could be resolved only in the regime when the beam spot size was much larger than the plasma wavelength, i.e. when the

relation between the plasma wake field response,  $U_w$ , and the beam probability density,  $\psi_m$ , was strictly local.

- In nonlinear strictly local regime, the existence of quantum beam vortices in the form of ring solitons has been shown numerically. Due to the interplay between the strong transverse effects of the PWF (collective and nonlinear effects) and the external magnetic field, the envelope oscillations with weak and strong focusing and defocusing have been observed for different values of  $m$ . On the basis of the similarity with the linear states, we have arrived at the conclusion that the nonlinear states with  $m \neq 0$  are associated with the vortex effect introduced by the orbital angular momentum. The conditions for instability/stability criteria for collapse that include the quantum nature of the beam particles have been also discussed.
- In order to investigate the effects of the moderate nonlocality in the nonlinear plasma response, we have solved numerically the pair of governing equations (3.3.3) and (3.3.4). The existence of stable hollow (ring) structures has been demonstrated also in this regime, after solving the full system of nonlinear equations in the cylindrically symmetric case. In particular, we have followed the evolution of a quantum ring in the form of an envelope dark soliton that has been observed to be stable for a very long time. Nevertheless, it appears to perform relatively small breathing as well as violent oscillations.
- Remarkably, besides the modulus of the wave function through the rotating structures, also the phase exhibits a topological structure characterized by the helicity which actually accounts for both orbital and spin angular momenta for non zero vortex charge  $m$ . Such a property has been predicted in both the linear and nonlinear cases.
- This investigation seems to be useful to design the plasma-based focusing schemes. In particular, in the quantum regime, it seems to work to focus relativistic electron/positron beams to the nanoscales (nanobeams) for very compact final stage of linear colliders.

## Electromagnetic radiation pulses

We have theoretically studied the selfconsistent interaction between an ultra-strong, ultra-short laser pulse in the form of a pancake ( $L_z \ll L_\perp$ ) and an unmagnetized plasma with the ions taken to be immobile. Within the framework of the laser wake field excitation, our study has been mainly referred, as a concrete example, to the FLAME

laser which is currently employed as a facility in the Frascati National Laboratories of INFN for different plasma-based acceleration projects including the self-injection case. For the maximum laser power  $W_{max} \sim 220$  TW, we have considered three different regimes of the laser intensities, corresponding to different transverse spot sizes of the pancake, respectively. Since in our physical problem the laser intensity ranges from  $10^{14}$  to  $10^{20}$  W/cm<sup>2</sup>, the motion of the plasma electrons has been assumed to be in the fully relativistic regime. In addition, due also to the concomitant role of the high intensity and the high gradient of the laser field profiles, the radiation pressure effects (ponderomotive force) fairly overcome those arising from the electron kinetic pressure, so that the plasma can be regarded as being cold. We have adopted a fluid plasma model, described by the relativistic Lorentz-Maxwell equations, from which we have derived and solved numerically the nonlinear equations that describe a plasma penetrated by an ultrashort, ultrastrong laser pulse, in the fully relativistic regime. We used the numerical method of lines and the calculations were performed on a standard PC. To derive those equations, we have first determined the leading order part of our set of fluid equations in terms of a stationary 1D solution propagating with the speed of light. We have showed that, in the reference frame that is moving at the group velocity of the laser light, this solution have allowed us to reduce our system of fluid equations in a pair of coupled nonlinear partial differential equations for the four-potential. They describe the spatio-temporal evolution of the modulated e.m. wave that is coupled with the Langmuir wave via the nonlinearities arising from the relativistic effects. A Zakharov-like system of equations has been obtained beyond the slowly-varying amplitude approximation. It consists of a parabolic wave equation governing the nonlinear high-frequency propagation of  $A_{\perp 0}$  that is coupled with the slow plasma response equation through the electric potential variation that, in turn, is driven by  $A_{\perp 0}$ .

The investigation can be summarized as follows:

- In the weak and moderate intensity regimes, a nonlinear Schrodinger equation with a reactive nonlocal nonlinear term has been obtained and numerically studied in both 1D and 2D cases. The evolution of the pancake has been followed for times that are comparable with the transit time of the pulse through the accelerators interaction chamber ( $\sim 10$  cm) and studied the interplay between the spreading and the collapse (filamentation) of the pulse in the transverse direction, in spite of the numerical limitations imposed by the maximum resolution of  $64 \times 64$  points, that we have used.
- We have shown that the 2D evolution of a pancake in the weak and moderate intensity regimes is unstable, but the collapse is not very fast. We have followed

the evolution until the times during which the pulse travels (in the laboratory frame) the distance of about 17 cm, which is almost two times longer than the actual size of the interaction chamber in the laser accelerator device. While the envelope of the laser pulse was not much affected by the collapse, a relatively slow transverse contraction of the electrostatic potential was observed. In addition, we would like to emphasize that pulses whose intensities fall in the weak or moderate intensity ranges behave similarly to the standard NLS solitons and survive unchanged during a time sufficiently longer than required for the laser accelerator scheme. Thus, within this preliminary analysis, we do not expect that the transverse collapse constitutes a critical limitation for the accelerator scheme under consideration here.

- In the strong intensity regime, we have outlined the role of the saturation of the nonlinear and nonlocal plasma response relevant to the pancake self-consistent evolution. For the typical maximum power and suitable choice of the longitudinal and the transverse dimensions of FLAME that preserve the 1D hydrodynamical approximation (see Section 4.2.1), we have found the appropriate set of Zakharov equations governing the pancake evolution that we have compared to the corresponding set of equation valid for the weak and moderate intensity regimes.
- Remarkably, our approach provides a physical model in terms of the pair of coupled nonlinear partial differential equations (Zakharov-like system), widely used in plasma physics and in many other areas of nonlinear physics, that give suitable and appropriate descriptions of the laser-plasma interaction in the diverse regimes considered in this paper. Their analytical and numerical solutions (the latter have been obtained by a standard PC) may be very helpful and relevant to the interpretation of the results given by the standard simulation codes presently widely employed to describe the very violent self-consistent laser-plasma interactions.
- We want to outline that a special care must be taken when the longitudinal non-locality, as described by the pair of equations (4.3.8) and (4.3.9), is considered under the assumption such that  $\phi \sim 1$ . In fact, for consistency, one must account for the feedback from the electrostatic wake (which is a spatially extended structure) to the electromagnetic pulse (which is localized in the direction of propagation).
- Although the classical works [4,5,14,15,109–113] regard the relativistic plasma

in a moderate intensity regime as a cold fluid [108], it is worth noting that the nonlinear contribution to the off-diagonal terms in the electron stress tensor may give rise to the non-curlfree component of the time dependent ponderomotive force [129], that is one among the known mechanisms for the generation of quasi-stationary, mega-Gauss magnetic fields. Alternatively, it is usually thought [106] that the creation of a quasistationary magnetic field by a laser pulse with a duration  $< 0.1$  ps, in a homogeneous, collisionless, and tenuous plasma, is likely to come from the jets of fast electrons arising in laser plasma. These jets are subject to the Weibel instability, leading to the current filamentation and the generation of a magnetic field [130]. As the latter is located mostly in the plasma wake, behind the main pulse [106, 130], it is not expected to affect significantly the propagation of the laser pulse. For the spatial structure of such wake magnetic field see e.g., [131] and references therein. The magnetic field has been known to have a focusing effect on relativistic electrons in the plasma wakefield accelerator context [132]. The experimental results definitely indicate that the lifetimes of magnetic fields are considerably longer (by orders of magnitude) than the laser pulse duration [106]. The role of the self-generated magnetic field is beyond the scope of the present work, and it will be the subject of a future study.

# List of Publications related to the thesis

R. Fedele, **F. Tanjia**, S. De Nicola, and D. Jovanović, and C. Ronsivalle “Wave theories of non-laminar charged particle beams: from quantum to thermal regime”, Submitted.

**F. Tanjia**, “Self-consistent Plasma Wake Field Interaction and Ring Solitons in paraxial Beam Transport”, to be published in *Il Nuovo Cimento C - Colloquia and Communication in Physics* (Invited Article as a special communication by the committee of the *XCVIII Congresso Nazionale, Società Italiana di Fisica*, Napoli, Italy).

**F. Tanjia**, R. Fedele, S. De Nicola, D. Jovanović, and A. Mannan, “The quantum plasma lens concept: a preliminary investigation”, to be published in *J. Plasma Phys.*

D. Jovanović, R. Fedele, **F. Tanjia**, S. De Nicola, and M. Belić, “Coherent quantum hollow beam creation in a plasma wakefield accelerator”, *J. Plasma Phys*, in press, doi:10.1017/S0022377813000111.

R. Fedele, **F. Tanjia**, S. De Nicola, D. Jovanović, and P. K. Shukla, “Quantum ring solitons and nonlocal effects in plasma wake field excitations”, *Phys. Plasmas* **19**, 102106 (2012).

D. Jovanović, R. Fedele, **F. Tanjia**, and S. De Nicola, “Quantum ring soliton formation by strongly nonlocal plasma wake field response to a relativistic electron beam”, *Eur. Phys. Lett.* **100**, 5502 (2012).

D. Jovanović, R. Fedele, **F. Tanjia**, and S. De Nicola, “Nonlocal effects in the self-consistent nonlinear 3D propagation of an ultrastrong, femtosecond laser pulse in plasmas”, *Eur. Phys. J. D* **66**, 328 (2012).

R. Fedele, **F. Tanjia**, S. De Nicola, D. Jovanović, and P. K. Shukla, “Self consistent nonlinear transverse quantum dynamics of a cold relativistic electron beam in a magnetized plasma”, *AIP Conf. Proc.* **1421**, 212 (2012).

**F. Tanjia**, S. De Nicola, R. Fedele, P. K. Shukla, and D. Jovanović, “Quantumlike description of the nonlinear and collective effects on relativistic electron beams in strongly magnetized plasmas”, *Proc. 38th EPS Conf. on Plasma Physics, Strasbourg, France* **35G**, P5.021, ISBN 2-914771-68-1 (2011).

R. Fedele, **F. Tanjia**, S. De Nicola, P. K. Shukla, and D. Jovanović, “Self consistent thermal wave model description of the transverse dynamics for relativistic charged particle beams in magnetoactive plasmas”, *Proc. 38th EPS Conf. on Plasma Physics, Strasbourg, France* **35G**, P5.006, ISBN 2-914771-68-1 (2011).

D. Jovanović, R. Fedele, **F. Tanjia**, and S. De Nicola, “Propagation of ultrastrong femtosecond laser pulses in PLASMON-X”, *Proc. 38th EPS Conf. on Plasma Physics, Strasbourg, France* **35G**, O3.205, ISBN 2-914771-68-1 (2011).

# Appendix A

## Kinetic model: The Vlasov-Maxwell system

The kinetic model of plasma was developed by Vlasov [34] where he considered the plasma as a set of macro particles of dimensions of the order of the Debye length  $\lambda_D$ . These are treated like particles of the system in all respects. The Vlasov model is based on the theory of Hartree's mean field approximation [71]. In this approximation, the interaction between many interacting charged particles can be exemplified, assuming that each individual particle moves in a field (average) generated by all the other particles of the system and thought of as an external field to the system. However, it depends on the instantaneous distribution of the particles of the system and is defined at every point of the space. This model is introduced by using the so-called *phase space of single-particle of Boltzmann* or *reduced phase space* (sometimes also called  *$\mu$  space*) [133]. A point  $P$  of this space is a dynamical state of a single particle.  $P$  has therefore six coordinates  $(\mathbf{r}, \mathbf{v}) = (x, y, z, v_x, v_y, v_z)$ , where  $\mathbf{r} = (x, y, z)$  is the position of the generic particle in the configuration space and  $\mathbf{v} = (v_x, v_y, v_z)$  is its velocity.

Let us suppose that we have a system consisting of a large number of identical particles to be in dynamical states that are continuously distributed in  $\mu$  space with the scales of the order of the Debye lengths. We define the Boltzmann distribution function of such a system of identical particles as the function  $f = f(\mathbf{r}, \mathbf{v}, t)$  such that the number  $dN$  for dynamical states of  $\mu$  space by a volume  $d^3r d^3v$  is  $dN = f(\mathbf{r}, \mathbf{v}, t) d^3r d^3v$ . Given the uniqueness of solutions of the equations of motion of individual particles (with assigned initial conditions), this system is a set of identical particles but distinguishable. Consequently, the dynamical states (points in  $\mu$  space) are in correspondence with the particles of the system. Then, at every instant  $t$ , the total number of dynamical states coincides with the total number  $N$  of the particles in the system.

Therefore

$$N = \int f(\mathbf{r}, \mathbf{v}, t) d^3r d^3v. \quad (\text{A.0.1})$$

Note that, if the particles of the system retain their identity (for example, absence of processes of ionization and/or recombination, decays, etc.),  $N$  remains unchanged over time. It follows that  $f(\mathbf{r}, \mathbf{v}, t)$  is normalizable. Then, once normalized, i.e.,  $\int f(\mathbf{r}, \mathbf{v}, t) d^3r d^3v = 1$ , thus meaning of probability density in the  $\mu$  space. With a kinetic model and in terms of such a distribution function, it is possible to describe any physical system composed of a very large number of charged particles interacting on scales comparable to  $\lambda_D$ . For instance, such systems are the charged-particle beams that are ordinarily produced and/or used in a machine accelerator or naturally produced in astrophysics; the plasmas that are ordinarily generated and/or used in the laboratory for many final scientific and technological applications or which are present in the diversified temperature and density in astrophysics. In particular, in a plasma, each species  $s$  of identical particles ( $s = \text{various species of ions, electrons}$ ) of a plasma. Let us suppose that there  $n_0$  are processes that can change the identity of the particles of each species and collisions at short range are actually negligible (assuming *collisionless plasma*). Given the *one-to-one* correspondence between the particles and dynamical states, during the evolution of the system in an arbitrary volume of  $\mu$ -space, an equal number of dynamical states *enter* and *go out* per unitary time. It corresponds to assume an equation of continuity for a (continuous) system of dynamical points that are representative of each species, where  $f_s(\mathbf{r}, \mathbf{v}, t)$  is their density and  $\mathbf{U}^{(6)} = (\dot{\mathbf{r}}, \dot{\mathbf{v}}) = (\mathbf{v}, \mathbf{a})$  is their velocity field, where  $\mathbf{a}$  is the instantaneous acceleration of a single particle. Then

$$\partial_t f_s + \nabla^{(6)} \cdot (f_s \mathbf{U}^{(6)}) = 0, \quad (\text{A.0.2})$$

where  $\nabla^{(6)} = (\partial_x, \partial_y, \partial_z, \partial_{v_x}, \partial_{v_y}, \partial_{v_z})$  is the gradient operator in 6-dimensional  $\mu$  space. Note that the quantities

$$n_s(\mathbf{r}, t) = \int f_s(\mathbf{r}, \mathbf{v}, t) d^3v, \quad (\text{A.0.3})$$

$$\mathbf{V}_s(\mathbf{r}, t) = \frac{\int \mathbf{v} f_s(\mathbf{r}, \mathbf{v}, t) d^3v}{n_s}, \quad (\text{A.0.4})$$

are macroscopic quantities and representing the density and the velocity (also called *current velocity* or *field velocity* of the fluid) associated with the species  $s$ . Taking into account that: (i)  $\mathbf{r}$  and  $\mathbf{v}$  are independent variables, (ii) the force field acting on the species  $s$  is  $\mathbf{F}_s = \mathbf{F}_s(\mathbf{r}, \mathbf{v}, t)$ , the equation of motion of a single particle (mass  $m_s$ ) is  $\mathbf{a} = \mathbf{F}_s(\mathbf{r}, \mathbf{v}, t)/m_s$ , then Eq. (A.0.2) becomes

$$\partial_t f_s + \mathbf{v} \cdot \nabla_{\mathbf{r}} f_s + \frac{\mathbf{F}_s}{m_s} \cdot \nabla_{\mathbf{v}} f_s + \frac{f_s}{m_s} (\nabla_{\mathbf{v}} \cdot \mathbf{F}_s) = 0,$$

where  $\nabla_{\mathbf{r}} = (\partial_x, \partial_y, \partial_z)$  and  $\nabla_{\mathbf{v}} = (\partial_{v_x}, \partial_{v_y}, \partial_{v_z})$  are the gradient operators in the configuration space and velocity space, respectively. The force field  $\mathbf{F}_s(\mathbf{r}, \mathbf{v}, t)$  can generally be the sum of external fields and the fields produced by the particles of the system (self-consistent fields). Let us confine our attention to fields only self-consistent, say  $\mathbf{F}_s = q_s[\mathbf{E} + \mathbf{v} \times \mathbf{B}]$ , where the fields  $\mathbf{E} = \mathbf{E}(\mathbf{r}, t)$  and  $\mathbf{B} = \mathbf{B}(\mathbf{r}, t)$  satisfy suitable Maxwell's equations. Note that the electromagnetic (EM) field sources are given by the distribution of charges and total currents (i.e., due to the contribution of all species) in the system. Taking into account of the above assumption and observing that, in the case of the EM Lorentz force,  $\nabla_{\mathbf{v}} \cdot \mathbf{F}_s = 0$ , we obtain the following system of coupled equations, said Vlasov-Maxwell (in cgs unit):

$$\partial_t f_s + \mathbf{v} \cdot \nabla_{\mathbf{r}} f_s + \frac{q_s}{m_s} [\mathbf{E} + \mathbf{v} \times \mathbf{B}] \cdot \nabla_{\mathbf{v}} f_s = 0 \quad (\text{A.0.5})$$

$$\nabla \cdot \mathbf{E} = 4\pi\rho, \quad (\text{A.0.6})$$

$$\nabla \cdot \mathbf{B} = 0 \quad (\text{A.0.7})$$

$$\nabla \times \mathbf{B} = \frac{4\pi}{c} \mathbf{j} + \frac{1}{c} \frac{\partial \mathbf{E}}{\partial t}, \quad (\text{A.0.8})$$

$$\nabla \times \mathbf{E} = -\frac{1}{c} \frac{\partial \mathbf{B}}{\partial t}, \quad (\text{A.0.9})$$

where  $s$  is the *various species of ions, electrons* and  $\rho$  and  $\mathbf{j}$  is the total charge density and current density, respectively, viz.,

$$\rho = \sum_s q_s n_s(\mathbf{r}, t) = \rho(\mathbf{r}, t) \quad (\text{A.0.10})$$

$$\mathbf{j} = \sum_s q_s n_s(\mathbf{r}, t) \mathbf{V}_s(\mathbf{r}, t) = \mathbf{j}(\mathbf{r}, t). \quad (\text{A.0.11})$$

The system of equation (A.0.5) - (A.0.11) is known as *Vlasov-Maxwell system*. It describes the self-consistent spatio-temporal evolution of the plasma according to the kinetic theory. It is worth noting to describe briefly some important aspects of this system of equations.

- For each  $s$ , Eq. (A.0.5) is called *kinetic equation of Vlasov* of the species  $s$ . It can be regarded as a kind of kinetic equation of Boltzmann in which the collisions are negligible. Actually, the presence of long-range interactions action is contained in the term of the Lorentz force and is described in the approximation of the mean field. However, the inclusion of the collective effects, makes the Vlasov equation profoundly different from the Boltzmann equation. An important aspect of this diversity is, for example, the development of processes of *non-dissipative damping* (known as *Landau damping*) of the collective oscillation modes of the system (plasma waves) with character of reversibility. In the

kinetic theory of Vlasov, such processes are describe in terms of the very large number of resonant interactions between the collective modes of the system and the individual particles [134].

- For each  $s$ , the first member of Eq. (A.0.5) can be regarded as the derivative of  $f_s$ . In fact, since  $\nabla_{\mathbf{v}} \cdot \mathbf{F}_s = 0$ , we observe that:

$$\partial_t f_s + \mathbf{v} \cdot \nabla_{\mathbf{r}} f_s + \frac{\mathbf{F}_s}{m_s} \cdot \nabla_{\mathbf{v}} f_s = \partial_t f_s + \dot{\mathbf{r}} \cdot \nabla_{\mathbf{r}} f_s + \dot{\mathbf{v}} \cdot \nabla_{\mathbf{v}} f_s = \frac{df_s}{dt}.$$

Consequently, from Eq. (A.0.5), it follows that  $df_s/dt = 0$ . Thus, the distribution function  $f_s$  is preserved along the characteristics  $\mathbf{r} = \mathbf{r}(t)$  and  $\mathbf{v} = \mathbf{v}(t)$ . This result has the following simple physical interpretation. Since each  $f_s$  represents the density of the dynamical states in  $\mu$ - space, these states constitute an incompressible fluid. It follows that, by virtue of the conservation of the number of the dynamical states in an arbitrary volume of  $\mu$ - space (continuity equation), the volume of the  $\mu$ - space associated with each subset of particles of the species  $s$  is preserved (*Liouville theorem in  $\mu$ - space*). Thus, it is easy to see that the same conservation property extends to the phase space volume associated with each subset containing all the species of the plasma.

- The coupling between the mathematical equations of the system (A.0.5) - (A.0.11) results in the following representation of the self-consistency of the Vlasov-Maxwell description. In principle, once the initial and boundary conditions are given, the Vlasov equation of each species can be integrated. Then, the resulting  $f_s$  can be used to determine the charge and current densities. In turn, the latter allows us to find the fields  $\mathbf{E}$  and  $\mathbf{B}$  by means of the Maxwell's equations, provided that appropriate boundary and initial conditions are given. It turns out that to determine explicitly  $f_s$  from (A.0.5), we must already know explicitly the fields  $\mathbf{E}$  and  $\mathbf{B}$ , but, on the other hand, to determine explicitly the latter by Maxwell's equations we need to know explicitly the distribution of the sources (charges and currents) and therefore  $f_s$ .
- The system of equations (A.0.5) - (A.0.11) is a system of differential equations with nonlinear partial derivative. The *sources of nonlinearity* can be identified in the third term of the left-hand side of Eq. (A.0.5) and, because of Eq. (A.0.11), in the first term of the right-hand side of Eq. (A.0.8). The nonlinearity of the system (A.0.5) - (A.0.11) makes it impossible to apply the superposition principle, i.e., a linear combination of solutions of the system of equations (A.0.5) - (A.0.11) is not a solution of the same system.

# Appendix B

## Fluid model: Lorentz-Maxwell system

We now want to derive the equations that govern the behavior of each species at scales much larger than the corresponding Debye length. This is usually done by reducing the description given in the  $\mu$ -space to the configurations space. This is done by integrating the Vlasov equation after it has been multiplied by appropriate monomials or polynomials of the velocity or its components.

Let us consider a homogeneous and isotropic plasma that is free from the action of any external fields. We denote by  $\hat{L}_s$  the following differential operator in the  $\mu$ -space as

$$\hat{L}_s = \partial_t + \mathbf{v} \cdot \nabla_{\mathbf{r}} + \frac{q_s}{m_s} \left[ \mathbf{E}(\mathbf{r}, t) + \frac{\mathbf{v}}{c} \times \mathbf{B}(\mathbf{r}, t) \right] \cdot \nabla_{\mathbf{v}}.$$

Then, the Vlasov equation (A.0.5) for the distribution function of the  $s$ -th species can be written as

$$\hat{L}_s f_s = 0. \quad (\text{B.0.1})$$

Now if  $g(v_i)$  is a generic function of  $\mathbf{v}$  or of its components  $v_i (i = x, y, z)$ , multiplying Eq. (B.0.1) by  $g$  and integrating, we obtain

$$\int g(v_i) \hat{L}_s f_s d^3 v = 0. \quad (\text{B.0.2})$$

We introduce also the following quantities (the integrations are extended to the entire velocity space):

1. *Moment of zero order of  $f_s$* , the scalar quantity

$$I_s^{(0)} = \int f_s(\mathbf{r}, \mathbf{v}, t) d^3 v. \quad (\text{B.0.3})$$

2. *First order moment of  $f_s$* , the vector quantity:

$$\mathbf{I}_s^{(1)} = \int \mathbf{v} f_s(\mathbf{r}, \mathbf{v}, t) d^3 v = \mathbf{I}_s^{(1)}(\mathbf{r}, \mathbf{v}, t); \quad (\text{B.0.4})$$

3. *Second order moment of  $f_s$ , the tensor quantity:*

$$\hat{\mathbf{I}}_s^{(2)} = \int \mathbf{v}\mathbf{v}f_s(\mathbf{r}, \mathbf{v}, t)d^3v = \hat{\mathbf{I}}_s^{(2)}(\mathbf{r}, \mathbf{v}, t), \quad (\text{B.0.5})$$

where  $\mathbf{v}\mathbf{v}$  is the *dyadic product* (component by component product with general terms  $v_i v_j$ ,  $i, j = x, y, z$ ) of  $v$  by itself. According to the preceding paragraph:

- $I_s^{(0)}$  coincides with the numerical density  $n_s(\mathbf{r}, t)$
- $\mathbf{I}_s^{(1)}$  coincides with the product of the numerical density and the current velocity  $\mathbf{V}_s(\mathbf{r}, t)$  concerning the species  $s$ , i.e.,  $\mathbf{I}_s^{(1)} = n_s(\mathbf{r}, t)\mathbf{V}_s(\mathbf{r}, t)$ . For this reason,  $\mathbf{I}_s^{(1)}$  is also called "*current density of species  $s$* ".

In addition, the quantity

$$\hat{\mathbf{P}}_s \equiv m_s \hat{\mathbf{I}}_s^{(2)}(\mathbf{r}, t) = m_s \int \mathbf{v}\mathbf{v}f_s(\mathbf{v})d^3v = m_s n_s \frac{\int \mathbf{v}\mathbf{v}f_s(\mathbf{r}, \mathbf{v}, t)d^3v}{\int f_s(\mathbf{r}, \mathbf{v}, t)d^3v} \quad (\text{B.0.6})$$

defines the *flux momentum density tensor of the species  $s$* . Denoting the average of tensor  $\mathbf{v}\mathbf{v}$  with respect to  $f_s$  by  $\langle \mathbf{v}\mathbf{v} \rangle_s$ , we can write

$$\hat{\mathbf{I}}_s^{(2)} = \frac{\hat{\mathbf{P}}_s}{m_s} = n_s \langle \mathbf{v}\mathbf{v} \rangle_s. \quad (\text{B.0.7})$$

In order to obtain a set of fluid equations for the plasma, we evaluate the integral of Eq. (B.0.2) for appropriate choices of  $g$ . The integration indicated by (B.0.2) leads to:

- for  $g = 1$ ,

$$\partial_t I_s^{(0)} + \nabla \cdot \mathbf{I}_s^{(1)} = 0; \quad (\text{B.0.8})$$

- for  $g = \mathbf{v}$ ,

$$\partial_t \mathbf{I}_s^{(1)} + \nabla \cdot \hat{\mathbf{I}}_s^{(2)} - \frac{q_s}{m_s} I_s^{(0)} \left[ \mathbf{E} + \frac{\mathbf{I}_s^{(1)}}{c} \times \mathbf{B} \right] = 0. \quad (\text{B.0.9})$$

Note that, Eq. (B.0.8), which has been obtained from the zero-order moment of Vlasov equation, can be regarded as the time evolution equation for the zero order moment  $I_s^{(0)}$ . However, it requires to know the first order moment  $\mathbf{I}_s^{(1)}$ . Furthermore, Eq. (B.0.9), which has been obtained from the first order moment of the Vlasov equation, one can relate to as an time evolution equation for the first order moment. However, it involves the second order moment  $\hat{\mathbf{I}}_s^{(2)}$ . If we calculate the second order moment of Vlasov equation, we obtain an evolution equation for the second order moment. However,

apart from the moments of order zero and one, it would contain the third order moment, as well. In general, an evolution equation for the moment of order  $n$ , involves moments of lower order, but it would also contain the moments of order  $n + 1$ .

The fluid model of plasma that we intend to present here is the one that is obtained by truncating the above described hierarchy of moment equations to the first order moment equation. To do this, it will be necessary to impose some physical conditions making it possible to express  $\hat{\mathbf{I}}_s^{(2)}$  in terms of moments of lower order (*closure reports*). The description that comes from this truncation can not coincide with the kinetic one, but it is only an approximation of that one. In particular, since the kinetic model applies on scales comparable to  $\lambda_D$ , the operations of average involved by the moments of the distribution functions introduce an effect of *smoothing*. It shows that the spatial variations of the physical quantities with scales very greater than  $\lambda_D$ .

If  $\lambda$  is the characteristic length of the spatial variation of the physical quantities involved in our description, then the condition of validity of a fluid model is expressed by

$$\lambda_D \ll \lambda.$$

This operation of *smoothing* can be best understood as follows: for each species  $s$  express velocity  $\mathbf{v}$  as the sum of a part corresponding to its average with respect to  $f_s$  and another average with respect to anything than  $f_s$ :

$$\mathbf{v} = \mathbf{V}_s + \mathbf{u} \quad (\text{B.0.10})$$

where  $\mathbf{V}_s = \langle \mathbf{v} \rangle_s$  and  $\langle \mathbf{u} \rangle_s = 0$ . Therefore,  $\mathbf{u}$  is the *random velocity* of the particle that takes into account their thermal motion. Taking into account of Eq. (A.0.3) and (A.0.4), into Eqs. (B.0.3) - (B.0.7) and (B.0.10), Eqs. (B.0.8) and (B.0.9) become

$$\frac{\partial n_s}{\partial t} + \nabla \cdot (n_s \mathbf{V}_s) = 0, \quad (\text{B.0.11})$$

$$\frac{\partial \mathbf{V}_s}{\partial t} + (\mathbf{V}_s \cdot \nabla) \mathbf{V}_s = \frac{q_s}{m_s} \left( \mathbf{E} + \frac{\mathbf{V}_s}{c} \times \mathbf{B} \right) - \frac{\nabla \cdot \hat{\mathbf{p}}_s}{m_s n_s}, \quad (\text{B.0.12})$$

where  $\hat{\mathbf{p}}_s$  is the *pressure tensor* on the species  $s$ , defined as

$$\hat{\mathbf{p}}_s = m_s n_s \langle \mathbf{u} \mathbf{u} \rangle_s = m_s \int f_s \mathbf{u} \mathbf{u} d^3 u. \quad (\text{B.0.13})$$

Since the collisions are considered negligible (the plasma is supposed to be highly diluted with also high temperature) and if no other form of dissipation are important, then we can assume the following isotropic form for the pressure tensor

$$\hat{\mathbf{p}}_s = p_s \hat{\mathbf{I}}, \quad (\text{B.0.14})$$

where  $\hat{\mathbf{I}}$  is the identity tensor and  $p_s$  is the scalar pressure of the species  $s$ . It is also assumed to be related to  $n_s$  and temperatures  $T_s$  through the equation of state for ideal gas, i.e.,  $p_s = n_s k_B T_s$ , where  $k_B$  is the Boltzmann constant. The most recurrent forms of closure of the system consisting of Eqs. (A.0.6) - (A.0.11) and (B.0.11) and (B.0.12) are the following one corresponds to the so-called *adiabatic hypothesis*, i.e.,

$$\frac{T_s}{n_s^{\gamma_s-1}} = \text{constant}$$

where  $\gamma_s$  is the ratio of specific heats at constant pressure and constant volume of species  $s$ . In this case it is easy to see that the (B.0.12) becomes:

$$\left( \frac{\partial}{\partial t} + \mathbf{V}_s \cdot \nabla \right) \mathbf{V}_s = \frac{q_s}{m_s} \left( \mathbf{E} + \frac{\mathbf{V}_s}{c} \times \mathbf{B} \right) - \gamma_s \frac{k_B T_s}{m_s} \frac{\nabla n}{n_s}. \quad (\text{B.0.15})$$

The other hypothesis is called *isothermal* and corresponds to assume  $\nabla T_s = 0$ , for which case Eq. (B.0.12) can be written as

$$\left( \frac{\partial}{\partial t} + \mathbf{V}_s \cdot \nabla \right) \mathbf{V}_s = \frac{q_s}{m_s} \left( \mathbf{E} + \frac{\mathbf{V}_s}{c} \times \mathbf{B} \right) - \frac{k_B T_s}{m_s} \frac{\nabla n}{n_s}. \quad (\text{B.0.16})$$

The system of equations consisting of (A.0.6) - (A.0.11) and (B.0.15) or (B.0.16) (made for all species) is known as *Lorentz-Maxwell (LM) system* in *adiabatic approximation* or in *isothermal approximation*, respectively.

## B.1 EM and ES modes in unmagnetized plasma

Let us consider, for simplicity, a collisionless, homogeneous, and isotropic plasma consists of only two fluids: one ion species and electrons. Such a system is described by the system of equations of LM formed in the paragraph B. A stationary state of the system can be identified from the plasma quiescent condition:

$$\mathbf{E} = 0, \quad \mathbf{B} = 0, \quad \mathbf{V}_s = 0, \quad n_s = n_{0s}, \quad (\text{B.1.1})$$

where  $n_{0s}$  are positive constants (each of these is the unperturbed density of species  $s$ ).

The conditions (B.1.1) states that in equilibrium conditions the various components of the plasma velocity have a zero current and self-compatible macroscopic fields are zero. Since  $\mathbf{E}$  is related to the density of total charge of Poisson's equation, it follows that in equilibrium there is local charge neutrality. Consequently:

$$\sum_{n=i,e} n_{0s} q_s = 0,$$

where  $Z$  is the atomic number of ions. The condition of local neutrality thus implies

$$Zn_{0i} = n_{0e} = n_0. \quad (\text{B.1.2})$$

Introducing small perturbations of the quantities with respect to the equilibrium state, we get

$$\mathbf{E} = \mathbf{E}_1, \quad \mathbf{B} = \mathbf{B}_1, \quad \mathbf{V} = \mathbf{V}_{s1}, \quad n_s = n_{0s} + n_{1s} = n_0 + n_{1s}, \quad (\text{B.1.3})$$

where subscript defines first order perturbation of the respective quantities. Substituting Eqs.(B.1.3) in the LM system and neglecting terms of higher order, we obtain the following system of linearized equation

$$\frac{\partial n_{e1}}{\partial t} + n_0 \nabla \cdot \mathbf{V}_{e1} = 0, \quad (\text{B.1.4})$$

$$\frac{\partial n_{i1}}{\partial t} + n_0 \nabla \cdot \mathbf{V}_{i1} = 0, \quad (\text{B.1.5})$$

$$\frac{\partial \mathbf{V}_{e1}}{\partial t} = -\frac{e}{m_e} \mathbf{E}_1 - \frac{1}{n_0 m_e} \left( \frac{\partial p_{e1}}{\partial n_{e1}} \right)_0 \nabla n_{e1}, \quad (\text{B.1.6})$$

$$\frac{\partial \mathbf{V}_{i1}}{\partial t} = \frac{e}{m_i} \mathbf{E}_1 - \frac{1}{n_0 m_i} \left( \frac{\partial p_{i1}}{\partial n_{i1}} \right)_0 \nabla n_{i1}, \quad (\text{B.1.7})$$

$$\nabla \cdot \mathbf{E}_1 = 4\pi e (n_{i1} - n_{e1}), \quad (\text{B.1.8})$$

$$\nabla \times \mathbf{E}_1 = -\frac{1}{c} \frac{\partial \mathbf{B}_1}{\partial t}, \quad (\text{B.1.9})$$

$$\nabla \cdot \mathbf{B}_1 = 0, \quad (\text{B.1.10})$$

$$\nabla \times \mathbf{B}_1 = \frac{4\pi e n_0}{c} (\mathbf{V}_{i1} - \mathbf{V}_{e1}) + \frac{1}{c} \frac{\partial \mathbf{E}_1}{\partial t}, \quad (\text{B.1.11})$$

where  $(\partial p_{s1}/\partial n_{s1})_0$  denotes the derivative of order zero of the kinetic pressure with respect to the density, relatively to the species  $s$ . From this system we want to extract high-frequency modes.

### B.1.1 High-frequency modes

Since  $m_i \gg m_e$ , for modes of high frequency it can be said that modes involve the response of only electrons at any stresses of the system. This corresponds to assume infinite inertia for the ion components, which formally can be assumed by taking the limit  $m_i \rightarrow \infty$  in the system of equations (B.1.4)-(B.1.11). In this approximation, the

latter is reduced to the following system

$$\frac{\partial n_{e1}}{\partial t} + n_0 \nabla \cdot \mathbf{V}_{e1} = 0 \quad (\text{B.1.12})$$

$$\frac{\partial \mathbf{V}_{e1}}{\partial t} = -\frac{e}{m_e} \mathbf{E}_1 - \frac{1}{m_e} \left( \frac{\partial p_{e1}}{\partial n_{e1}} \right)_0 \frac{\nabla n_{e1}}{n_0} \quad (\text{B.1.13})$$

$$\nabla \cdot \mathbf{E}_1 = -4\pi e n_{e1} \quad (\text{B.1.14})$$

$$\nabla \times \mathbf{E}_1 = -\frac{1}{c} \frac{\partial \mathbf{B}_1}{\partial t} \quad (\text{B.1.15})$$

$$\nabla \cdot \mathbf{B}_1 = 0 \quad (\text{B.1.16})$$

$$\nabla \times \mathbf{B}_1 = -\frac{4\pi e n_0}{c} \mathbf{V}_{e1} + \frac{1}{c} \frac{\partial \mathbf{E}_1}{\partial t}. \quad (\text{B.1.17})$$

Note that in this approximation ions constitute a background of positive charge. By combining Eqs. (B.1.12) - (B.1.16), it is easy to obtain the following wave equation

$$\frac{1}{c^2} \frac{\partial^2 \mathbf{E}_1}{\partial t^2} - \nabla^2 \mathbf{E}_1 + \frac{\omega_{pe}^2}{c^2} \mathbf{E}_1 + \left[ 1 - \frac{1}{m_e c^2} \left( \frac{\partial p_{e1}}{\partial n_{e1}} \right)_0 \right] \nabla (\nabla \cdot \mathbf{E}_1) = 0. \quad (\text{B.1.18})$$

Given the linearity of the equation (B.1.18),  $\mathbf{E}_1$  can be expressed as a superposition of waves through the Fourier integral

$$\mathbf{E}_1(\mathbf{r}, t) = \frac{1}{(2\pi)^4} \int \tilde{\mathbf{E}}_1(\mathbf{k}, \omega) \exp(i\mathbf{k} \cdot \mathbf{r} - i\omega t) d^3 k d\omega. \quad (\text{B.1.19})$$

With  $\tilde{\mathbf{E}}_1(\mathbf{k}, \omega)$  is given by the Fourier transform of  $\mathbf{E}_1(\mathbf{r}, t)$ , which leads algebraic equation

$$\hat{\mathbf{D}}(\mathbf{k}, \omega) \cdot \tilde{\mathbf{E}}_1(\mathbf{k}, \omega) = 0 \quad (\text{B.1.20})$$

where the tensor  $\hat{\mathbf{D}}$  is defined by

$$\hat{\mathbf{D}}(\mathbf{k}, \omega) = \left( -\frac{\omega^2}{c^2} + \mathbf{k}^2 + \frac{\omega_{pe}^2}{c^2} \right) \hat{\mathbf{I}} + \left[ \frac{1}{m_e c^2} \left( \frac{\partial p_e}{\partial n_e} \right)_0 - 1 \right] \mathbf{k}\mathbf{k}. \quad (\text{B.1.21})$$

Here  $\hat{\mathbf{I}}$  is the isotropic tensor and  $\mathbf{k}\mathbf{k}$  represents the dyadic product of  $\mathbf{k}$  with itself. So that there are solutions of (B.1.20) other than the trivial, the determinant of  $\hat{\mathbf{D}}$  must vanish. By imposing this cancellation condition and expressing  $\tilde{\mathbf{E}}_1$  as the sum of the parallel to  $\mathbf{k}$ , which we denote by  $\tilde{\mathbf{E}}_{1\parallel}$ , and that of perpendicular to the wave vector, which we denote by  $\tilde{\mathbf{E}}_{1\perp}$ , we obtain the following dispersion relations

(i) Purely longitudinal modes:

$$\omega^2 = \omega_{pe}^2 + \frac{1}{m_e} \left( \frac{\partial p_{e1}}{\partial n_{e1}} \right)_0 k^2 \quad (\text{B.1.22})$$

(ii) Purely transverse modes:

$$\omega^2 = \omega_{pe}^2 + c^2 k^2 \quad (\text{B.1.23})$$

The principle properties of these relations can be summarized as follows:

- Unlike the propagation of EM waves in vacuum, the propagation does not occur in plasma only with purely transverse waves.
- Both the equations (B.1.22) and (B.1.23) show the existence of a *cut-off* frequency that coincides with the electron plasma frequency. So, in linear theory, high frequency modes of frequencies less than  $\omega_{pe}$  can not propagate.
- Both the equations (B.1.22) and (B.1.23) show that plasma is a dispersive medium: the phase velocity ( $v_f = \omega/k$ ) and the group velocity ( $v_g = d\omega/dk$ ) are different.
- For wavenumbers sufficiently high (wavelength  $\lambda = 2\pi/k$  sufficiently small) Eq. (B.1.23) becomes

$$\omega \simeq \pm ck,$$

which coincides with the dispersion relation of the EM waves in a vacuum. This implies that for wavenumbers sufficiently high, the plasma is transparent to the propagation of purely transverse fields.

- In adiabatic approximation Eq. (B.1.22) becomes

$$\omega^2 = \omega_{pe}^2 \left( 1 + \gamma_e \lambda_{De}^2 k^2 \right), \quad (\text{B.1.24})$$

where  $\lambda_{De}^2$  and  $\gamma_e$  are Debye length and adiabatic exponent of electrons. However, since the fluid theory is valid in the limit  $\lambda_{De} k \ll 1$ , Eq. (B.1.24) is approximated to

$$\omega = \omega_{pe} \left( 1 + \frac{\gamma_e}{2} \lambda_{De}^2 k^2 \right). \quad (\text{B.1.25})$$

This means that, in fluid theory, it does not make any sense to take very high values of  $k$  to predict an asymptotic non-dispersive behavior. Since  $\lambda_{De} k \ll 1$ , the frequencies of the longitudinal modes are confined to values around their cut-off, i.e.,  $\omega_{pe}$ . Also note that the Fourier transform of Eq. (B.1.16) results that  $\mathbf{k} \cdot \tilde{\mathbf{B}}_1 = 0$ . Consequently,  $\tilde{\mathbf{B}}_1$  is always transverse, and in turn implies that the propagation described by Eqs. (B.1.24) and (B.1.25) is associated only to fluctuations of longitudinal electric field. Since, by virtue of Eq. (B.1.8),  $\tilde{\mathbf{E}}_{1\parallel}$  is supported by fluctuations of electron density, these modes are also called electrostatic (ES). In fact,  $\tilde{\mathbf{E}}_{1\parallel}$  varies in space and time, yet this physical circumstance

corresponds to a particular solution of Maxwell's equations, which is not associated with fluctuations of magnetic field, consistent with the conditions  $\nabla \times \mathbf{E}_1 = 0$  and  $\nabla \times \mathbf{B}_1 = 0$ . Thanks to Eq (B.1.17), the second condition implies that, for a purely ES possible solution, a perfect compensation between conduction current and displacement current must be realized.

- Finally, we observe that Eqs. (B.1.22) and (B.1.23) for  $k = 0$  collapse in the same dispersion relation,  $\omega = \omega_{pe}$ , which also describes plasma oscillations. Indeed, since in this case the group velocity is zero, one can not demonstrate any process propagation. Furthermore, for purely longitudinal modes, if  $k \neq 0$ , the propagation mechanism is ensured by the spatial dispersion of which is responsible for the thermal agitation of the particles in the plasma (in this case the electric component). For purely transverse modes, the spatial dispersion is ensured by the coupling between the mutual fluctuations of electric and magnetic fields like in a vacuum.

# Appendix C

## Slowly-varying amplitude approximation

Let us consider the following wave equation

$$-\frac{1}{c^2} \frac{\partial^2 \Phi}{\partial t^2} + \frac{\partial^2 \Phi}{\partial x^2} + \frac{\partial^2 \Phi}{\partial y^2} + \frac{\partial^2 \Phi}{\partial z^2} = 0. \quad (\text{C.0.1})$$

let us consider that  $\Phi(x, y, z, t)$  has the form  $\Phi(x, y, z) = \phi(x, y, z) \exp(-i\omega t)$ , in which frequency  $\omega$  and wave number  $k$  are related via the dispersion relation  $c^2 k^2 / \omega^2 = n^2$ , where  $n(x, y, z)$  is the refractive index of the medium. Then Eq. (C.0.1) reduces to the Helmholtz equation

$$\nabla^2 \phi + \frac{k^2}{n^2} \phi = 0. \quad (\text{C.0.2})$$

It is supposed that the medium has small modulations,  $n_1$ , compared to an unperturbed value  $n_0$ , such that  $n = n_0 + n_1(x, y, z)$  with  $n_1 \ll n_0$ . We also choose  $k = k_0 n_0$ , where  $k_0$  is the wave number in vacuum. Now we look for an approximate solution of (C.0.2) of the form

$$\phi(x, y, z) = \Psi(x, y, z) \exp(ik_0 z), \quad (\text{C.0.3})$$

where  $\Psi$  is a complex function. Thus Eq. (C.0.2) becomes

$$\nabla_{\perp}^2 \Psi + \frac{\partial^2 \Psi}{\partial z^2} + 2ik_0 \frac{\partial \Psi}{\partial z} - 2k_0^2 \frac{n_1}{n_0} \Psi = 0. \quad (\text{C.0.4})$$

Now if we assume that  $\Psi$  is a very slow function compared to the exponential term  $\exp(ik_0 z)$ , we can eventually assume

$$\left| \frac{\partial^2 \Psi}{\partial z^2} \right| \ll \left| 2ik_0 \frac{\partial \Psi}{\partial z} \right|.$$

This allows us to write Eq. (C.0.4) neglecting the second derivatives of  $\Psi$ , with respect to  $z$ , and we obtain the following equation for the parabolic complex wave function

$$\nabla_{\perp}^2 \Psi + 2ik_0 \frac{\partial \Psi}{\partial z} - 2k_0^2 \frac{n_1}{n_0} \Psi = 0. \quad (\text{C.0.5})$$

Equation (C.0.5) has the same form like a paraxial wave equation. Therefore, the *slowly-varying amplitude approximation* is the analog of the *paraxial approximation*. In fact, the ‘slowly’ varying complex amplitude takes into account the differences between the beam and a plane wave, namely the non-uniformity in the intensity distribution, the slight curvature of the wave-fronts, the evolution of the beam with respect to the propagation coordinate and the phase shift.

# Appendix D

## Virial equation

Let us consider a relativistic charged-particle beam is traveling along the  $z$ - axis with velocity  $\beta c$  ( $\beta \simeq 1$ ) under the action of an external potential. The motion of each single particle is associated with an unperturbed total energy  $m_0\gamma_0c^2$  ( $m_0$  and  $\gamma_0$  being the particle rest mass and the unperturbed relativistic factor, respectively). Let us additionally suppose that the beam has an interaction with the surroundings in the transverse plane only in such a way that, in the co-moving frame, the transverse motion of each single-particle is associated with an effective Hamiltonian  $\mathcal{H} = \mathcal{H}(\mathbf{r}_\perp, \mathcal{P}_\perp, \xi)$  as

$$\mathcal{H}(\mathbf{r}_\perp, \mathcal{P}_\perp, \xi) = \frac{1}{2}\mathcal{P}_\perp^2 + \mathcal{U}, \quad (\text{D.0.1})$$

where,  $\mathbf{r}_\perp$  and  $\mathcal{P}_\perp$  are the conjugate variables of transverse position and momentum, respectively,  $\xi = z - \beta ct \simeq z - ct$  is the time-like variable, and  $\mathcal{U}$  is the external potential. The quantities  $\mathcal{H}$  and  $\mathcal{U}$ , and  $\mathcal{P}_\perp$  are dimensionless quantities with respect to  $m_0\gamma_0c^2$  and  $m_0\gamma_0c$ , respectively. Following ‘quantumlike’ or ‘quantum’ description, we can introduce the following quantization rules:  $\mathcal{H} \rightarrow \hat{\mathcal{H}} = i\epsilon\partial/\partial\xi$ ,  $\mathcal{P}_\perp \rightarrow \hat{\mathcal{P}}_\perp = -i\epsilon\nabla_\perp$ , and  $\mathcal{U} \rightarrow \hat{\mathcal{U}}$ , where  $\epsilon$  is the emittance (generic dispersion parameter,  $\epsilon = \epsilon_t, \epsilon_c$ , depending on the considered regime, thermal or quantum, respectively). Then, Eq. (D.0.1) can be written as the following 2D Schrödinger-like equation

$$i\epsilon\frac{\partial\Psi}{\partial\xi} = -\frac{\epsilon^2}{2}\nabla_\perp^2\Psi + \mathcal{U}\Psi, \quad (\text{D.0.2})$$

where  $\Psi = \Psi(\mathbf{r}_\perp, \xi)$  is the beam wave function (BWF), so that its squared modulus is proportional to the beam density and  $\hat{\mathcal{U}}$  assumed to be a multiplicative operator. From Eq. (D.0.2), it is easily proven that the following continuity equation holds

$$\frac{\partial|\Psi|^2}{\partial\xi} + \nabla_\perp \cdot \Upsilon = 0, \quad (\text{D.0.3})$$

where

$$\Upsilon = \frac{-i\epsilon}{2} (\Psi^* \nabla_{\perp} \Psi - \Psi \nabla_{\perp} \Psi^*). \quad (\text{D.0.4})$$

By integrating Eq. (D.0.3) over all the transverse plane, we easily get the following norm conservation law, viz.,

$$\frac{d\mathcal{N}}{d\xi} = 0, \quad (\text{D.0.5})$$

where the norm is defined as  $\mathcal{N} = \int |\Psi|^2 d^2 r_{\perp}$ . According to Eq. (D.0.2), and to the Hamiltonian defined by Eq. (D.0.1), the quantum-like or quantum definition of the total beam energy is given by

$$\mathcal{E} = \langle \hat{\mathcal{H}} \rangle = \frac{1}{\mathcal{N}} \int \Psi^* \hat{\mathcal{H}} \Psi d^2 r_{\perp}. \quad (\text{D.0.6})$$

Consequently, it is easily seen that the total time-like variation of  $\mathcal{E}$  is

$$\frac{d\mathcal{E}}{d\xi} = \frac{1}{\mathcal{N}} \int |\Psi|^2 \frac{\partial \mathcal{U}}{\partial \xi} d^2 r_{\perp}, \quad (\text{D.0.7})$$

Let us introduce the effective transverse size of the beam  $\sigma_{\perp}$ , namely

$$\sigma_{\perp}^2 \equiv \langle (\hat{\mathbf{r}}_{\perp} - \langle \hat{\mathbf{r}}_{\perp} \rangle)^2 \rangle = \langle \hat{\mathbf{r}}_{\perp}^2 \rangle - \langle \hat{\mathbf{r}}_{\perp} \rangle^2 = \frac{1}{\mathcal{N}} \int \hat{\mathbf{r}}_{\perp}^2 |\Psi|^2 d^2 r_{\perp} - \left( \frac{1}{\mathcal{N}} \int \hat{\mathbf{r}}_{\perp} |\Psi|^2 d^2 r_{\perp} \right)^2. \quad (\text{D.0.8})$$

Note that:

$$\frac{d}{d\xi} \langle \hat{\mathbf{r}}_{\perp} \rangle = -\frac{i\epsilon}{2\mathcal{N}} \int (\Psi^* \nabla_{\perp} \Psi - \Psi \nabla_{\perp} \Psi^*) d^2 r_{\perp}. \quad (\text{D.0.9})$$

Then, differentiating Eq. (D.0.8), we finally get the following equation

$$\frac{d\sigma_{\perp}^2}{d\xi} = -\frac{i\epsilon}{\mathcal{N}} \int (\hat{\mathbf{r}}_{\perp} - \langle \hat{\mathbf{r}}_{\perp} \rangle) \cdot (\Psi^* \nabla_{\perp} \Psi - \Psi \nabla_{\perp} \Psi^*) d^2 r_{\perp}. \quad (\text{D.0.10})$$

Let us now define the average of the operator  $(\hat{\mathbf{r}}_{\perp} - \langle \hat{\mathbf{r}}_{\perp} \rangle) \cdot (\hat{\mathcal{P}}_{\perp} - \langle \hat{\mathcal{P}}_{\perp} \rangle)$  as the following symmetrized form:

$$\begin{aligned} & \langle (\hat{\mathbf{r}}_{\perp} - \langle \hat{\mathbf{r}}_{\perp} \rangle) \cdot (\hat{\mathcal{P}}_{\perp} - \langle \hat{\mathcal{P}}_{\perp} \rangle) \rangle \equiv \\ & \frac{1}{2\mathcal{N}} \int \Psi^* \left[ (\hat{\mathbf{r}}_{\perp} - \langle \hat{\mathbf{r}}_{\perp} \rangle) \cdot (\hat{\mathcal{P}}_{\perp} - \langle \hat{\mathcal{P}}_{\perp} \rangle) + (\hat{\mathcal{P}}_{\perp} - \langle \hat{\mathcal{P}}_{\perp} \rangle) \cdot (\hat{\mathbf{r}}_{\perp} - \langle \hat{\mathbf{r}}_{\perp} \rangle) \right] \Psi d^2 r_{\perp} = \\ & \left\langle \frac{\hat{\mathbf{r}}_{\perp} \cdot \hat{\mathcal{P}}_{\perp} + \hat{\mathcal{P}}_{\perp} \cdot \hat{\mathbf{r}}_{\perp}}{2} \right\rangle - \langle \hat{\mathbf{r}}_{\perp} \rangle \cdot \langle \hat{\mathcal{P}}_{\perp} \rangle. \end{aligned} \quad (\text{D.0.11})$$

Making use of Eqs. (D.0.10) and (D.0.11), it is easy to show that

$$\frac{1}{2} \frac{d\sigma_{\perp}^2}{d\xi} = \langle (\hat{\mathbf{r}}_{\perp} - \langle \hat{\mathbf{r}}_{\perp} \rangle) \cdot (\hat{\mathcal{P}}_{\perp} - \langle \hat{\mathcal{P}}_{\perp} \rangle) \rangle, \quad (\text{D.0.12})$$

$$\frac{d}{d\xi} \langle \hat{\mathbf{r}}_{\perp} \rangle = \langle \hat{\mathcal{P}}_{\perp} \rangle, \quad (\text{D.0.13})$$

$$\frac{d}{d\xi} \langle \hat{\mathcal{P}}_{\perp} \rangle = -\langle \nabla_{\perp} \mathcal{U} \rangle. \quad (\text{D.0.14})$$

In case of the average of  $\hat{\mathbf{r}}_{\perp}$  and  $\hat{\mathcal{P}}_{\perp}$  are zero, viz.,  $\langle \hat{\mathbf{r}}_{\perp} \rangle = \langle \hat{\mathcal{P}}_{\perp} \rangle = 0$ , Eqs. (D.0.12) - (D.0.14) reduce to

$$\frac{d\sigma_{\perp}^2}{d\xi} = 2 \langle \hat{\mathbf{r}}_{\perp} \cdot \hat{\mathcal{P}}_{\perp} \rangle. \quad (\text{D.0.15})$$

Differentiating Eq. (D.0.15) with respect to  $\xi$ , we get

$$\frac{d^2\sigma_{\perp}^2}{d\xi^2} = 2 \frac{d}{d\xi} \langle \hat{\mathbf{r}}_{\perp} \cdot \hat{\mathcal{P}}_{\perp} \rangle, \quad (\text{D.0.16})$$

Since  $\hat{\mathbf{r}}_{\perp}$  and  $\hat{\mathcal{P}}_{\perp}$  do not depend on  $\xi$  explicitly, we can use the Ehrenfest's theorem [135] for the operator  $\langle \hat{\mathbf{r}}_{\perp} \cdot \hat{\mathcal{P}}_{\perp} \rangle$  such that

$$\frac{d}{d\xi} \langle \hat{\mathbf{r}}_{\perp} \cdot \hat{\mathcal{P}}_{\perp} \rangle = \frac{1}{i\epsilon} \langle [\hat{\mathbf{r}}_{\perp} \cdot \hat{\mathcal{P}}_{\perp}, \hat{\mathcal{H}}] \rangle. \quad (\text{D.0.17})$$

This leads us to the examination of the commutator  $[\hat{\mathbf{r}}_{\perp} \cdot \hat{\mathcal{P}}_{\perp}, \hat{\mathcal{H}}]$  as

$$[\hat{\mathbf{r}}_{\perp} \cdot \hat{\mathcal{P}}_{\perp}, \hat{\mathcal{H}}] = \left[ \hat{\mathbf{r}}_{\perp} \cdot \hat{\mathcal{P}}_{\perp}, \frac{\hat{\mathcal{P}}_{\perp}^2}{2} + \hat{\mathcal{U}} \right] \equiv \left[ \hat{x}_i \hat{p}_i, \frac{\hat{p}_j \hat{p}_j}{2} \right] + [\hat{x}_i \hat{p}_i, \mathcal{U}(\hat{x})]. \quad (\text{D.0.18})$$

Recalling  $[\hat{x}_i, \hat{p}_i] = i\epsilon\delta_{ij}$  and  $[\hat{p}_i, \hat{p}_j] = 0$ , the first commutator is quite straightforward, and can be written as

$$\begin{aligned} \left[ \hat{x}_i \hat{p}_i, \frac{\hat{p}_j \hat{p}_j}{2} \right] &= \frac{1}{2} (\hat{x}_i \hat{p}_i \hat{p}_j \hat{p}_j - \hat{p}_j \hat{p}_j \hat{x}_i \hat{p}_i) \\ &= \frac{1}{2} \left( \hat{x}_i \hat{p}_i \hat{p}_j \hat{p}_j - \hat{x}_i \underbrace{\hat{p}_j \hat{p}_j \hat{p}_i}_{=\hat{p}_i \hat{p}_j \hat{p}_i} + i\hbar \hat{p}_i \hat{p}_i + i\epsilon \hat{p}_i \hat{p}_i \right) \\ &= 2i\epsilon \frac{\hat{p}_i \hat{p}_i}{2} \equiv 2i\epsilon \frac{\hat{\mathcal{P}}_{\perp}^2}{2}. \end{aligned} \quad (\text{D.0.19})$$

For the second commutator in Eq. (D.0.18), we first remark that the potential  $\mathcal{U}(\hat{x})$  commutes with all  $\hat{x}_i$ , as can be seen by series expansion of  $\mathcal{U}$ . Therefore

$$[\hat{x}_i \hat{p}_i, \mathcal{U}(\hat{x})] = \hat{x}_i \hat{p}_i \mathcal{U}(\hat{x}) - \mathcal{U}(\hat{x}) \hat{x}_i \hat{p}_i = \hat{x}_i \hat{p}_i \mathcal{U}(\hat{x}) - \hat{x}_i \mathcal{U}(\hat{x}) \hat{p}_i = \hat{x}_i [\hat{p}_i, \mathcal{U}(\hat{x})] \quad (\text{D.0.20})$$

We may now recall the formula  $[\hat{p}_i, \mathcal{U}(\hat{x})] = -i\epsilon \partial \mathcal{U} / \partial \hat{x}_i$ , then Eq. (D.0.20) can be written as

$$[\hat{x}_i \hat{p}_i, \mathcal{U}(\hat{x})] = -i\epsilon \hat{x}_i \frac{\partial \mathcal{U}}{\partial \hat{x}_i} \equiv (\hat{\mathbf{r}}_{\perp} \cdot \hat{\mathcal{P}}_{\perp}) \mathcal{U}. \quad (\text{D.0.21})$$

Substituting Eqs. (D.0.19) and (D.0.21) into (D.0.18), we get

$$[\hat{\mathbf{r}}_{\perp} \cdot \hat{\mathcal{P}}_{\perp}, \hat{\mathcal{H}}] = 2i\epsilon \frac{\hat{\mathcal{P}}_{\perp}^2}{2} + (\hat{\mathbf{r}}_{\perp} \cdot \hat{\mathcal{P}}_{\perp}) \mathcal{U}. \quad (\text{D.0.22})$$

Therefore, Eq. (D.0.17) can be written as

$$\frac{d}{d\xi} \langle \hat{\mathbf{r}}_{\perp} \cdot \hat{\mathcal{P}}_{\perp} \rangle = \frac{1}{i\epsilon} \left[ 2i\epsilon \left\langle \frac{\hat{\mathcal{P}}_{\perp}^2}{2} \right\rangle + \langle (\hat{\mathbf{r}}_{\perp} \cdot \hat{\mathcal{P}}_{\perp}) \mathcal{U} \rangle \right]. \quad (\text{D.0.23})$$

Thus, using Eq. (D.0.23), from (D.0.16), we get the virial equation

$$\frac{d^2 \sigma_{\perp}^2}{d\xi^2} = 4 \left\langle \frac{\hat{\mathcal{P}}_{\perp}^2}{2} \right\rangle + \frac{2}{i\epsilon} \langle (\hat{\mathbf{r}}_{\perp} \cdot \hat{\mathcal{P}}_{\perp}) \mathcal{U} \rangle = 4 \frac{\epsilon^2}{2} \int |\nabla_{\perp} \Psi|^2 d^2 r_{\perp} - 2 \langle \mathbf{r}_{\perp} \cdot \nabla_{\perp} \mathcal{U} \rangle. \quad (\text{D.0.24})$$

Note that the first term at the right hand side of Eq. (D.0.24) corresponds to four times the averaged kinetic energy associated with the transverse motion. Thus, virial equation can be cast as

$$\frac{d^2 \sigma_{\perp}^2}{d\xi^2} = 4 [\mathcal{E} - \langle \mathcal{U} \rangle] - 2 \langle \mathbf{r}_{\perp} \cdot \nabla_{\perp} \mathcal{U} \rangle. \quad (\text{D.0.25})$$

# Bibliography

- [1] F. F. Chen. *Handbook of Plasma Physics*, chapter 11: Laser Accelerators, pages 483–517.
- [2] J. M. Dawson. *From Particles to Plasmas*, page 131. Addison Wesley, Reading, MA, 1959.
- [3] J. M. Dawson. Nonlinear electron oscillations in a cold plasma. *Phys. Rev.*, 113:383387, 1959.
- [4] T. Tajima and J. M. Dawson. Laser electron accelerator. *Phys. Rev. Lett.*, 43:267–270, 1979.
- [5] M. N. Rosenbluth and C. S. Liu. Excitation of plasma waves by two laser beams. *Phys. Rev. Lett.*, 29:701–705, 1972.
- [6] C. Joshi, W. B. Mori, T. Katsouleas, J. M. Dawson, J. M. Kindel, and D. W. Forslund. Ultrahigh gradient particle acceleration by intense laser-driven plasma density waves. *Nature*, 311:525–529, 1984.
- [7] C. M. Tang, P. Sprangle, and R. N. Sudan. Dynamics of space-charge waves in the laser beat wave accelerator. *Phys. Fluids*, 28:1974–1983, 1985.
- [8] R. Fedele, U. de Angelis, and T. Katsouleas. Generation of radial fields in the beat-wave accelerator for gaussian pump profiles. *Phys. Rev. A*, 33:4412–4414, 1986.
- [9] W. Horton and T. Tajima. Pump depletion in the plasma-beat-wave accelerator. *Phys. Rev. A*, 34:4110–4119, 1986.
- [10] W. B. Mori, C. Joshi, J. M. Dawson, D. W. Forslund, and J. M. Kindel. Evolution of self-focusing of intense electromagnetic waves in plasma. *Phys. Rev. Lett.*, 60:1298–1301, 1988.

- [11] P. Gibbon and A. R. Bell. Cascade focusing in the beat-wave accelerator. *Phys. Rev. Lett.*, 61:1599–1602, 1988.
- [12] C. E. Clayton et al. Ultrahigh-gradient acceleration of injected electrons by laser-excited relativistic electron plasma waves. *Phys. Rev. Lett.*, 70:37–40, 1993.
- [13] M. Everett et al. Trapped electron acceleration by a laser-driven relativistic plasma wave. *Nature*, 368:527–529, 1994.
- [14] L. M. Gorbunov and V. I. Kirsanov. Excitation of plasma waves by an electromagnetic wave packet. *Sov. Phys. JETP*, 66:290–294, 1987.
- [15] L. M. Gorbunov and V. I. Kirsanov. Excitation of plasma-waves by short electromagnetic wave-packets. *Zh. Eksp. Teor. Fiz.*, 93:509–518, 1987.
- [16] P. Sprangle, E. Esarey, A. Ting, and G. Joyce. Laser wakefield acceleration and relativistic optical guiding. *Appl. Phys. Lett.*, 53:2146–2148, 1988.
- [17] F. Amiranoff et al. Observation of laser wakefield acceleration of electrons. *Phys. Rev. Lett.*, 81:995–998, 1998.
- [18] V. Malka et al. Electron acceleration by a wake field forced by an intense ultra-short laser pulse. *Sci.*, 298:1596–1600, 2002.
- [19] S. V. Bulanov, V. I. Kirsanov, and A. S. Sakharov. Excitation of ultrarelativistic plasma waves by pulse of electromagnetic radiation. *JETP Lett.*, 50:198–201, 1989.
- [20] V. I. Berezhiani and I. G. Murusidze. Relativistic wake-field generation by an intense laser pulse in a plasma. *Phys. Lett. A*, 148:338–340, 1990.
- [21] P. Sprangle, E. Esarey, and A. Ting. Nonlinear interaction of intense laser pulses in plasmas. *Phys. Rev. A*, 41:4463–4469, 1990.
- [22] P. Sprangle, E. Esarey, and A. Ting. Nonlinear theory of intense laser-plasma interactions. *Phys. Rev. Lett.*, 64:2011–2014, 1990.
- [23] P. Sprangle, E. Esarey, J. Krall, and G. Joyce. Propagation and guiding of intense laser pulses in plasmas. *Phys. Rev. Lett.*, 69:2200–2203, 1992.

- [24] E. E. Esarey, A. Ting, P. Sprangle, D. Umstadter, and X. Liu. Nonlinear analysis of relativistic harmonic generation by intense lasers in plasmas. *IEEE Trans. Plasma Sci.*, 21:95–104, 1993.
- [25] P. Chen, J. M. Dawson, R. W. Huff, and T. Katsouleas. Acceleration of electrons by the interaction of a bunched electron beam with a plasma. *Phys. Rev. Lett.*, 54:693–696, 1985.
- [26] J. B. Rosenzweig, D. B. Cline, B. Cole, H. Figueroa, and W. Gai. Experimental observation of plasma wake-field acceleration. *Phys. Rev. Lett.*, 61:98–101, 1988.
- [27] J. B. Rosenzweig, B. Breizman, T. Katsouleas, and J. J. Su. Acceleration and focusing of electrons in two-dimensional nonlinear plasma wake fields. *Phys. Rev. A*, 44:R6189–R6192, 1991.
- [28] R. Fedele, F. Tanjia, S. De Nicola, D. Jovanović, and P. K. Shukla. Quantum ring solitons and nonlocal effects in plasma wake field excitations. *Phys. Plasmas*, 19:102106 (1–15), 2012.
- [29] R. Fedele, F. Tanjia, S. De Nicola, D. Jovanović, and P. K. Shukla. Self consistent nonlinear transverse quantum dynamics of a cold relativistic electron beam in a magnetized plasma. *AIP Conf. Proc.*, 1421:212–228, 2012.
- [30] D. Jovanović, R. Fedele, F. Tanjia, S. De Nicola, and L. A. Gizzi. Nonlocal effects in the self-consistent nonlinear 3d propagation of an ultrastrong, femtosecond laser pulse in plasmas. *Eur. Phys. J. D*, 66:328 (1–16), 2012.
- [31] L. Tonks and I. Langmuir. Oscillations in ionized gases. *Phys. Rev.*, 33:195–210, 1929.
- [32] D. R. Nicholson. *Introduction to Plasma Theory*. John Wiley & Sons Ltd., New York, 1983.
- [33] F. F. Chen. *Introduction to plasma physics and controlled fusion*. Plenum Press, New York, 2 edition, 1984.
- [34] P. Sturrock. *Plasma Physics: An Introduction to the Theory of Astrophysical, Geophysical, and Laboratory Plasmas*. Cambridge University Press, New York, 1994.

- [35] J. D. Jackson. *Classical Electrodynamics*. John Wiley & Sons Ltd., New York, 1998.
- [36] W. K. H. Panofsky and W. A. Wenzel. Some considerations concerning the transverse deflection of charged particles in radio-frequency fields. *Rev. Sci. Instrum.*, 27:967, 1956.
- [37] E. Esarey, A. Ting, and P. Sprangle. Relativistic focusing and beat wave phase velocity control in the plasma beat wave accelerator. *Appl. Phys. Lett.*, 53:1266–1268, 1988.
- [38] C. E. Clayton, C. Joshi, C. Darrow, and D. Umstadter. Relativistic plasma-wave excitation by collinear optical mixing. *Phys. Rev. Lett.*, 54:2343–2346, 1985.
- [39] E. Esarey, C. B. Schroeder, and W. P. Leemans. Physics of laser-driven plasma-based electron accelerators. *Rev. Mod. Phys.*, 81:1229–1285, 2009.
- [40] H. Hamster, A. Sullivan, S. Gordon, W. White, and R. W. Falcone. Subpicosecond, electromagnetic pulses from intense laser-plasma interaction. *Phys. Rev. Lett.*, 71:2725–2728, 1998.
- [41] Y. Kitagawa et al. Electron acceleration in an ultraintense-laser-illuminated capillary. *Phys. Rev. Lett.*, 92:205002–205005, 2004.
- [42] P. Muggli and M. J. Hogan. Review of high-energy plasma wakefield experiments. *C. R. Phys.*, 10:116–129, 2009.
- [43] S. Lee et al. Energy doubler for a linear collider. *Phys. Rev. ST Accel. Beams*, 5:121301–121304, 2002.
- [44] L. de Broglie. Sur la possibilité de relier les phénomènes d’interférences et de diffraction à la théorie des quanta de lumière. *Compt. Rend.*, 183:447, 1926.
- [45] E. Schrödinger. Quantisierung als eigenwertproblem (zweite mitteilung). *Ann. Phys. Lpz.*, 79:489–527, 1926.
- [46] N. Bohr. *On the quantum theory of line spectra*, volume I: On the general theory, II: On the hydrogen spectrum, III: On the spectra elements of higher atomic structure of 8. Danske Vidensk. Selsk. Skrifter, Naturvidensk. og Mathem, Copenhagen, 1918-1922.
- [47] A. Messiah. *Quantum Mechanics*. NorthHolland Pub., Amsterdam, 1961.

- [48] J. A. Arnaud. *Beam and Fiber Optics*. Academic, New York, 1976.
- [49] V.I. Karpmann. *Nonlinear Waves in Dispersive Media*. Pergamon Press, Oxford, 1975.
- [50] R. Glauber. Photon correlations. *Phys. Rev. Lett.*, 10:84–86, 1963.
- [51] E. C. G. Sudarshan. Equivalence of semiclassical and quantum mechanical descriptions of statistical light beams. *Phys. Rev. Lett.*, 10:277–279, 1963.
- [52] M. A. Leontovich. A method for the solution of the problem of the propagation of electromagnetic waves along the surface of the earth. *Izv. Akad. Nauk SSSR, Ser. Fiz.*, 8:16, 1944.
- [53] M. A. Leontovich and V. A. Fock. Solution of the problem of propagation of electromagnetic waves along the earths surface by the method of parabolic equation. *Zh. Eksp. Teor. Fiz.*, 16:557–573, 1946.
- [54] G. B. Whitham. *Linear and Nonlinear Waves*. Wiley, New York, 1974.
- [55] G. P. Agrawal. *Nonlinear Fiber Optics*. Academic Press, San Diego, 1995.
- [56] D. Gloge and D. Marcuse. Formal quantum theory of light rays. *J. Opt. Soc. Am. A*, 59:1629–1631, 1969.
- [57] P. Sturrock. *Static and Dynamic Electron Optics: An Account of Focusing in Lens, Deflector and Accelerator*. Cambridge University Press, London, 1995.
- [58] J. Lawson. *The Physics of Charged-Particle Beams*. Clarendon Press, Oxford, 2nd edition, 1988.
- [59] R. Fedele and G. Miele. A thermal wave model for relativistic charged particle beam propagation. *Nuovo Cim. D*, 13:1527–1544, 1991.
- [60] H. P. Yuen. Two-photon coherent states of the radiation field. *Phys. Rev. A*, 13:2226–2243, 1976.
- [61] R. Fedele and G. Miele. Spherical aberrations in the thermal-wave model for luminosity estimates in particle accelerators. *Phys. Rev. A*, 46:6634–6639, 1992.
- [62] S. De Nicola, R. Fedele, V. I. Man’ko, and G. Miele. Coherent states for particle beams in the thermal wave model. *Phys. Scr.*, 52:191–198, 1995.

- [63] R. Fedele, F. Galluccio, and G. Miele. Aberrations in the thermal wave model: Comparison with particle tracking simulations. *Phys. Lett. A*, 185:93–98, 1994.
- [64] R. Fedele and P. K. Shukla. Self-consistent interaction between the plasma wake field and the driving relativistic electron beam. *Phys. Rev. A*, 45:4045–4049, 1992.
- [65] R. Fedele and V. G. Vaccaro. Thermal wave model for nonlinear longitudinal dynamics of a relativistic charged particle bunch in cold plasmas. *Phys. Scr.*, T-52:36–39, 1994.
- [66] R. Fedele, L. Palumbo, and V. G. Vaccaro. A novel approach to the nonlinear longitudinal dynamics in particle accelerators. In H. Henke, H. Homeyer, and Ch. Petit-Jean-Genaz, editors, *Proceedings of the Third European Particle Accelerator Conference, EPAC 92*, page 762, Berlin, March 1992. Editions Frontieres.
- [67] R. Fedele, G. Miele, L. Palumbo, and V. G. Vaccaro. Thermal wave model for nonlinear longitudinal dynamics in particle accelerators. *Phys. Lett. A*, 179:407413, 1993.
- [68] R. Fedele, G. Miele, and L. Palumbo. Radiation damping and quantum excitation for longitudinal charged particle dynamics in the thermal wave model. *Phys. Lett. A*, 194:113–118, 1994.
- [69] D. Anderson, R. Fedele, V. Vaccaro, M. Lisak, A. Berntson, and S. Johansson. Modulational instabilities within the thermal wave model description of high energy charged particle beam dynamics. *Phys. Lett. A*, 258:244–248, 1999.
- [70] P. Johannisson et al. Nonlocal effects in high-energy charged-particle beams. *Phys. Rev. E*, 69:066501–066507, 2004.
- [71] D. R. Hartree. *The calculation of Atomic Structures*. John Wiley & Sons Ltd., New York, 1957.
- [72] R. Fedele, F. Tanjia, S. De Nicola, P. K. Shukla, and D. Jovanović. Self consistent thermal wave model description of the transverse dynamics for relativistic charged particle beams in magnetoactive plasmas. In A. Becoulet, T. Hoang, and U. Stroth, editors, *Proc. 38th EPS Conf. Plasma Phys.*, volume 35G, Strasbourg, France, 2011. Eur. Phys. Soc.

- [73] F. Tanjia, S. De Nicola, R. Fedele, P. K. Shukla, and D. Jovanović. Quantumlike description of the nonlinear and collective effects on relativistic electron beams in strongly magnetized plasmas. In A. Becoulet, T. Hoang, and U. Stroth, editors, *Proc. 38th EPS Conf. Plasma Phys.*, volume 35G, Strasbourg, France, 2011. Eur. Phys. Soc.
- [74] D. Jovanović, R. Fedele, F. Tanjia, S. De Nicola, and M. Belić. Quantum ring soliton formation by strongly nonlocal plasma wake field response to a relativistic electron beam. *Eur. Phys. Lett.*, 100:5502–5507, 2012.
- [75] F. Tanjia, R. Fedele, S. De Nicola, D. Jovanović, and A. Mannan. The quantum plasma lens concept: a preliminary investigation. to be published in *J. Plasma Phys.*
- [76] D. Jovanović, R. Fedele, F. Tanjia, S. De Nicola, and M. Belić. Coherent quantum hollow beam creation in a plasma wakefield accelerator. to be published in *J. Plasma Phys.*
- [77] R. Fedele, F. Galluccio, V. I. Man’ko, and G. Miele. Full phase-space analysis of particle beam transport in the thermal wave model. *Phys. Lett. A*, 209:263–276, 1995.
- [78] R. Fedele and V. I. Man’ko. Quantumlike corrections and semiclassical description of charged-particle beam transport. *Phys. Rev. E*, 58:992–1001, 1998.
- [79] R. Jagannathan, R. Simon, E. C. G. Sudarshan, and N. Mukunda. Quantum theory of magnetic electron lenses based on the dirac equation. *Phys. Lett. A*, 134:457–464, 1989.
- [80] R. Jagannathan. Quantum theory of electron lenses based on the dirac equation. *Phys. Rev. A*, 42:6674–6689, 1990.
- [81] S. A. Khan and R. Jagannathan. Quantum mechanics of charged-particle beam transport through magnetic lenses. *Phys. Rev. E*, 51:2510–2515, 1995.
- [82] A. A. Sokolov and I. M. Ternov. On polarization and spin effects in the theory of synchrotron radiation. *Dokl. Akad. Nauk Ser. Fiz.*, 153:1052–1054, 1964.
- [83] A. A. Sokolov and I. M. Ternov. On polarization and spin effects in the theory of synchrotron radiation. *Sov. Phys. Dokl.*, 8:1203–1205, 1964.
- [84] J. Kessler. *Polarized Electrons*. Springer, Berlin, 2nd edition, 1985.

- [85] V. A. Bordovitsyn, editor. *Synchrotron Radiation Theory and its Development: in Memory of I.M. Ternov*. World Scientific, Singapore, 1999.
- [86] Z. Huang, P. Chen, and R.D. Ruth. Radiation reaction in a continuous focusing channel. *Phys. Rev. Lett.*, 74:1759–1762, 1995.
- [87] Z. Huang and R.D. Ruth. Effects of focusing on radiation damping and quantum excitation in electron storage rings. *Phys. Rev. Lett.*, 80:2318–2321, 1998.
- [88] Z. Huang and R.D. Ruth. Radiation damping and quantum excitation in a focusing-dominated storage ring. In H. Henke, H. Homeyer, and Ch. Petit-Jean-Genaz, editors, *15th ICFA Advanced Beam Dynamics Workshop on Quantum Aspects of Beam Physics*, Monterey, CA, USA, 1998.
- [89] G. Preparata. Quantum field theory of the free-electron laser. *Phys. Rev. A*, 38:233–237, 1988.
- [90] R. Bonifacio, M.M. Cola, N. Piovella, and G.R.M. Robb. A quantum model for collective recoil lasing. *Europhys. Lett.*, 69:55–60, 2005.
- [91] R. Bonifacio, N. Piovella, and G.R.M. Robb. Quantum theory of sase fel. *Nucl. Instrum. Methods Phys. Res. A*, 543:645–652, 2005.
- [92] E.P. Gross. Structure of a quantized vortex in boson systems. *Nuovo Cim.*, 20:454–457, 1961.
- [93] L.P. Pitaevskii. Vortex lines in an imperfect bose gas. *Sov. Phys. JETP*, 13:451–454, 1961.
- [94] D. Jovanović, R.Fedele, F. Tanjia, S. De Nicola, and L. A. Gizzi. Propagation of ultrastrong femtosecond laser pulses in plasmon-x. In A. Becoulet, T. Hoang, and U. Stroth, editors, *Proc. 38th EPS Conf. Plasma Phys.*, volume 35G, Strasbourg, France, 2011. Eur. Phys. Soc.
- [95] A.G. Khachatryan et al. Conceptual design of a laser wakefield acceleration experiment with external bunch injection. *Nucl. Instrum. Methods Phys. Res. A*, 566:244–249, 2006.
- [96] S. Kalmykov, S.A. Yi, V. Khudik, and G. Shvets. Electron self-injection and trapping into an evolving plasma bubble. *Phys. Rev. Lett.*, 103:135004–135007, 2009.

- [97] G. Turchetti et al. Optical acceleration activity in italy: Plasmonx. Prometheus project, 2010.
- [98] C. Benedetti et al. Nta plasmonx, 2008.
- [99] L.A. Gizzi et al. An integrated approach to ultraintense laser sciences: The plasmon-x project. *Eur. Phys. J. Special Topics*, 175:3–10, 2009.
- [100] D. Giulietti et al. Plasma acceleration and monochromatic x-ray production, 2006.
- [101] C. de Martinis et al. Status of the sparx fel project. In *Proceedings of EPAC 2006*, Edinburgh, Scotland, July 2006. EPAC.
- [102] A. Giulietti et al. Prepulse effect on intense femtosecond laser pulse propagation in gas. *Phys. Plasmas*, 13:093103 (1–6), 2006.
- [103] F. Broggi and L. Serafini. Energy deposition effects of the x photon beam on the mirror of plasmon-x experiment at li 2fe. report SPARC-EBD-10/01, INFN, 2010.
- [104] A. Pukhov. Strong field interaction of laser radiation. *Rep. Prog. Phys.*, 66:47–101, 2003.
- [105] S. Augst, D. D. Meyerhofer, D. Strickland, and S. L. Chint. Laser ionization of noble gases by coulomb-barrier suppression. *J. Opt. Soc. Am. B*, 8:858–867, 1991.
- [106] V. S. Belyaev. Generation of fast charged particles and superstrong magnetic fields in the interaction of ultrashort high-intensity laser pulses with solid targets. *Phys. Usp.*, 51:793–814, 2008.
- [107] A. Giulietti. Seminario plasmonx risultati dell'esperimento ilil/slic ed indicazioni per plasmonx, 2007.
- [108] J. Meyer ter Vehn, A. Pukhov, and Z.M. Sheng. Relativistic laser-plasma interaction. In D. Batani, C.J. Joachain, S. Martellucci, and A.N. Chester, editors, *Proc. 30th Course of the International School of Quantum Electronics on Atoms, Solids and Plasmas in Super-Intense Laser Fields*, page 167, Erice, Italy, 2000. Springer.
- [109] V.I. Berezhiani and S.M. Mahajan. Wake fields in semiconductor plasmas. *Phys. Rev. Lett.*, 73:1837–1840, 1994.

- [110] A. Sharma, I. Kourakis, and P.K. Shukla. Spatiotemporal evolution of high-power relativistic laser pulses in electron-positron-ion plasmas. *Phys. Rev. E*, 82:016402–016408, 2010.
- [111] A. Sharma and I. Kourakis. Spatial evolution of a q-gaussian laser beam in relativistic plasma. *Laser Part.*, 28:479–489, 2010.
- [112] E. Esarey, P. Sprangle, J. Krall, and A. Ting. Overview of plasma-based accelerator concepts. *IEEE Trans. Plasma Sci.*, 24:253–288, 1996.
- [113] R. Bingham, J.T. Mendonça, and P.K. Shukla. Plasma based charged-particle accelerators. *Plasma Phys. Control. Fusion*, 46:R1–R23, 2004.
- [114] R.E. Kidder. *Interaction of intense photon and electron beams with plasmas*, *Physics of High Energy Density*, page 306. Academic Press, New York, 1971.
- [115] U. Peschel, T. Peschel, and F. Lederer. Temporal solitary waves near linear resonances. *J. Opt. Soc. Am. B*, 14:2994–3002, 1997.
- [116] J. B. Johnson. A low voltage cathode ray oscillograph. *J. Opt. Soc. Am.*, 6:701–712, 1922.
- [117] P. Chen. A possible final focusing mechanism for linear colliders. *Part. Accel.*, 20:171–182, 1987.
- [118] P. Chen, T. Katsouleas J. J. Su, and J. M. Dawson. Plasma focusing for high-energy beams. *IEEE Trans. Plasma Sci.*, 15:218–225, 1987.
- [119] J. J. Su, T. Katsouleas, J. M. Dawson, and R. Fedele. Plasma lenses for focusing particle beams. *Phys. Rev. A*, 41:3321–3331, 1990.
- [120] R. Fedele and E. J. N. Wilson. A proposal to use a plasma lens to achieve a 12 nm spot at the end of clic. *Nuov. Cim. D*, 12:1497–1508, 1990.
- [121] J. B. Rosenzweig et al. Demonstration of electron beam self-focusing in plasma wake fields. *Phys. Fluids B*, 2:1376–1383, 1990.
- [122] H. Nakanishi et al. Direct observation of plasma-lens effect. *Phys. Rev. Lett.*, 66:1870–1873, 1991.
- [123] G. Hairapetian et al. Experimental demonstration of dynamic focusing of a relativistic electron bunch by an overdense plasma lens. *Phys. Rev. Lett.*, 72:2403–2406, 1994.

- [124] G. Hairapetian et al. Transverse dynamics of a short, relativistic electron bunch in a plasma lens. *Phys. Plasmas*, 2:2555–2561, 1995.
- [125] R. Govil, W. P. Leemans, E. Y. Backhaus, and J. S. Wurtele. Observation of return current effects in a passive plasma lens. *Phys. Rev. Lett.*, 83:3202–3205, 1999.
- [126] N. Barov and J. B. Rosenzweig. Propagation of short electron pulses in underdense plasmas. *Phys. Rev. E*, 49:4407–4416, 1994.
- [127] R. Fedele, F. Tanjia, D. Jovanović, S. De Nicola, and C. Ronsivalle. Wave theories of non-laminar charged particle beams: from quantum to thermal regime. submitted to *J. Plasma Phys.*
- [128] F. J. Sacherer. Rms envelope equations with space charge. *IEEE Trans. Nucl. Sci.*, NS-18:1105–1107, 1971.
- [129] B. Qiao, X. T. He, and S.-P. Zhu. Fluid theory for quasistatic magnetic field generation in intense laser plasma interaction. *Phys. Plasmas*, 13:053106 (1–7), 2006.
- [130] F. Pegoraro, S. V. Bulanov, F. Califano, and M. Lontano. Nonlinear development of the weibel instability and magnetic field generation in collisionless plasmas. *Phys. Scr.*, T63:262–265, 1996.
- [131] D. Jovanović, F. Pegoraro, and F. Califano. Perpendicular electron trapping associated with nonlinear whistlers. *Phys. Plasmas*, 8:3217–3226, 2001.
- [132] L. M. Gorbunov, P. Mora, and T. M. Antonsen. Quasistatic magnetic field generated by a short laser pulse in an underdense plasma. *Phys. Plasmas*, 4:4358–4368, 1997.
- [133] K. Huang. *Statistical Mechanics*. John Wiley & Sons Ltd., New York, 2 edition, 1987.
- [134] A. I. Akhiezer et al. *Collective oscillations in a plasma*. Pergamon, Oxford, 1967.
- [135] P. Ehrenfest. Bemerkung über die angenäherte gültigkeit der klassischen mechanik innerhalb der quantenmechanik. *Zeitschrift für Physik*, 45:455–457, 1927.